NASA Technical Paper 3008

September 1990

The Langley 14- by 22-Foot Subsonic Tunnel: Description, Flow Characteristics, and Guide for Users

Garl L. Gentry, Jr.,
P. Frank Quinto,
Gregory M. Gatlin,
and Zachary T. Applin

NASA

NASA Technical Paper 3008

1990

The Langley 14- by 22-Foot Subsonic Tunnel: Description, Flow Characteristics, and Guide for Users

Garl L. Gentry, Jr.,
P. Frank Quinto,
Gregory M. Gatlin,
and Zachary T. Applin
Langley Research Center
Hampton, Virginia

National Aeronautics and Space Administration
Office of Management
Scientific and Technical Information Division

Contents

q_{ind}	dynamic pressure measured 12 ft upstream of tunnel station 0, psf
q_∞	dynamic pressure, psf
S	wing area, ft^2
U_∞	free-stream tunnel velocity, ft/sec
u	longitudinal velocity component of local measured flow, ft/sec
$\widetilde{u}$	rms longitudinal velocity component of local flow, ft/sec
V_∞	velocity, ft/sec
w	tunnel-circuit width at indicated station, ft
x	longitudinal distance referenced to station 0, ft
z	vertical distance above tunnel floor, ft or in.
α	angle of attack, deg
β	angle of sideslip, deg
θ_h	angle between floor and ceiling, deg
θ_k	knuckle angle, deg
θ_S	angle of vertical strut at station 40, deg
θ_w	angle between opposite walls, deg
2θ	diffuser equivalent cone angle, $2\tan^{-1}\left(\frac{A_2^{1/2}-A_1^{1/2}}{L\pi^{1/2}}\right)$, deg

Abbreviations:

A/B	afterbody sting
BLRS	boundary-layer removal system
C.G.	center of gravity
dia.	diameter
ESP	electronically scanned pressure
L.E.	leading edge
LV	laser velocimeter
MIF	model interface
MPA	model preparation area
max	maximum
O.D.	outside diameter
OPT.	optional
RAD.	radius
RTC	rotor test cell
rms	root mean square
Sta.	tunnel station
T.E.	trailing edge

General Description of Facility

The Wind Tunnel

The Langley 14- by 22-Foot Subsonic Tunnel, shown in figure 1, is a closed-circuit, single-return, atmospheric wind tunnel with a maximum speed of about 338 ft/sec. The maximum unit Reynolds number is 2.1×10^6 per foot. The test section can be operated in a variety of configurations to minimize aerodynamic wall interference on the model. A schematic of the tunnel is shown in figure 2, and cross-sectional areas of the closed test section are presented in table 1. A general sketch showing the location of the major components of the tunnel is presented in figure 3. All the stations (Sta.) presented are referenced to station 0 which is the beginning of the test section. Detailed coordinate parameters defining the shapes of the first diffuser and the contraction section are presented in tables 2 and 3, respectively.

Settling chamber and contraction. Good flow quality is an essential element of the 14- by 22-Foot Tunnel. Low levels of test-section turbulence are achieved through the combined effects of a fan diffuser grid, a flow-straightening honeycomb, four antiturbulence screens, and a 9-to-1 contraction ratio. The square-mesh grid shown in figure 4 is located at the end of the fourth diffuser to reduce flow separation and provide uniform flow with low turbulence downstream of the fan in the fourth diffuser. The honeycomb and screens are located upstream of the test section in the settling chamber that is 57 ft wide by 50 ft high (fig. 5). The honeycomb has 0.375-in. hexagonal cells and is 5 in. deep. The four screens are located 30, 39, 46, and 53 in., respectively, downstream of the honeycomb. The geometric characteristics of the screens are given in chart A.

Chart A

Screen	Mesh	Wire diameter, in.	Porosity, percent
1	15	0.0120	67
2	20	.0080	70
3	22	.0075	70
4	25	.0065	70

Summary

The Langley 14- by 22-Foot Subsonic Tunnel is a closed-circuit, single-return, atmospheric wind tunnel with a test section that can be operated in a variety of configurations—closed, slotted, partially open, and open. The closed test-section configuration is 14.5 ft high by 21.75 ft wide by 50 ft long with a maximum speed of about 338 ft/sec. The open test-section configuration, which has a maximum speed of about 270 ft/sec, is formed by raising the ceiling and walls to form a floor-only configuration. The tunnel may be configured with a moving-belt ground plane and a floor boundary-layer removal system at the entrance to the test section for ground-effects testing. In addition, the tunnel has a two-component laser velocimeter, a frequency-modulated tape system for dynamic data acquisition, flow-visualization equipment, and acoustic testing capabilities. This report provides users of the 14- by 22-Foot Subsonic Tunnel with information required for planning experimental investigations including the use of test hardware and model support systems.

Introduction

The need for obtaining an improved understanding of the aerodynamics of vertical/short takeoff and landing (V/STOL) aircraft configurations, and the unusual test requirements associated with V/STOL aerodynamic research, led in 1970 to the design and construction of the Langley 14 -by 22-Foot Subsonic Tunnel (initially named the V/STOL Tunnel and later the 4- by 7-Meter Tunnel). This facility was designed to address two critical problems encountered in previous V/STOL testing in conventional wind tunnels. The first of these problems was the distortion of the tunnel flow resulting from the strong downwash generated by the V/STOL model lift fans or jets. The second was the interaction of the floor boundary layer with the vertical or forward-facing propulsion flow components from the model in such a way as to render conventional wall corrections meaningless. The tunnel was designed to accommodate wall effects with a large test section to provide a large ratio of test-section size to model size. Variable test-section configurations were designed to minimize the effects of the walls and model-generated downwash. These configurations include the following: a fully closed test section, a closed test section with slotted walls, a test section with either one or both sidewalls removed, and an open test section closed only on the floor. A boundary-layer removal system and moving-belt ground plane were designed to prevent the formation of a floor boundary layer in the test section and provide a uniform vertical velocity distribution for ground-effects testing.

The Langley 14- by 22-Foot Subsonic Tunnel is also ideally suited for low-speed tests to determine high-lift stability and control, aerodynamic performance, rotorcraft acoustics, turboprop performance, and basic wake and flow field surveys. An extensive flow improvement modification was completed in 1985 to provide better flow distribution and to reduce turbulence levels (refs. 1–3).

The purpose of this paper is to provide general information necessary for planning experimental investigations in the 14- by 22-Foot Tunnel. A general tunnel description and the flow characteristics are provided with detailed user information on instrumentation, data acquisition, test hardware, and specialized auxiliary equipment.

Symbols

A_1	area at location 1, ft^2
A_2	area at location 2, ft^2
AR	aspect ratio
b	wing span, ft
C_L	lift coefficient, $Lift/q_\infty S$
c_r	root chord, ft
$F_{D,b}$	drag-force correction to balance, lbf
h	tunnel-circuit height at indicated station, ft
L	centerline length, ft
p_s	static pressure, psf

The floor, ceiling, and walls have 3-in-high fairings to cover the support hardware for the honeycomb and screens.

Test section. The test section is 50 ft long and may be operated in a closed configuration or in any of several open configurations. The maximum speed for the closed configuration is 338 ft/sec, and the maximum speed for the fully open configuration is 270 ft/sec. In the closed configuration, the test section is 21.75 ft wide by 14.50 ft high (fig. 6). The tunnel has two test bays; the center of the front bay is located at station 17.75 and the center of the rear bay is located at station 40. The model support cart shown in figure 6 can be installed in either bay. The test-section walls, ceiling, and floor have continuous longitudinal slots with adjustable covers that may be opened to reduce wall effects on research models. The wall and ceiling slots are shown fully closed in figure 7. The slot opening can be varied to provide ventilation areas ranging from 0 to 10.48 percent of the total test-section wall, ceiling, and floor surface area. In general, the model size dictates the use of the slots. A large model could use the slots and apply no wall corrections, whereas a small model could be tested without the use of either the slots or the wall corrections. This method of minimizing wall effects was suggested in reference 4 and was explored in detail in reference 5. The test-section sidewalls have a divergence of approximately 0.1° from front to back to allow for boundary-layer growth. There are numerous observation windows in both walls, and the walls and ceiling are all equipped with high-intensity lights for photographic, filming, and video needs. The open test-section configuration (fig. 8) was incorporated into the tunnel design to aid in reducing vertical interference effects for powered-lift aircraft or helicopter lifting systems by providing for recirculation-free testing (ref. 6). For the open configuration, the ceiling and sidewalls are raised to a height of 24.5 ft above the test-section floor, and the flow collector, shown in figures 9(a) and 9(b), is moved into the proper position.

The test section is housed within a test chamber that is 61.6 ft high by 77 ft wide by 82 ft long. This chamber is designed to maintain a constant static pressure on the research models being investigated. The chamber walls are lined with acoustic panels that provide a sound absorption coefficient of approximately 0.95. The acoustic panels are constructed of a fibrous glass inner core wrapped in fiberglass cloth No. 1526. The inner core is sandwiched between perforated sheets of 22-gauge zinc-coated steel, and the panels are mounted in specially-designed channels attached to the test chamber structure. A close-up view of these acoustic panels is shown in figure 9(c).

Power section and drive fan. Test-section airflow is produced by a 40-ft-diameter, nine-bladed fan (fig. 10(a)) that is powered by a 6650-hp, three-phase alternating-current (ac) induction motor mounted in tandem with a 1350-hp direct-current (dc) motor. Both are variable-speed motors on a common shaft with the fixed-pitch fan. These motors are housed inside the nacelle shown in figure 10(b). The test-section wind speed is controlled by varying the fan speed. The two motors can be operated together to provide full power, or the dc motor may be operated alone for low-speed testing. In the single-motor operation (dc motor only), the fan can be operated up to 145 rpm, which corresponds to a test-section dynamic pressure of 35 psf in the closed test-section configuration. In tandem operation, the ac motor starts automatically at a fan speed of 80 rpm. The fan blades are 40 ft in diameter less a nominal 0.25-in. gap for radial clearance between the tip of the blade and the tunnel wall. The blades incorporate Clark-Y airfoil sections and are made of laminated spruce with a protective fiberglass cover on the leading edge. The fan hub is 13.33 ft in diameter and is supported on bearings that are on the ends of the fan drive shaft inside the nacelle. The spinner is a low-drag cowl that turns with the blades.

Support Areas

Control and data acquisition rooms. The control room is located adjacent to the test section as shown in figure 2. All functions associated with a test, including the control of the tunnel, model attitude, auxiliary compressed air, and variable-frequency electric-motor power systems, are controlled from this room. A photograph of the current control room is presented in figure 11. Television cameras and monitors are available for viewing the test section while the tunnel is running. A data acquisition room is located adjacent to the control room and contains the computer systems necessary for tunnel operation, data acquisition, and off-line data processing.

Model preparation areas. The pretest model assembly and posttest disassembly are done in the model preparation area (MPA) as shown in figure 2. Four model carts complete with model support systems are available for model assembly. The model is completely assembled and all components are checked for proper fit. In the MPA all instrumentation is installed, checked, and calibrated. There are four buildup test sites in the MPA. Common instrumentation interfaces are provided with quick connections at all sites. In addition, static tests of powered models can be accomplished at these sites.

When the model is scheduled for tunnel testing, the model, instrumentation, and cart are moved as a unit into the test section. In the tunnel the top of the model cart becomes part of the test section (floor).

Rotor test cell. Another part of the model preparation area is the rotor test cell (RTC). The RTC is a high-bay area that is 69 ft high by 42 ft wide by 48 ft long with a steel chain link fence around the walls; it is arranged specifically for the buildup and testing of powered rotor models in hover. Two walls of the RTC have louvers that can be opened to alleviate some of the recirculation of air from the hovering rotor. The ambient temperature and pressure, as well as the dew point, are measured by instrumentation located in the RTC. The model instrumentation is connected through the in-house cabling to the data acquisition system.

Aerodynamic Characteristics

Airflow Control and Measurement

Tunnel airflow control. A number of devices for controlling and conditioning the tunnel airflow are located throughout the tunnel circuit. An adjustable air intake in the first diffuser and a fixed-area exhaust exit just upstream of the third corner, as shown in figure 2, are used for tunnel temperature control.

The tunnel also has a set of flow-control vanes located between the first and second corners. These vanes open to permit maximum airflow and close to restrict airflow in a manner similar to that of split flaps on a wing (fig. 12). The vanes are designed with symmetrical airfoil-shaped struts with a 9-ft chord to withstand a dynamic pressure of 40 psf normal to the surface. These vanes provide a large, controllable flow resistance in the tunnel circuit to assist in low-speed operation. The increased resistance requires that the drive-fan speed be increased to achieve a given velocity in the test section. The resulting increase in fan operating speed allows more precise control of the desired low test-section speed. For test-section speeds greater than about 59 ft/sec, the flow-control vanes are normally not used. The vanes are also used to close the tunnel circuit to prevent circulation of airflow during static tests of powered models.

Each vane has a trailing-edge flap that was added to improve the turning of the flow so that the flow would remain attached to the inner wall downstream of the second corner. The trailing-edge flap (flow deflector), which was designed to be 1.5 ft long and to deflect 25°, is most effective at high speed (above 59 ft/sec) when the flow-control vanes are fully open, as shown in figure 12(c). When the flow-control vanes are closed to improve low-speed control, the trailing-edge flaps are in the wake of the flow-control vanes and their effects are essentially removed, as shown in figure 12(d).

All four corners of the tunnel have fixed turning vanes that are designed to guide the airflow around the turns to minimize losses and to improve the flow quality of the tunnel. Table 4 gives the number of vanes, their spacing, and the relative porosity for each of the corners. Figure 13 shows a debris-catching screen located across the lower one-third of the second-corner turning vanes to prevent any large foreign object from contact with the fan blades.

Tunnel speed measurements. As previously discussed, test-section wind speed, and therefore dynamic pressure, is controlled by varying the tunnel fan speed. Tests are generally conducted at constant dynamic pressure or velocity. The dynamic pressure in the test section is monitored by using both a static pressure probe located 12 ft upstream of the test section and a total pressure probe located 59.4 ft upstream of the test section in the settling chamber (2 ft downstream of the last turbulence screen). Photographs of both pressure probes are presented in figure 14. The upstream location of the static port was chosen to minimize any effects from model recirculation flow interference. The static and total pressure probes are connected to a precision 208.8-psf differential, fused-quartz, bourdon pressure transducer with a digital readout. This transducer has a measured accuracy of ±0.08 psf of the full-scale reading. The instrument is located in the control room and displays the differential pressure between the static and total pressure readings, which is referred to herein as the indicated dynamic pressure (q_{ind}). This indicated dynamic pressure is related to the actual dynamic pressure of the test section by means of calibration curves that have been determined for the different test-section configurations (ref. 7). The pressure transducer readings are input continually to the computer system and corrected for instrument error and environmental factors. Displays of corrected test-section dynamic pressure as well as computed test-section velocity are both available on the operator console. The velocity corrections include the effects of changes in tunnel temperature and density.

Flow Characteristics

Test-section static pressure distribution. Wind speeds for testing in the 14- by 22-Foot Tunnel are established by setting an indicated dynamic

pressure that has been calibrated as a function of measured dynamic pressure in the test section, as discussed in the previous section. The ratio of q_{ind} to q_∞ is a constant value and changes only with a change of tunnel configuration (open or closed) or with the use of the boundary-layer removal system. Each tunnel configuration has been independently calibrated.

During the calibration, a centerline probe with streamwise static pressure orifices (fig. 15) was used to determine the longitudinal static pressure gradient. The probe extended from a point 20 ft inside the contraction section rearward to the end of the test section. A structural support at tunnel station 54 held the back end of the probe while three sets of cables supported the rest of the probe, as shown in the photograph presented in figure 15(b). The tunnel was clear of all items except for support hardware. The five configurations tested were: (1) a closed test section, (2) a closed test section using boundary-layer suction, (3) an open test section (ceiling and walls removed), (4) an open test section using boundary-layer suction, and (5) a closed test section with only ceiling slots open. This last configuration was used for overhead flow-visualization observations and photographic documentation.

Centerline static pressure measurements were made for the tunnel-empty condition to determine the dynamic pressure distribution in the streamwise direction. Results of these tests are presented in figures 16–20 as plots of local static pressure versus tunnel longitudinal location at several tunnel speeds. Increasing the tunnel speed resulted in an increase in static pressure gradient for all the closed test-section configurations (figs. 16–18).

Predicted longitudinal static pressures computed using the inviscid numerical method described in reference 8 are compared with a measured dynamic pressure in figure 19. The predicted curve has a slight pressure gradient opposite in direction from the measured gradient because of the divergence in the tunnel sidewalls. The data indicated that for the tunnel to be relieved of the pressure gradient, the tunnel walls need higher divergence angles. Centerline static pressure data were obtained with the centerline probe for test-section dynamic pressures up to 140 psf for the closed test-section configuration and for dynamic pressures up to 90 psf for the open test-section configuration. For each test-section dynamic pressure, a first-order, least-squares curve fit was applied to the static pressure data obtained between tunnel stations 5 and 30. The resulting static pressure variations were plotted against test-section dynamic pressure in figure 20(a) for closed test-section configurations. The pressure distribution along the centerline of the test section was also measured with the boundary-layer removal system operational and with all slots closed as shown in figure 20(b). The static pressure variations for the closed test-section configuration with ceiling slots open are presented against free-stream dynamic pressure in figure 20(c).

Since the angle in the walls, ceiling, and floor geometry cannot be changed, the tunnel user must mathematically correct the drag component of the model tested as described in reference 7 or as shown in the following equation:

$$\Delta F_{D,b} = \frac{\partial p_s}{\partial x} \times \text{Model volume}$$

where $\partial p_s/\partial x$ is obtained from figure 20, depending on the test-section configuration.

The open test-section configuration shown in figures 21 and 22 has essentially zero pressure gradient as expected.

Comparison of centerline and wall pressures. Static pressure wall data for the closed test-section configuration along with the centerline probe data are presented in figure 23 for tunnel station −50 (in the contraction cone) to station 100 (in the first diffuser). The data show that as the flow accelerates through the final portion of the contraction cone, the velocity at the centerline is less than that at the sidewalls of the tunnel. This lower dynamic pressure at the centerline is caused by the large nacelle that houses the drive motor. From tunnel station 0 (the entrance to the test section) to station 30, however, there is very good agreement between the wall data and the centerline probe data, and it is in this area that the buoyancy effect in the test section can be seen. A least-squares curve fit through the centerline probe data reveals that between tunnel stations 5 and 30 the static pressure decreases 0.0959 psf/ft. Static pressure data from the centerline probe gradually decrease from tunnel station 30 to station 40 as the free-stream flow adjusts to the effects from the 3-ft slot opening between tunnel stations 37 and 40. Static pressure begins to increase as the flow enters the diffuser at tunnel station 50.

Static pressure data showing the free-stream flow behavior through the test section for the open test-section configuration are presented in figure 24. The same lower dynamic pressure is seen at the centerline in the final portion of the contraction cone as seen for the closed test-section configuration. A least-squares curve fit for pressure data between tunnel stations 5 and 30 reveals that the static pressure decreases 0.0076 psf/ft. As expected, this amount is much less than that for the closed test-section configuration. A decreased static pressure is seen at the entrance to the diffuser because of the entrainment of test

chamber air into the free stream between the flow collector and the diffuser.

An additional tunnel configuration investigated was the closed test-section configuration with the test-section ceiling slots open. Static pressure data showing the behavior of the flow through the test section for this configuration are presented in figure 25. These data are very similar to those for the closed test-section configuration except that between tunnel stations 5 and 30, the static pressure decreases only 0.0757 psf/ft. It is expected that the static pressure gradient would be less for this configuration because the boundary-layer buildup on the ceiling is being relieved through the slots. Decreased static pressure is seen at the entrance to the diffuser because of the entrainment of test chamber air into the free stream between the flow collector and the diffuser.

Circuit static pressure distribution. Static pressure data have been obtained around the entire wind-tunnel circuit on both the outer and inner walls to document the static pressure distribution. Values of the static pressure around the tunnel circuit are presented for the closed test-section configuration in figure 26. These data are presented for a test-section dynamic pressure of 70 psf as determined by the calibration curve. The static pressure data show a smooth acceleration of the flow in the contraction cone with a good correlation between the outer and inner walls. As the free stream enters the test section, however, there is a slight disturbance at tunnel station 0. This is a result of a gap in the tunnel circuit where the contraction cone ends and the test section begins. The flow accelerates slightly through the test section, as will be discussed in detail later, and then increases to its highest velocity at tunnel station 40. The pressure drop that appears at tunnel station 40 results from a 3-ft slot opening (between tunnel stations 37 and 40) on the wall and ceiling slots. At this location, the low pressure in the test section entrains airflow from the test chamber. This inflow of test chamber air decreases the effective cross-sectional area and therefore increases the velocity of the free stream at station 40. The flow decelerates smoothly through the first diffuser; however, a slight decrease in pressure occurs on the outer wall of the tunnel at the location of the flow-control vanes. This decrease is due to the flow deflectors on the trailing edge of the flow-control vanes which create the effect of camber and thus increase the flow velocity on the outer-wall side of the vanes.

A pressure rise of approximately 19 psf occurs across the drive fan at tunnel station 352. A very slight decrease in pressure is seen downstream of the fan as the flow accelerates past the nacelle and its support fairings. Maximum static pressure in the tunnel circuit occurs near the end of the fourth diffuser just upstream of the grid, thus indicating that the grid is effectively producing the desired high-pressure region. The static pressure decreases slightly just downstream of the grid and remains relatively constant until the flow begins to accelerate at the entrance to the contraction cone.

A similar plot of static pressure around the tunnel circuit is presented for the open test-section configuration in figure 27. These data are also presented for a test-section dynamic pressure of 70 psf. The flow in the contraction cone appears to be the same as that for the closed test-section configuration except that it is a little smoother as it approaches tunnel station 0. The movable test-section walls extend into the first diffuser up to tunnel station 68, and therefore there are no static pressure wall data until tunnel station 70. However, at tunnel station 70 there is a large difference in static pressure (approximately 14 psf) when compared with the closed test-section configuration. This difference results from the entrainment of air from the test chamber into the free stream through the gap between the flow collector and the diffuser. The inflow of air acts to decrease the effective cross-sectional area seen by the free stream and produces the lowest static pressure in the tunnel circuit. The flow around the remainder of the tunnel circuit behaves in a manner similar to that for the closed test-section configuration with the exception of the pressure rise across the drive fan. The static pressure increase across the drive fan is approximately 11 psf greater for the open test-section configuration than for the closed test-section configuration. This difference illustrates the greater work load required of the drive fan when the wind tunnel is operated in the open test-section configuration.

Tunnel flow angularity. An indication of flow angularity has been determined with an NACA 0012 unswept, uncambered, elliptical wing model (fig. 28). The model was sting mounted to a six-component strain gauge balance in the front bay of the tunnel test section (fig. 29). Aerodynamic forces and moments were measured for the model in the upright and inverted positions at a dynamic pressure of 60 lb/ft^2 through an angle-of-attack range from $-6°$ to $6°$. Half the difference between the measured lift curves indicates an integrated upwash flow (vertical flow) of $0.15°$ (fig. 30). Figure 30(b) shows the upwash as a function of tunnel dynamic pressure. The side flow was determined in a similar manner with the use of a yaw mechanism at a dynamic pressure of 60 lb/ft^2 (fig. 31). Figure 31(b) shows the side flow as a function of tunnel dynamic pressure. These lift

curves indicate a flow angularity of 0.44 of side flow (coming from right to left looking upstream).

Boundary layer of test-section floor. Floor velocity profiles were determined from total pressure measurements obtained with a 30-in. total pressure rake. Simultaneous static pressure measurements were made by a separate probe located to one side of the rake and at a nominal height of 30 in. above the test-section floor. The general arrangement of the total pressure rake in this test section is shown in figure 32. The total pressure measurements were made at dynamic pressures of 20 to 100 lbf/ft^2 at a tunnel station 17.75 ft from the entrance to the test section. All the pressure data were obtained by means of electrically scanned pressure (ESP) modules described in the instrumentation section of this paper.

The boundary layer for the closed configuration was measured both with and without the boundary-layer removal system (BLRS) operating. Data without the use of the BLRS are presented in figure 33 and demonstrate that models should not be positioned less than 10 in. above the floor at any test configuration. The BLRS is designed to eliminate as much of the boundary layer as possible for ground-effects tests or for models in close proximity to the floor because of configuration setup (for example, a semispan model). The results of figure 33(b) show that the boundary-layer height was reduced to about 2 in. with the BLRS operating. These data were measured from the boundary-layer rake presented in table 5.

Tunnel turbulence. Figure 34 presents longitudinal turbulence intensity as a function of dynamic pressure for the closed test-section configuration. The data were obtained using a single normal-wire probe located on the tunnel centerline of a station 17.8 ft from the entrance to the test section. The probe used a 0.00015-in-diameter platinum-coated tungsten wire that was 0.050 in. long. The longitudinal turbulence intensity varies from approximately 0.3 to 0.1 percent over the dynamic pressure range presented.

The longitudinal turbulence intensity for the open test section is presented in figure 35. The hot-wire probe and location are exactly the same as for the closed test-section data. Generally, the turbulence level for the open test section is about 0.25 percent throughout the dynamic pressure range presented.

Model Support Systems

The wide variety of model configurations tested in the 14- by 22-Foot Tunnel has resulted in the development of a variety of support systems, stings, and balances as illustrated in figures 36–42. Each model support cart is designed as a stand-alone unit so that sting and model buildup, instrumentation checkout, and posttest model disassembly can be accomplished outside the test section. These features are essential because the elaborate instrumentation used on large models makes setup and checkout inside the test section prohibitive in terms of the tunnel occupancy time.

Model Support Carts 1 and 2

Model support carts 1 and 2 are shown in figure 36. Both carts are similar in design and consist of a support carriage, rotating turntable, and movable vertical-sting support mast. The carts each have a gear-driven pitch mechanism, which has the capability of pitching the model from $-14°$ to $14°$, and a chain-driven yaw mechanism, which has the capability of yawing the model from $-170°$ to $170°$.

The elevation or height adjustment of the model is accomplished by raising the mast using an electrically driven jack-screw mechanism on cart 1 and a hydraulically actuated mechanism on cart 2. The vertical motion capability on both units is 79 in. A fixed insert is available to provide an additional 15 in. in height for the entire sting assembly. The vertical drive mechanism can move the model from floor level to a position slightly above the tunnel centerline in a period of approximately 1 minute.

The model support carts each weigh approximately 80 000 lb and are moved to and from the model preparation area (MPA) on four air-bearing assemblies. The carts are raised into either the front or aft test bay by hydraulic lifts and, when mounted in place, the support cart becomes the floor of the test section.

Hardware for Model Support Carts 1 and 2

A variety of different sting arrangements are available for use on model support carts 1 and 2 as shown by the support hardware presented in figures 37–40. Two types of strain gauge balances are used most frequently in models tested in the 14- by 22-Foot Tunnel and they are referred to as 708-type and 729-type balances. Load ranges for several of these balances are given in table 6. Several sting systems have been designed so that the end of the sting will attach directly to one of these two balance types. Examples of these systems are shown in their completely assembled form in figure 37. This is not to say that only models using these two balances can be tested on these sting systems. Many other balances

may be used, and it is common for special adaptive hardware to be built for models that have not been tested previously in the 14- by 22-Foot Tunnel.

Angle-of-attack ranges other than that from $-14°$ to $14°$ are obtained with angled sections referred to as "knuckles". The knuckles are used to produce an angular offset in order to change the end points for a model angle-of-attack range or yaw-angle range. A descriptive sketch of a knuckle and a list of knuckles available for use are presented in figure 38.

A wide variety of model support stings have been fabricated and are available. Examples of some of the straight and bent stings available are presented in figures 39 and 40. These stings are in several lengths and typically have a diameter of 2 to 3 in. at the point where the sting would normally enter the back of a model. Certain models require the use of high-pressure air to simulate propulsion or to run various other systems. Stings designed specifically for use with such models are referred to as "air stings" and are shown in figure 40. In addition to the two bent air stings shown in figure 40, there is a straight air sting. All the air stings can be lengthened 18 in. by attaching an extension to the model end of the sting.

Prior to testing a model that uses high-pressure air, the balance to be used must be bench calibrated with the source air line attached. The bench calibration task usually requires about 8 weeks to complete. Several balance and sting combinations have already been calibrated and are ready for immediate use.

Both model support carts 1 and 2 are capable of supporting a model at the end of a 22.25-ft sting system as shown in figure 37. The maximum allowable load at the model center of gravity is 4000 lb in the vertical plane and 3500 lb in the horizontal plane. These values are for a total load consisting of a steady component plus a dynamic component, as well as the deadweight of the model.

High-α Vertical Strut

Special high-angle-of-attack (high-α), vertical-strut model support systems are available for attachment to model support cart 2 (fig. 41) to achieve angles of attack greater than 28°. The model is mounted directly to a special linkage at the top of the strut and is controlled in pitch and elevation by electrically driven motors. This special fitting at the top of the strut has a large fitting for heavy models and a smaller fitting for lighter models. The pitch control mechanism is gear driven and provides an angle-of-attack range of $-10°$ to $50°$ for the large fitting and $-10°$ to $40°$ for the smaller fitting. The elevation control mechanism is also gear driven and has a vertical range of 7.25 ft. Model yaw is provided by the use of the model cart yaw system as described previously. The vertical strut is designed for a 1200-lb model with the aerodynamic loads listed in chart B.

Model Support Cart 3

Model support cart 3 is shown in figure 42(a) and has an arc-sector model support (C-sting) with a pitch capability of -5 to $35°$, but it has no adjustable height capability. The C-sting was designed to position the model on the centerline of the tunnel for all pitch and yaw conditions. The design load for the cart is 17 000 lb in lift and 5000 lb in drag.

Chart B

Component	Load	
	Large fitting	Small fitting
Normal force, lb	±3 000	±1 000
Axial force, lb	±1 000	±500
Pitching moment, in-lb	±25 000	±15 000
Rolling moment, in-lb	±10 000	±5 000
Yawing moment, in-lb	±10 000	±5 000
Side force, lb	±1 000	±500

Model Support Cart 4

Model support cart 4 is a universal support system that utilizes a three-joint rotary sting (referred to as the $\alpha - \beta$ sting) as illustrated in figure 42(b). The vertical support mast is mounted in a structure supported by a tubular space frame in a manner similar to that used on carts 1 and 2. The design of cart 4 provides for a vertical mast translation of as much as 5.5 ft. The $\alpha - \beta$ sting, shown in more detail in figure 42(c), has an angle-of-attack range (α) from $-32°$ to $32°$ and an angle-of-sideslip range (β) from $-32°$ to $32°$. Any angle of attack and angle of sideslip within these ranges may be set while maintaining the

model location on the centerline of the tunnel. The straight air sting is shown attached at rotary sting joint 1 in figure 42(c). Model support cart 4 has the same load capacity as carts 1 and 2.

All model support carts, struts, and sting systems have a high-pressure air-supply capability or three-phase variable-frequency electric systems to provide power for propulsion system simulation on the models.

Model Propulsion Systems

The two primary means of providing for model-propulsion-system simulation in the 14- by 22-Foot Tunnel are by use of compressed air and electric motors. The compressed-air system is used for a wide range of applications to simulate direct jets, for powering air-driven turbine simulations, and for boundary-layer control, whereas the electric motors are used to supply power for propellers and rotors. The high-pressure compressed-air system is regulated from the tunnel control room and can supply from 0 to 4000 psi of air to the model. The maximum quantity of air available from the system is approximately 30.0 lbm/sec at 4000 psi. A central 4300-psia system receives high-pressure air from a primary source located at the Langley Research Center, and the air is then distributed to the control station in the test chamber and the model preparation area (MPA) . All models using the air-supply system must have high-pressure components designed and tested in accordance with references 9 and 10.

There are three variable-frequency electric supply systems available for use in the tunnel and in the MPA for electrically powered models. The largest of these systems, which is located in the test chamber beneath the tunnel test section, is a three-phase, 660-V, 210-A, variable-frequency (up to 440-Hz) generator rated at 240 kVA. This is the primary system used for electrically powered tests in the tunnel. The other two generators are 204-A, 150-kW, three-phase generators rated at 62.5 kVA with a frequency range from 10 to 400 Hz with a 200-hp limitation. These two generators are located in the building adjacent to the MPA. A feeder capable of transmitting the full output of both generators is provided from the generator to the test section and MPA.

Special Test Equipment

Special test equipment available for wind-tunnel investigations include the following: a moving-belt ground plane, a boundary-layer removal system, a laser velocimeter (LV) system, and several flow-visualization techniques.

Moving-Belt Ground Plane

The moving-belt ground plane provides a moving floor section that is 20 ft long and can provide a maximum ground speed of 120 ft/sec. This system contains a 14-ft wide continuous belt mounted on a cart that can be transported on transverse rollers as shown in figure 43. A typical test-section configuration using the moving-belt ground plane is shown in figure 6. The overall length of the belt is approximately 46 ft. It is made of 1/8-in-thick heat-woven wool (weighs 0.30 lb/ft^2) that has been treated to make it air impermeable. The life of the belt material has not yet been determined through wear; however, based on information from moving-belt systems in other tunnels, the running time expected from the belt would be approximately 1000 hr.

Boundary-Layer Removal System

The boundary-layer removal system is shown in figure 44 and consists of a blower and 900-hp drive motor, a suction plenum chamber, interconnecting ducts, and control valves. The system contains a centrifugal exhauster that is capable of moving 100 000 standard cubic feet per minute (scfm) and a butterfly-type airflow valve that is used to control the volume of air removed from the test section. The boundary layer entering the test section is removed from the floor by means of suction through a perforated plate that is 21 ft wide and 5.65 ft long. The location of the boundary-layer removal system in the test section is shown in figure 6. The boundary-layer removal system can be run regardless of the test-section configuration, and it is always used when the moving-belt ground plane is being used.

Laser Velocimeter System

A two-component laser velocimeter (LV) is available for making nonintrusive flow field velocity measurements. The LV system is operated in the backscatter mode and is normally configured to measure the longitudinal and vertical velocity components (ref. 11). The measurement sample volume is less than 0.39 in. long and is approximately 0.008 in. in diameter over the focal length of the system which is 9 to 25 ft. A 12-W argon-ion laser provides the light source and is typically operated at a 4-W output (in all lines) at the exit of the laser. The transmitting and receiving optics packages consist of two-component two-color units. The zoom lens system consists of a 3-in. clear-aperture negative lens and a 21-in. clear-aperture positive lens. The negative lens is computer controlled to provide the capability of positioning the sample volume laterally across the test section. In addition, the final folding mirror

can be panned and tilted, under computer control, to provide additional traversing capability. Bragg cells are incorporated in the system to alleviate directional ambiguity in each velocity component. A line diagram of the system is shown in figure 45(a), and a photograph of the system is presented in figure 45(b). This system is mounted on an x - y traversing rig shown in figure 45(c). The traversing rig can be operated either manually or under computer control with a positioning accuracy of ± 0.02 in. at a speed of 10 in/min. This rig provides an additional traversing capability of 7 ft vertical and ± 3 ft horizontal for the entire optics package. The traversing rig is mounted on wheels and can be moved to various positions along the test section. An isolated LV calibration room is located adjacent to the test chamber (fig. 2). This room enables calibration and preparation of the LV system to be conducted without interfering with normal tunnel operation. The operation of the LV is governed by the guidelines found in reference 12.

Flow Visualization

Several methods of flow visualization including simple yarn tufts, sublimating chemicals, liquid crystals, and fluorescent oil dyes are available for use at the tunnel. In addition, there are several smoke generators and smoke wands available for examining local flow characteristics as well as free-stream and wake characteristics. Sublimating chemical or liquid crystal techniques are available for investigations dealing with laminar-to-turbulent boundary-layer-transition phenomena. Fluorescent oil and minitufts illuminated with ultraviolet lights are routinely used for studying surface flow characteristics. In addition, smoke can be injected into the tunnel and the LV system can be configured to generate a light sheet that will illuminate a smoke screen for two-dimensional flow field analysis.

Data Acquisition System

Tests conducted in the 14- by 22-Foot Tunnel ordinarily fall into one of two categories: (1) static tests where time-averaged data are of primary concern, and (2) dynamic tests where time-dependent data are of primary concern. In both cases, the models are mounted rigidly in the tunnel by means of force balances and are restrained in all directions of motion. Tests of airplane configurations, wing sections, and various forms of bodies generally tend to be conducted as static tests. However, tests of powered helicopter models, rotors, and propellers tend primarily to be conducted as dynamic tests, and data are sampled continuously with respect to some reference time signal. Two separate data systems are used for the two types of tests: they may be operated as independent stand-alone systems, or they may be linked together to acquire data simultaneously against a governing reference signal.

Steady-State Data

The static-test data acquisition system is based on two ModComp Classic computers and is designed to acquire steady-state force and pressure data from models located either in the test section or in any of five test sites in the MPA. Either computer system can be used to support data acquisition during tunnel operation or model buildup and checkout in the MPA. This capability is accomplished through the use of several patch racks located in the tunnel control room.

The system can provide up to 50 V of direct-current excitation for the instrumentation channels, and it accepts analog, digital, and frequency inputs. Each computer is capable of acquiring data from 96 analog channels and 16 digital channels. The digital interface can be chained across computers to provide up to 32 digital channels on one system. The frequency input is acquired using digital channels. The lowest analog input range is -12.5 to 12.5 mV and the highest range is -10 to 10 V full scale. The digital inputs may be either five-digit 20-bit binary or six-digit binary-coded decimal.

Model instrumentation is connected to the data acquisition system via model interface (MIF) consoles. Each MIF console has the capability of 48 analog channels and 8 digital channels. The MIF consoles contain the excitation voltage sources for model instrumentation, tachometer interface for acquiring frequency inputs, and a thermocouple reference point. Also included are patching panels for auxiliary and video inputs.

Dynamic Data

Two frequency-modulator (FM) tape recorders are available for recording unsteady signals; the first of these is a basic 14-track tape recorder and the other is a computer-controlled, 28-track tape recorder with a Hewlett-Packard (HP) 1000 computer system as controller.

The HP-1000 computer also controls a Macrodyne 10-channel, analog-to-digital conversion unit that is capable of digitizing previously recorded analog data at speeds up to 100 000 samples per second. These digitized data are then stored on tape for further analysis.

Instrumentation

A collection of commonly used instrumentation is maintained at the facility and is available to users

upon request. This instrumentation consists primarily of various strain gauge balances, both differential and absolute pressure transducers, and accelerometers. In general, instrumentation that is unique to special user requirements will have to be supplied by the user unless it is provided through a special agreement with NASA.

Wiring Description

Instrumentation wiring is normally routed from the model through the model support system to a model interface (MIF) console located beneath the test section. The MIF console provides interface circuits for all data channels available on the data acquisition system, and auxiliary connections are available to support up to 1024 pressure measurements using the electronically scanned pressure (ESP) system or 2820 pressure measurements using scanivalve systems.

The thermocouples used in the 14- by 22-Foot Tunnel are iron-constantan, and a 32°F reference junction is provided in the MIF console.

The model instrumentation leads are normally installed in the model preparation area using user-supplied wiring with Government-furnished plugs for the wiring connection to the MIF console.

The facility has several identical MIF consoles to support model buildup and testing. Normally one MIF console is required per model setup. The MIF console allows functional checks and calibration of model instrumentation prior to tunnel entry. After model buildup and checkout in the MPA, the entire model assembly, including MIF console, is moved into the tunnel for testing.

Pressure Measurements

Multiple pressure measurements in the 14- by 22-Foot Tunnel utilize either the electronically scanned pressure (ESP) system or the scanivalve measuring system. The scanivalve control system is conventional and can operate 10 steppers. Each stepper can operate six 48-port scanivalve heads for a total of 2820 pressures with a reference pressure for each head.

The ESP system consists of a data acquisition and calibration unit, a pressure control unit, and up to 16 pressure-measuring modules having 32 ports each. The ESP system is designed to permit simultaneous measurement of up to 512 model pressures. A second ESP system provides an additional 512 pressures for a total of 1024 pressures. The ESP modules are normally mounted inside the model for best results. The nominal size of a current ESP module is 1.0 in. by 2.2 in. by 1.18 in., not including the pressure tubing. Specific application of ESP modules to a given model will need to account for physical arrangement, thermal protection, and possible variations in geometry of advanced ESP modules. Additional pressure measurements may be made with individual pressure transducers as test conditions may require.

Force Measurements

Model force and moment measurements are made with a sting-mounted, six-component strain gauge balance (accuracy within ±0.5 percent of full scale). A list of the balances available at the NASA Langley Research Center is available on request. For each balance the listing provides a brief dimensional description and the design load range for each of the components measured by the balance. The use of Langley balances is preferred and the selection should be made early in the test planning. The 708 and 729 are typical balances used in the 14- by 22-Foot Tunnel. Drawings of these two balances are shown in figure 46. These balances along with the others normally used in this tunnel are listed in table 6. All balances listed in table 6 are secured to the model support system by means of a tapered plug, anti-rotation key, and locking nut. Model requirements may sometimes require that a tapered socket be included as a part of the model (for example, an empennage assembly mounted to a fuselage by means of a balance). Taper gauges are available to ensure a precise fit of the balance in the tapered socket. Force balances supplied by users must meet rigid design requirements and be available for bench calibration at least 3 months prior to test entry.

In general, models shall be designed according to the requirements of reference 9. A model systems report is required for all model systems to be tested in the 14- by 22-Foot Tunnel. This report must be submitted to the Facility Safety Head at least 8 weeks prior to tunnel entry. The report will contain, as a minimum, as-built drawings of configurations to be tested, design conditions and loads, stress and stability reports, and required inspection and quality assurance reports. Delivery of the complete model system is required at least 6 weeks prior to tunnel entry. Some complex models may require additional setup time, and thus an earlier delivery date may be desirable. Model delivery and setup should be coordinated with the Tunnel Operations Engineer.

Data Processing

Pretest Information

Prior to the setup and checkout of a model in the model preparation area, certain information must be

provided to the Tunnel Operations Engineer. This should include a description of the model, its capabilities, the required instrumentation, special data acquisition and reduction needs, and a tentative test program. This information is used to schedule the use of various pieces of hardware as well as to provide inputs to the standard data acquisition and reduction software. As far as is practical prior to tunnel entry, any special data acquisition or reduction requirements must be identified and defined by the user to be incorporated into the system for checkout.

Once a model has been installed in the model preparation area, standard software is used to verify the integrity of the strain gauge balance and other model instrumentation. The software will also acquire the data needed to calibrate the model instrumentation and will provide appropriate sensitivity constants through specialized calibration algorithms. The standard data reduction software is then used to check the instrumentation for problems such as leaks in pressure measurement systems, balance-to-ground interference, and thermocouple ground loops.

On-Line Data Processing

On-line data processing programs provide the test engineer with information needed to direct the research investigation. The data are reduced to coefficient form for real-time graphic display or near-real-time tabular display on a line printer.

Final Data Processing

Final data processing is conducted off-line on a time-available basis. The data reduction program and graphic display programs provide the same capabilities that the real-time programs provide. The data may be copied to magnetic tape using a standard interface format for transmittal to remote computers.

User Cost

It is not normal practice to charge for tests that are of mutual interest to both the user and the U.S. Government. The data resulting from such a mutually beneficial test program reside in the public domain and will normally be analyzed and reported by Government researchers as formal NASA publications. It is recognized, however, that the unique features of the 14- by 22-Foot Tunnel may make it the only facility available for tests in which a potential user may have a proprietary concern that would be compromised by the general publication of results. The procedure to be used for access to the 14- by 22-Foot Tunnel is delineated in reference 13 (which can be obtained from Langley along with refs. 9, 10, and 12). Fees for the wind-tunnel tests are decided on a case-by-case basis by Langley management provided there is, in the opinion of the NASA Langley Technical Management, adequate justification for conducting such tests. Detailed cost information may be obtained from the Subsonic Aerodynamics Branch Head at the Langley Research Center by writing to:

NASA Langley Research Center
Head, Subsonic Aerodynamics Branch
Mail Stop 286
Hampton, VA 23665-5225

The initial contact for the 14- by 22-Foot Tunnel is the Subsonic Aerodynamics Branch Head. If the proposed test is feasible, a meeting is scheduled to establish a mutually acceptable plan as to how the program should proceed.

NASA Langley Research Center
Hampton, VA 23665-5225
July 11, 1990

References

1. Applin, Zachary T.: *Flow Improvements in the Circuit of the Langley 4- by 7-Meter Tunnel.* NASA TM-85662, 1983.
2. Sellers, William L., III; Applin, Zachary T.; Molloy, John K.; and Gentry, Garl L., Jr.: *Effect of Jet Exit Vanes on Flow Pulsations in an Open-Jet Wind Tunnel.* NASA TM-86299, 1985.
3. Applin, Zachary T.: *Modification to the NASA Langley 4- by 7-Meter Tunnel for Improved Rotorcraft Aerodynamics and Acoustics.* NASA paper presented at the American Helicopter Society National Specialist Meeting on Helicopter Testing Technology (Williamsburg, Virginia), Oct. 29—Nov. 1, 1984.
4. Wright, Ray H.: *Test Sections for Small Theoretical Wind-Tunnel-Boundary Interference on V/STOL Model.* NASA TR R-286, 1968.
5. Grunwald, Kalman J.: *Experimental Investigation of the Use of Slotted Test-Section Walls to Reduce Wall Interference for High-Lift-Model Testing.* NASA TN D-6292, 1971.
6. Heyson, Harry H.: *Theoretical Study of the Use of Variable Geometry in the Design of Minimal-Correction V/STOL Wind Tunnels.* NASA TR R-318, 1969.
7. Pope, Alan; and Harper, John J.: *Low-Speed Wind Tunnel Testing.* John Wiley & Sons, Inc., c.1966.
8. Ferguson, D. R.; and Keith, J. S.: *Modifications to the Streamtube Curvature Program. Volume I—Program Modifications and User's Manual.* NASA CR-132705, 1975.
9. *Wind-Tunnel Model Systems Criteria,* LHB 1710.15, NASA Langley Research Center, Aug. 1986.
10. *Safety Regulations Covering Pressurized Systems.* LHB 1710.40, NASA Langley Research Center, Nov. 1988.

11. Sellers, William L.; and Elliott, Joe W.: Applications of a Laser Velocimeter in the Langley 4- by 7-Meter Tunnel. *Flow Visualization and Laser Velocimetry for Wind Tunnels.* William W. Hunter, Jr., and Jerome T. Foughner, Jr., editors, NASA CP-2243, 1982, pp. 283–293.
12. *Nonionizing Radiation*, LHB 1710.8, NASA Langley Research Center, Sept. 1982.
13. *Development Work for Industry in NASA Wind Tunnels.* NMI 1300.1A, NASA Langley Research Center, Sept. 1986.

Table 1. Cross-Sectional Area of Closed Test-Section Tunnel

Component	Inlet area, ft^2	Outlet area, ft^2	Area ratio (outlet/inlet)	Length, ft
Contraction	2835.75	315.38	8.99	60.00
Test section	315.38	318.70	1.01	50.00
First diffuser[a]	318.70	850.50	2.67	142.50
Second diffuser	850.50	929.25	1.09	20.66
Third diffuser	929.25	1244.40	1.34	54.33
Fourth diffuser	1243.10	2835.75	2.28	170.00
Fan section	1244.40	1243.10	1.00	45.50
Return duct[b]	2835.75	2835.75	1.00	148.00

[a]For open test section, the first diffuser is shortened by 18 ft. [b]Return duct is between the fourth diffuser and the contraction.

Table 2. Coordinate Parameters for First Diffuser

x, ft	h, ft	w, ft	Area, ft^2	θ_h, deg	θ_w, deg
49.92	14.500	21.979	318.70		
				0	6.78
67.67	14.500	24.083	349.21		
				4.84	2.57
111.26	18.188	26.042	473.63		
				4.84	2.57
115.00	18.500	26.209	473.63		
				4.84	2.57
126.00	20.135	27.375	551.21		
				5.91	3.55
192.50	27.000	31.500	850.50		

Table 3. Coordinate Parameters for Contraction Section

x, ft	$h/2$, ft	$w/2$, ft	Area, ft^2	2θ, deg
−60	24.875	28.500	2835.750	−5.524
−59	24.883	28.458	2826.861	−20.572
−58	24.672	28.297	2792.548	−30.937
−57	24.427	28.052	2740.922	−47.103
−56	24.042	27.667	2660.611	−57.955
−55	23.552	27.177	2560.308	−63.784
−54	23.000	26.625	2449.500	−63.318
−53	22.458	26.083	2343.153	−63.362
−52	21.911	25.536	2238.164	−63.813
−51	21.365	24.990	2135.568	−63.780
−50	20.813	24.438	2034.422	−62.892
−49	20.271	23.896	1937.554	−64.226
−48	19.719	23.344	1841.238	−61.966
−47	19.188	22.813	1750.859	−64.364
−46	18.630	22.255	1658.477	−63.358
−45	18.089	21.714	1571.065	−63.414
−44	17.542	21.167	1485.194	−62.957
−43	17.000	20.625	1402.500	−63.848
−42	16.453	20.078	1321.392	−63.011
−41	15.359	18.984	1166.353	−64.350
−40	15.359	18.984	1166.353	−63.496
−39	14.813	18.438	1092.422	−57.258
−38	14.271	17.896	1021.554	−64.393
−37	13.719	17.344	951.738	−62.658
−36	13.181	16.807	886.234	−63.988
−35	12.630	16.255	821.227	−63.609
−34	12.089	15.714	759.815	−57.258
−33	11.609	15.234	707.446	−53.278
−32	11.167	14.792	660.694	−50.735
−31	10.750	14.375	618.125	−46.170
−30	10.375	14.000	581.000	−40.860
−29	10.052	13.677	549.933	−35.900
−28	9.766	13.391	523.071	−31.874
−27	9.516	13.141	500.165	−29.556
−26	9.286	12.911	479.607	−25.775
−25	9.089	12.714	462.190	−23.919
−24	8.901	12.526	445.979	−22.547
−23	8.729	12.354	431.366	−20.791
−22	8.568	12.193	417.854	−19.563
−21	8.417	12.042	405.403	−17.703
−20	8.281	11.906	394.395	−16.206
−19	8.156	11.781	384.363	−16.672

Table 3. Concluded

x, ft	$h/2$, ft	$w/2$, ft	Area, ft^2	2θ, deg
−18	8.036	11.661	374.867	−13.099
−17	7.938	11.563	367.109	−13.104
−16	7.839	11.464	359.430	−9.974
−15	7.760	11.385	353.422	−9.729
−14	7.688	11.313	347.859	−7.889
−13	7.625	11.250	343.125	−7.899
−12	7.568	11.193	338.813	−6.579
−11	7.516	11.141	334.915	−6.580
−10	7.469	11.094	331.426	−5.264
−9	7.427	11.052	328.339	−4.752
−8	7.391	11.016	325.649	−4.484
−7	7.359	10.984	323.353	−3.961
−6	7.328	10.953	321.063	−2.637
−5	7.307	10.932	319.542	−2.624
−4	7.286	10.911	318.024	−2.122
−3	7.271	10.896	316.887	−1.308
−2	7.260	10.885	316.131	−.537
−1	7.255	10.880	315.753	−1.055
0	7.250	10.875	315.375	0.000

Table 4. Turning Vanes in the 14- by 22-Foot Subsonic Tunnel

Turning vanes	Number of vanes	Vane spacing, in.	Porosity, percent
First corner	53	9.563	97.4
Second corner	53	9.563	97.4
Third corner	98	7.125	96.5
Fourth corner	202	3.000	91.7

Table 5. Boundary-Layer Rake Coordinate

Total pressure tube	z, in	Total pressure tube	z, in.
1	0.50	34	9.00
2	.75	35	9.25
3	1.00	36	9.50
4	1.25	37	9.75
5	1.50	38	10.00
6	1.75	39	10.50
7	2.00	40	11.00
8	2.25	41	11.50
9	2.50	42	12.00
10	2.75	43	12.50
11	3.00	44	13.00
12	3.25	45	13.50
13	3.50	46	14.00
14	3.75	47	14.50
15	4.00	48	15.50
16	4.25	49	16.00
17	4.50	50	16.50
18	4.75	51	17.00
19	5.25	52	17.50
20	5.50	53	18.00
21	5.75	54	18.50
22	6.00	55	19.00
23	6.25	56	19.50
24	6.50	57	20.00
25	6.75	58	21.00
26	7.00	59	22.00
27	7.25	60	23.00
28	7.50	61	24.00
29	7.75	62	26.00
30	8.00	63	27.00
31	8.25	64	28.00
32	8.50	65	29.00
33	8.75	66	30.00

Table 6. Balances Frequently Used in the 14- by 22-Foot Subsonic Tunnel

Balances	Normal force, lb	Axial force, lb	Pitching moment, in-lb	Rolling moment, in-lb	Yawing moment, in-lb	Side force, lb
708 types						
716	500	100	3000	1000	1000	300
708C	1200	125	2000	1000	2000	500
1613B	1200	450	2000	1000	2000	500
729 types						
729	2500	300	3500	2000	2000	500
748	1800	500	7000	4000	3000	1000
750	1000	500	4000	3000	3000	500

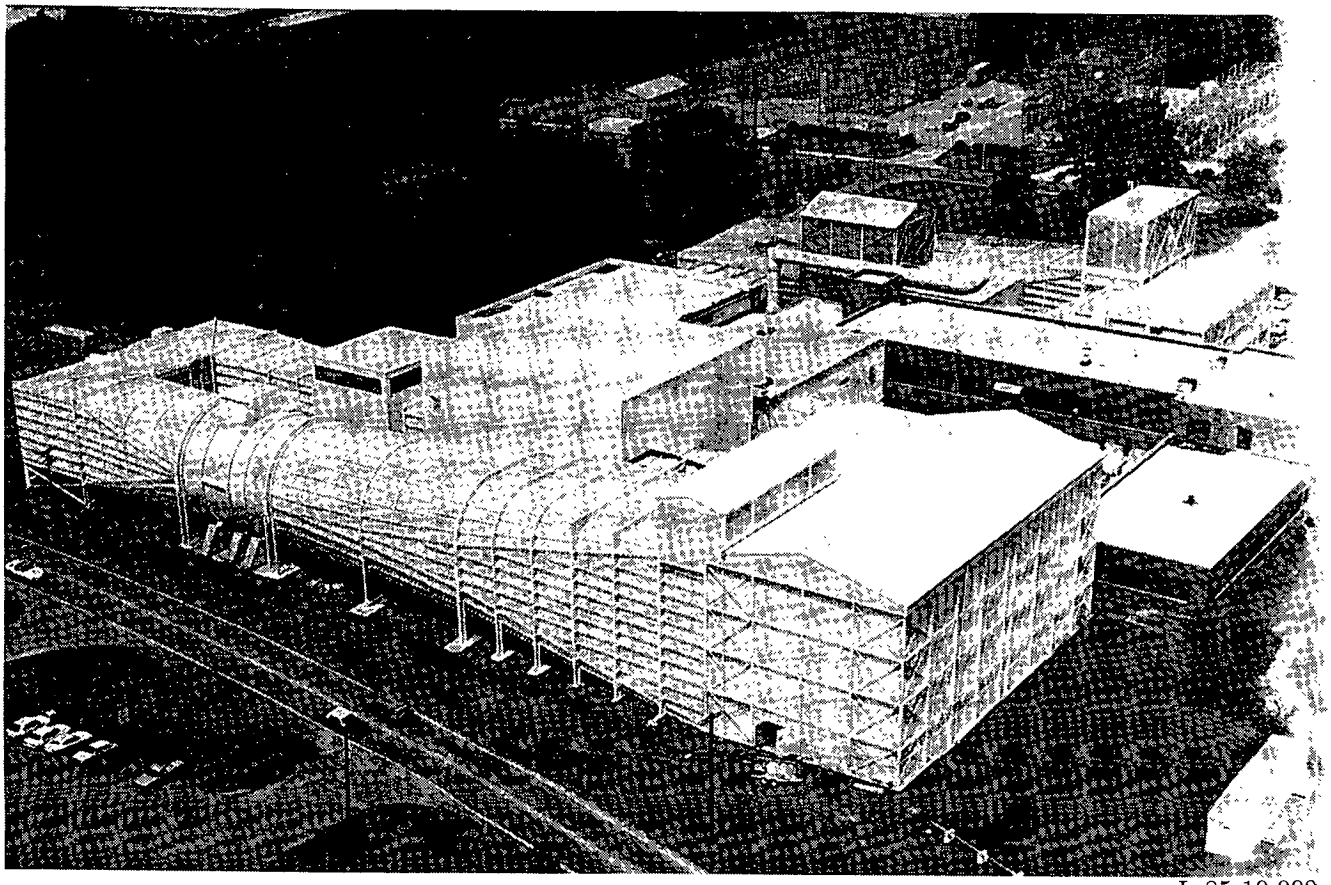

L-85-10,002

Figure 1. Aerial view of the Langley 14- by 22-Foot Subsonic Tunnel.

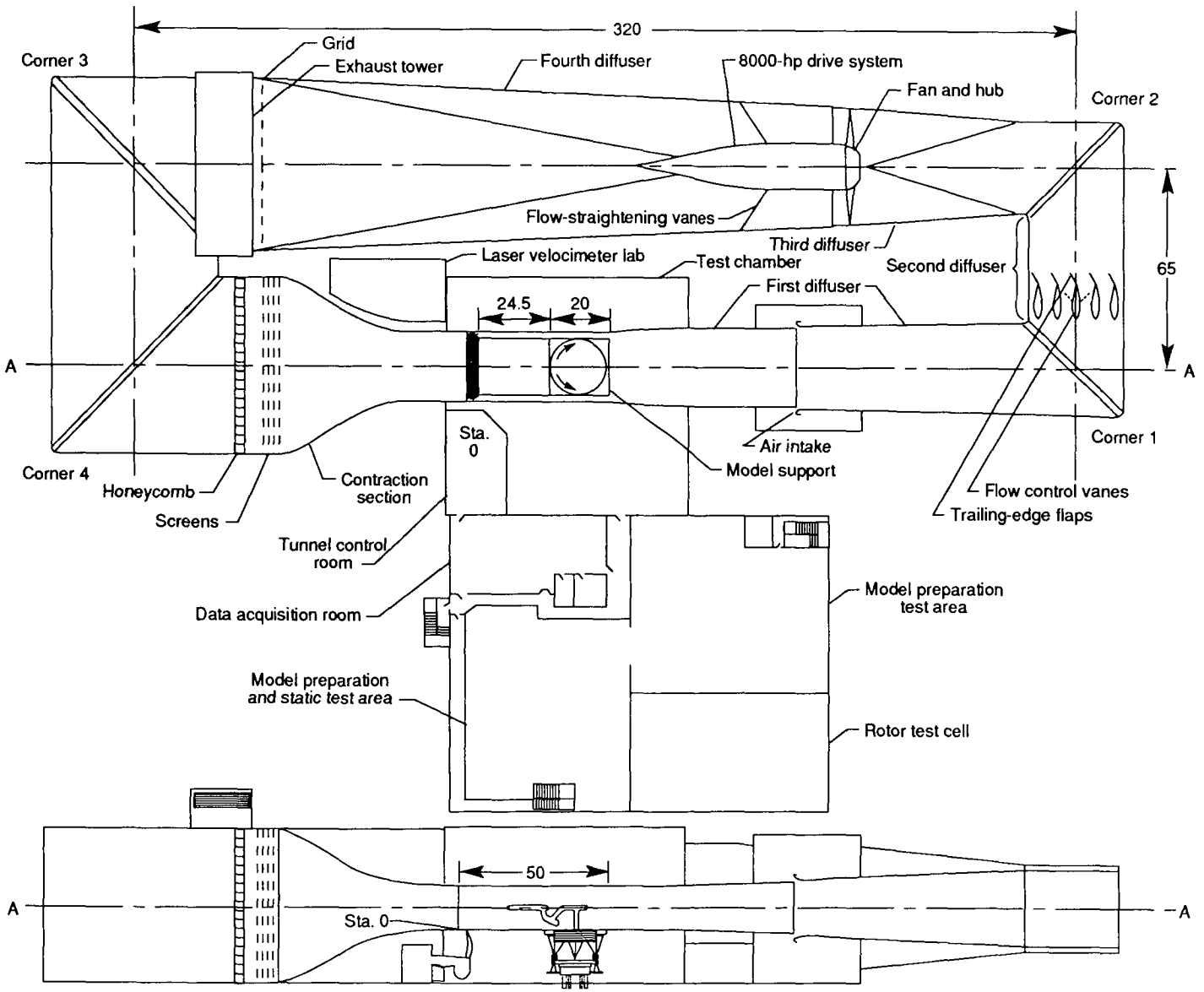

Figure 2. Schematic of the 14- by 22-Foot Tunnel and component sections. All dimensions are given in feet.

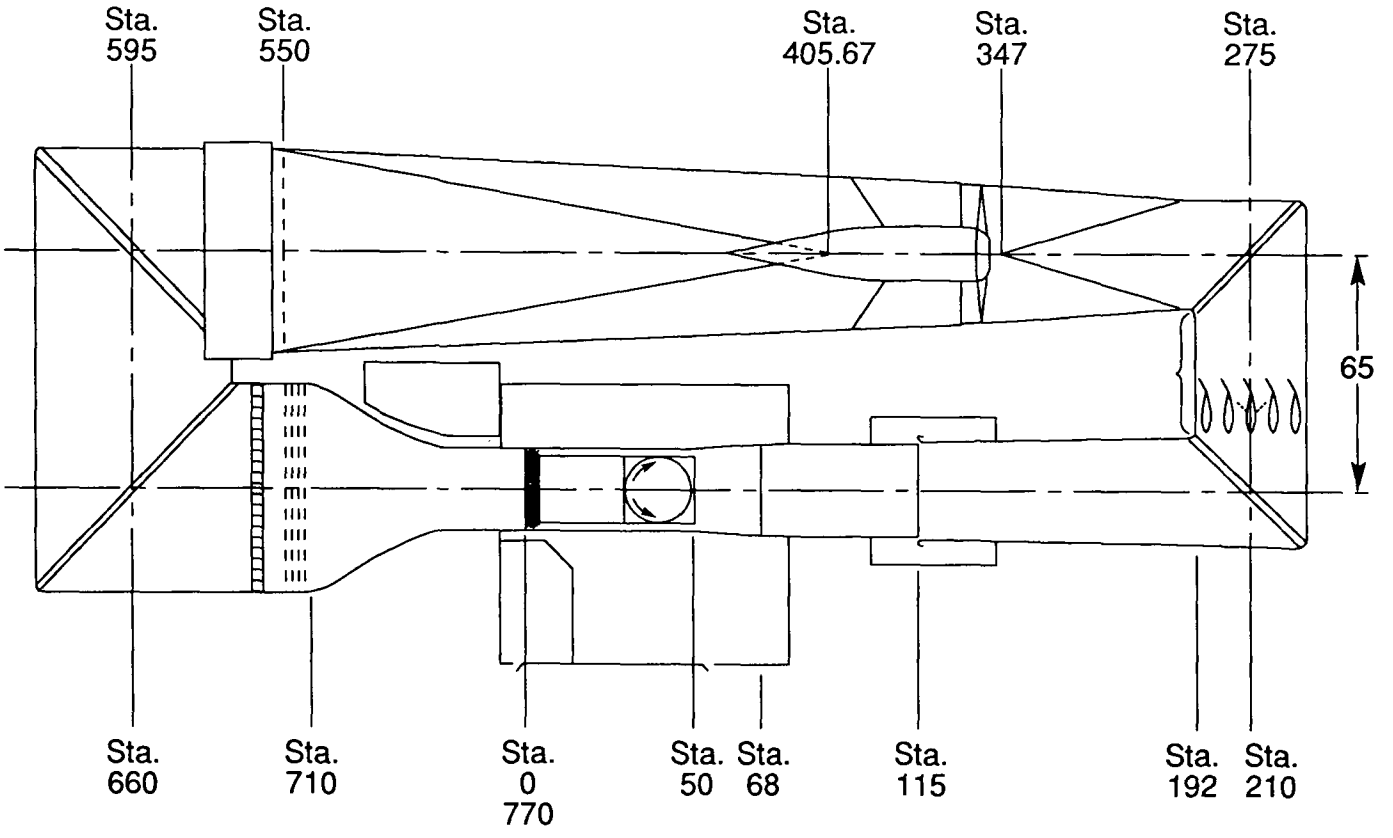

Figure 3. Plan view of the 14- by 22-Foot Tunnel showing locations of major component sections. All dimensions are given in feet.

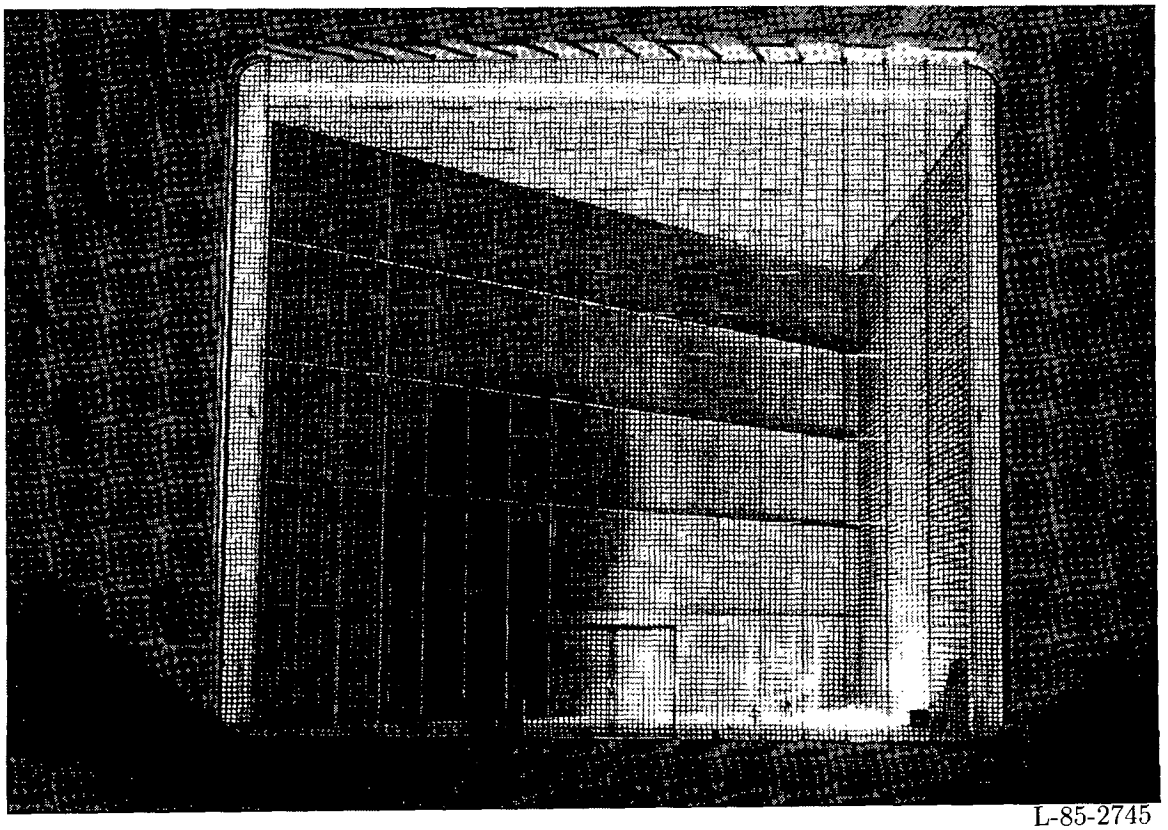

Figure 4. Photograph of square-mesh grid located at end of fourth diffuser.

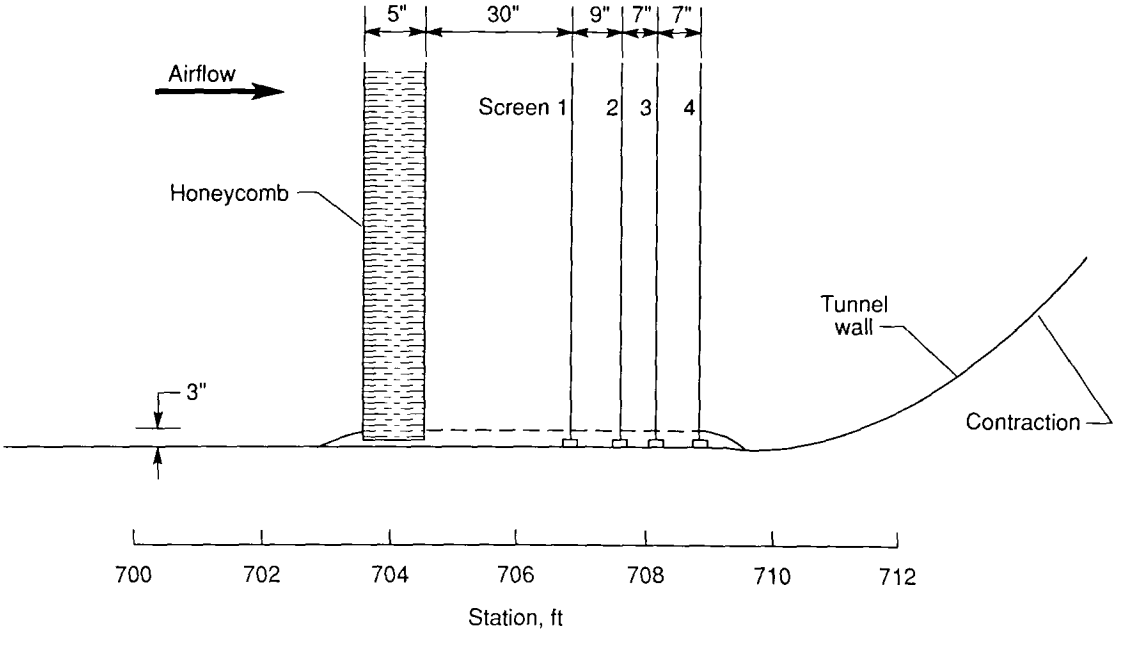

Figure 5. Sketch of honeycomb and antiturbulence screen in settling chamber.

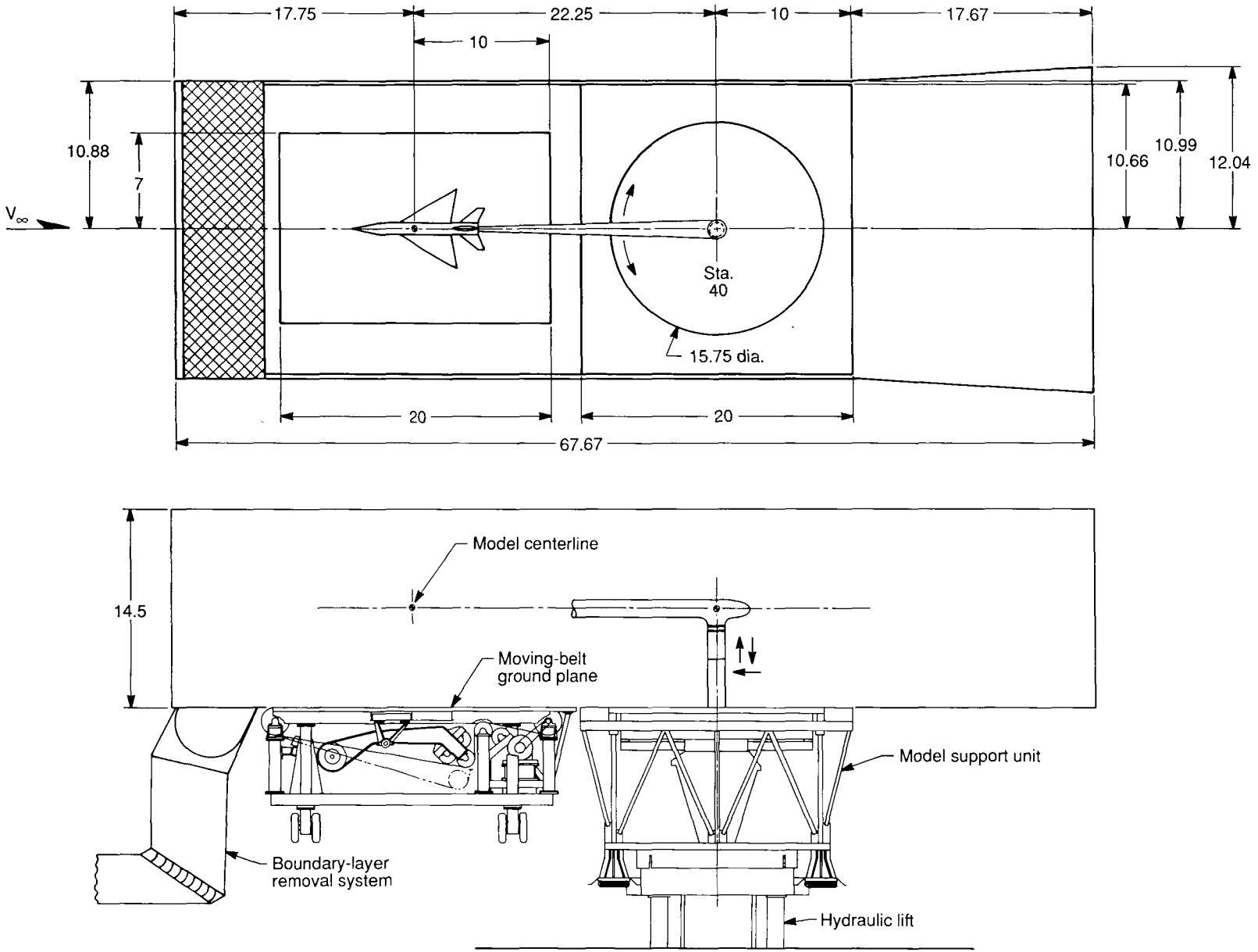

Figure 6. Closed test-section configuration. Dimensions are given in feet.

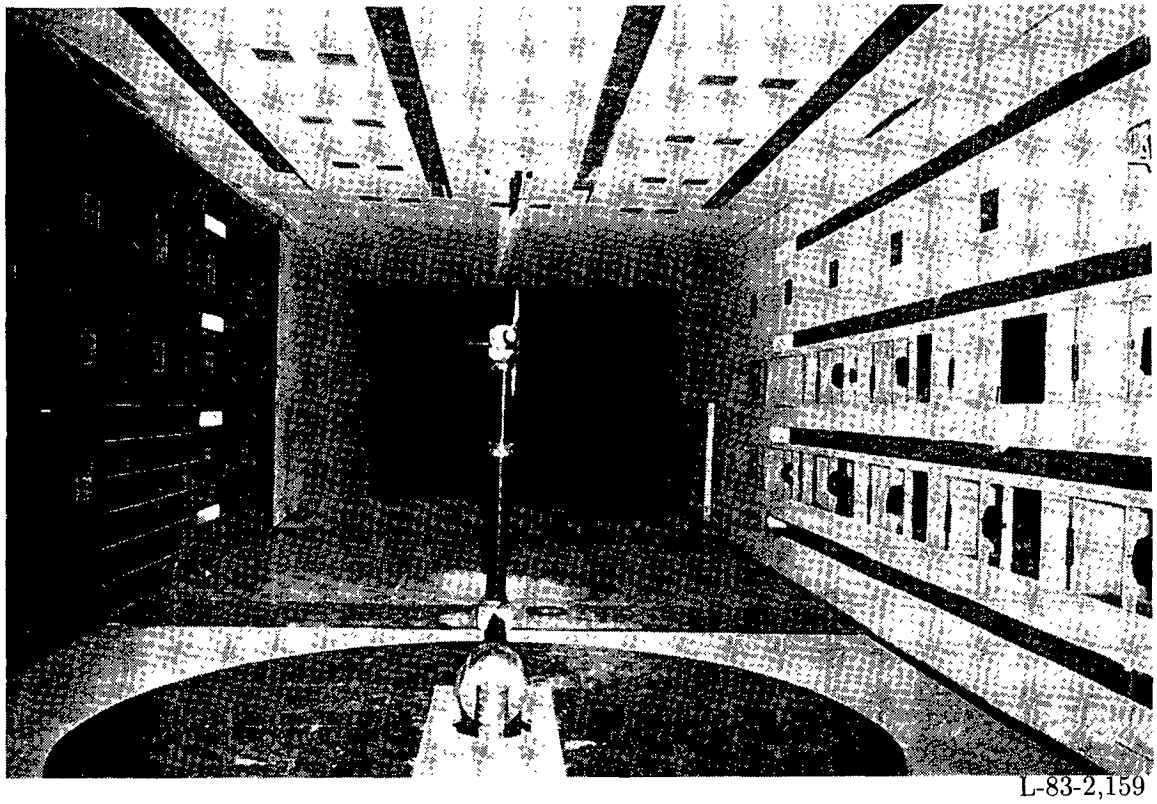

Figure 7. Photograph of closed test section showing longitudinal slots in wall and ceiling.

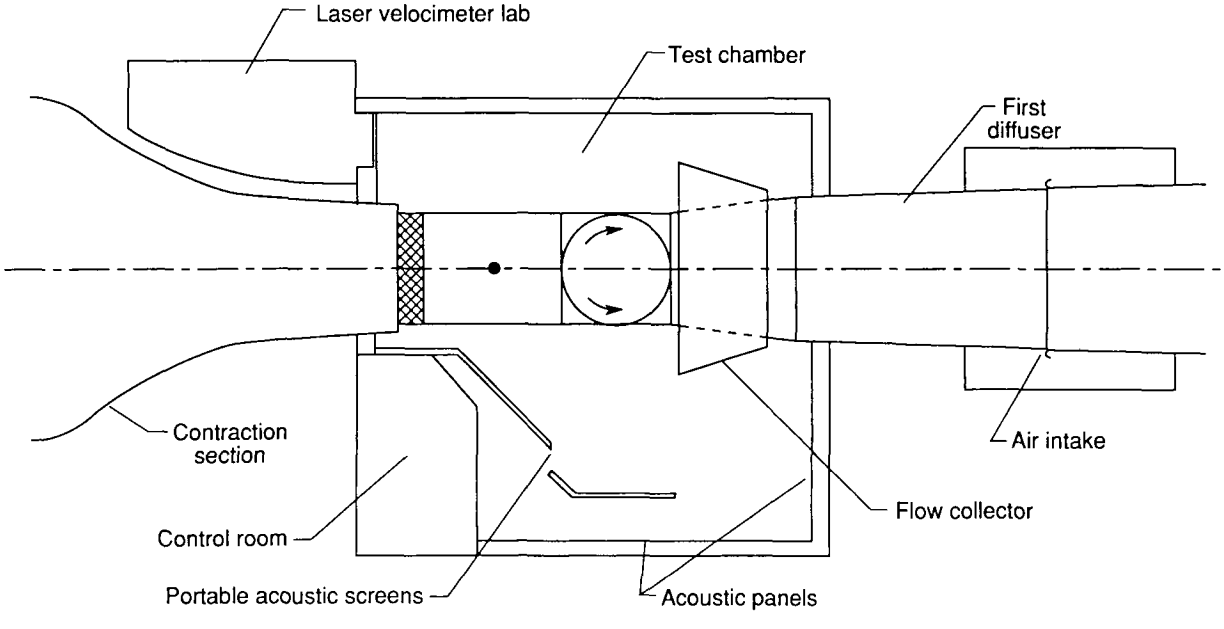

Figure 8. Sketch of open test-section configuration.

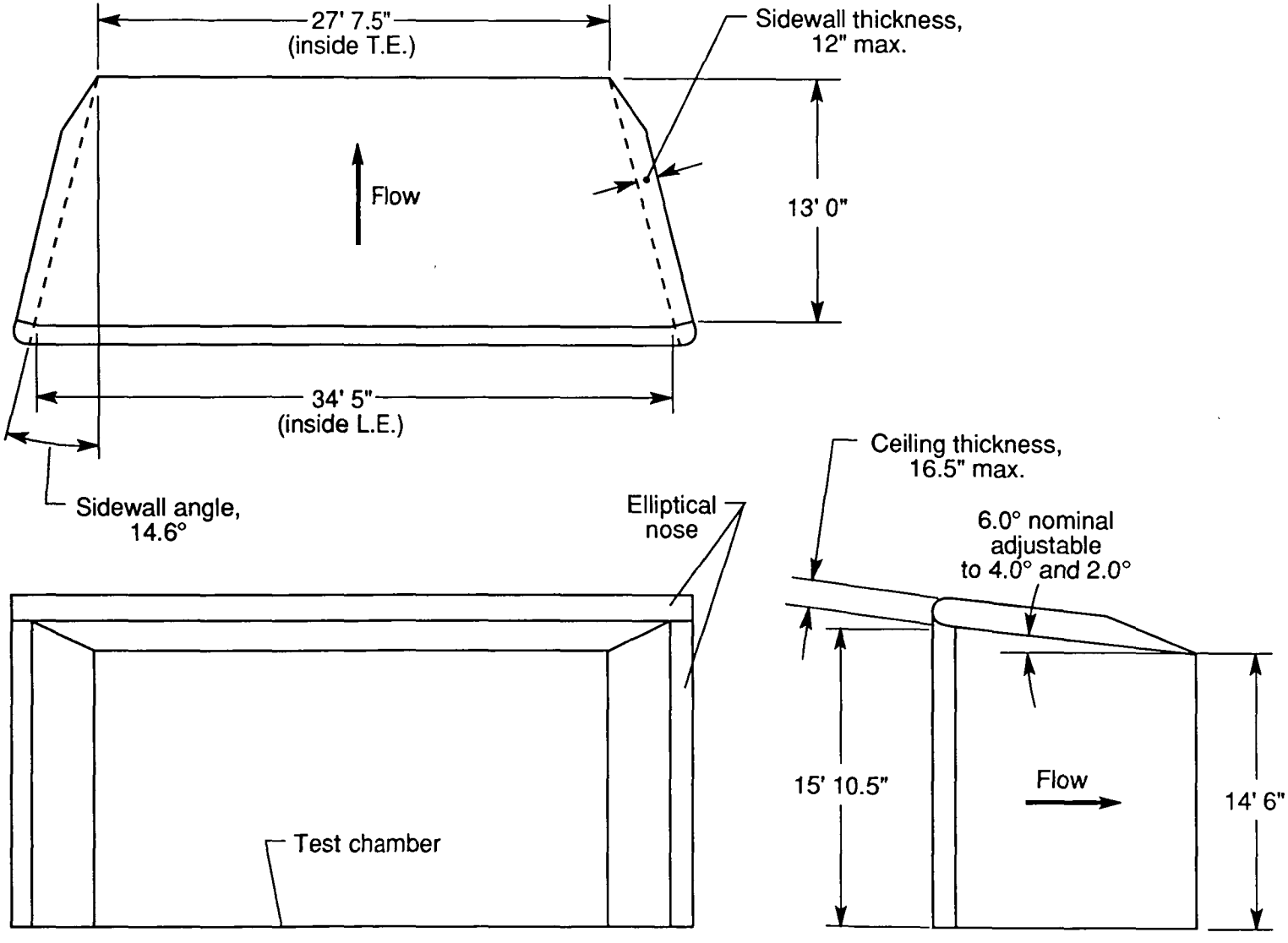

(a) Sketch of flow collector.

Figure 9. Flow collector used in open test-section configuration.

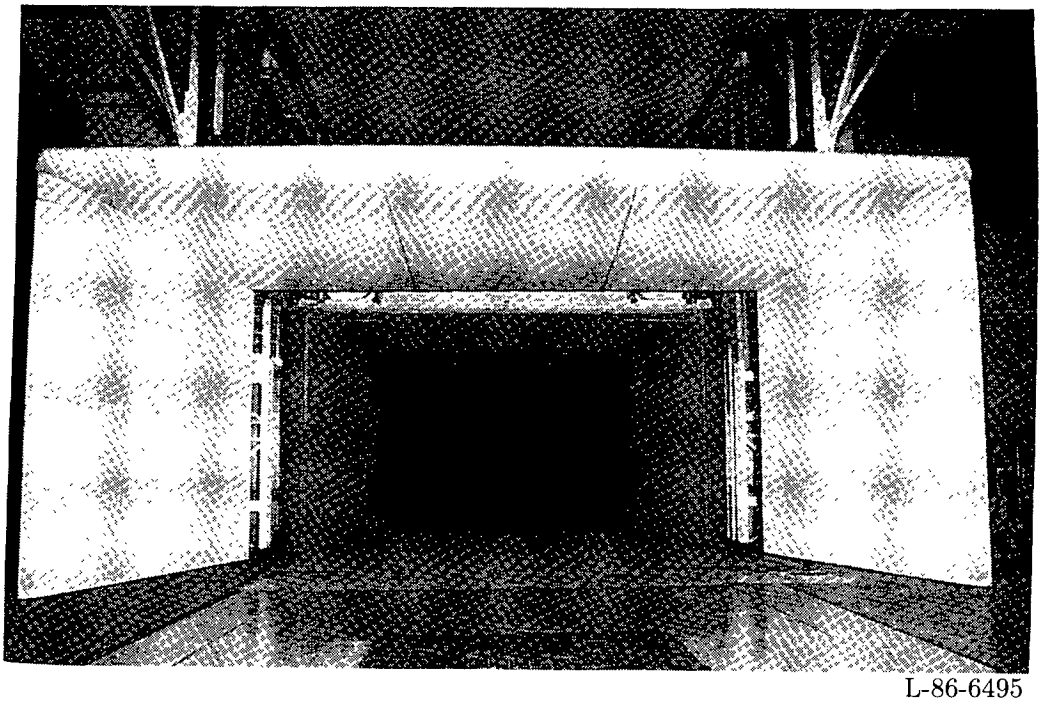

L-86-6495

(b) Photograph of flow collector.

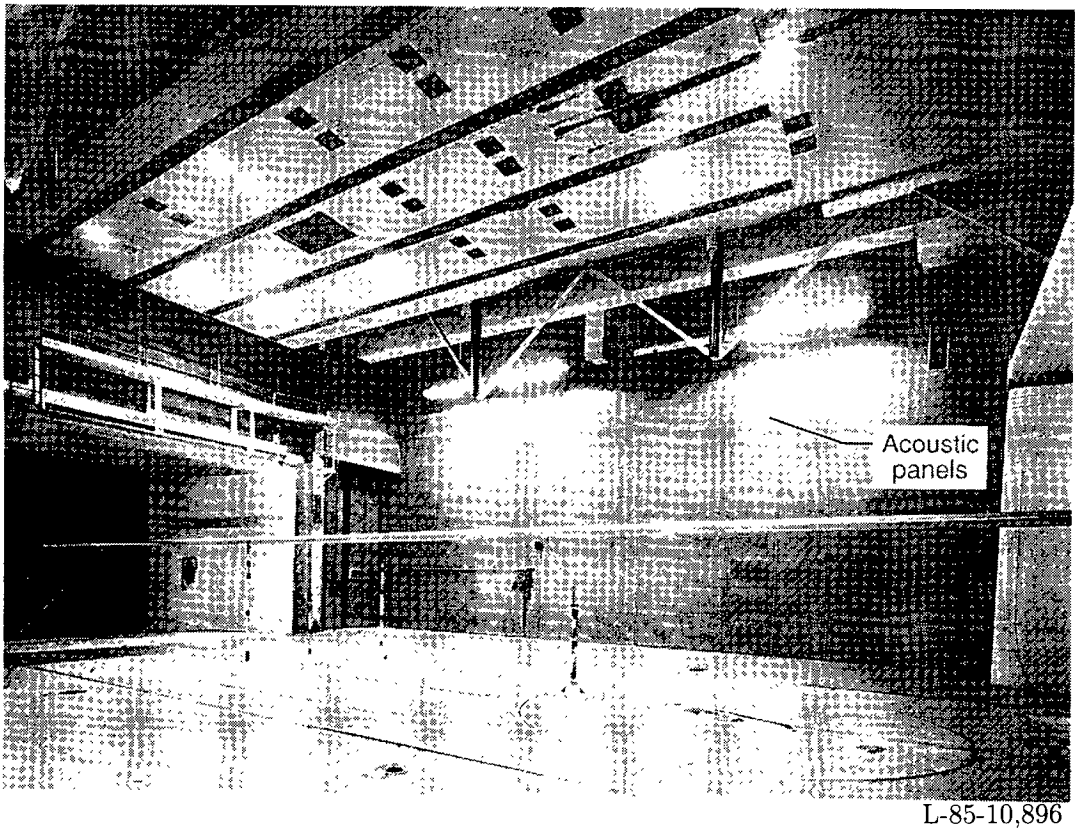

L-85-10,896

(c) Photograph of acoustic panels.

Figure 9. Concluded.

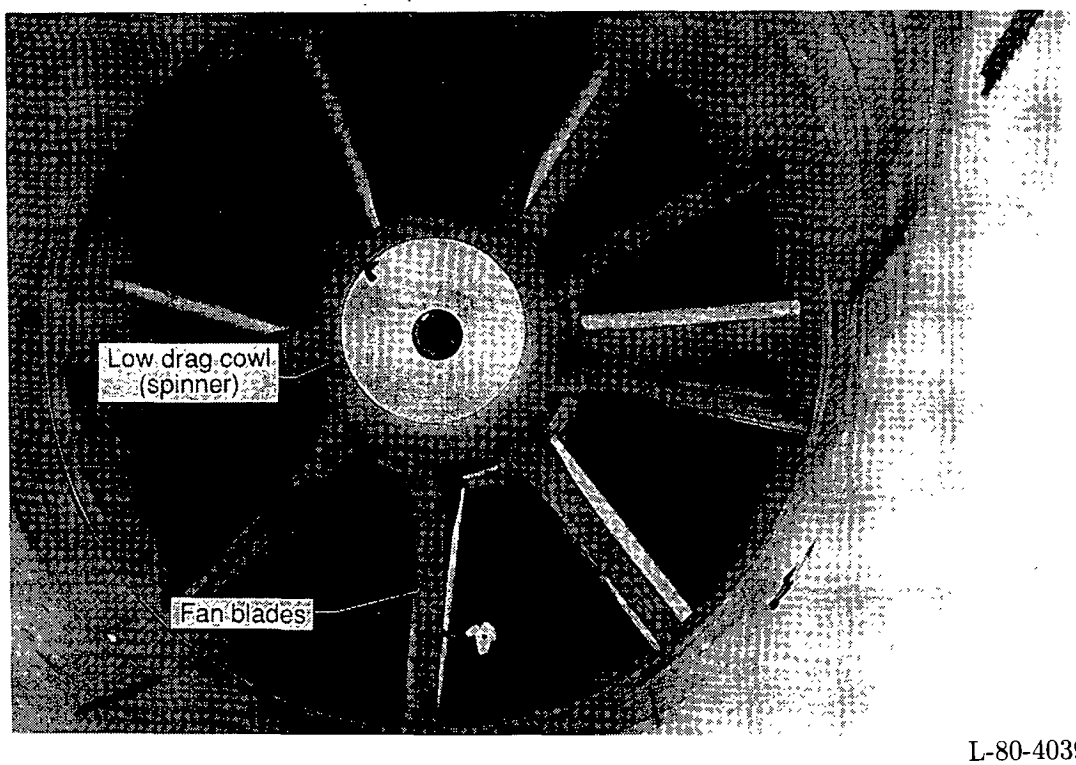

L-80-4039

(a) Upstream view of fan blade assembly.

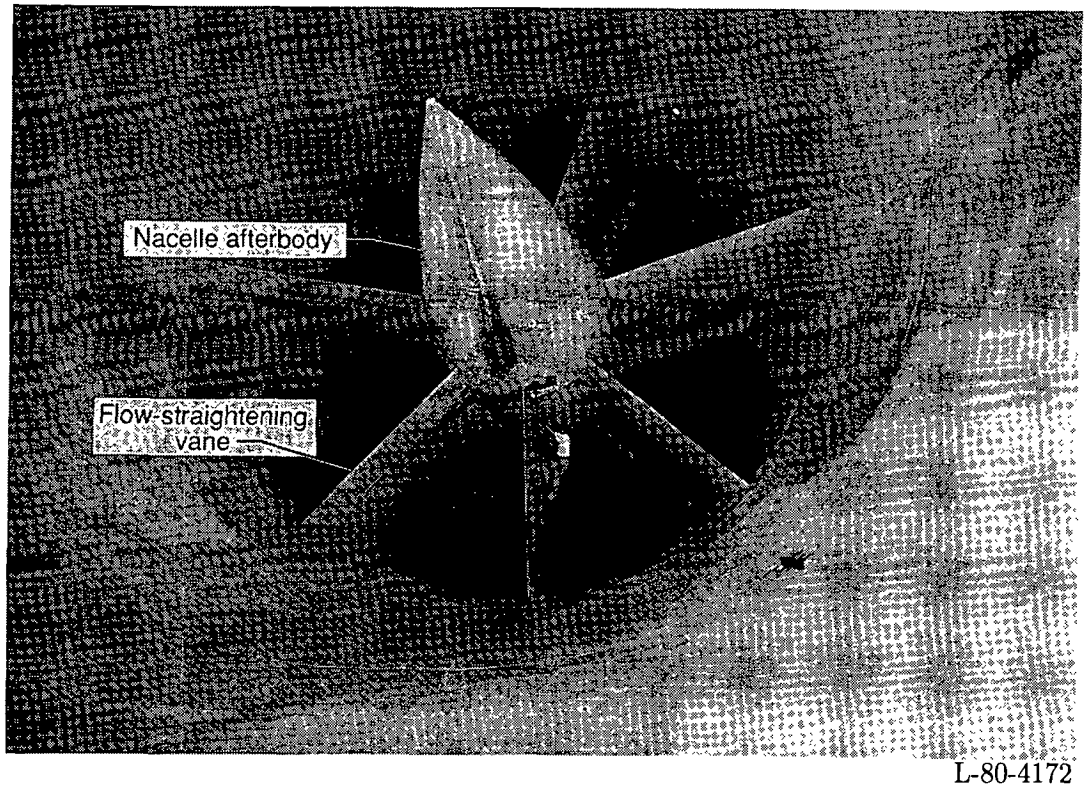

L-80-4172

(b) Nacelle.

Figure 10. Photographs of fan and nacelle assembly.

L-86-6497

Figure 11. Photograph of current control room in the 14- by 22-Foot Tunnel.

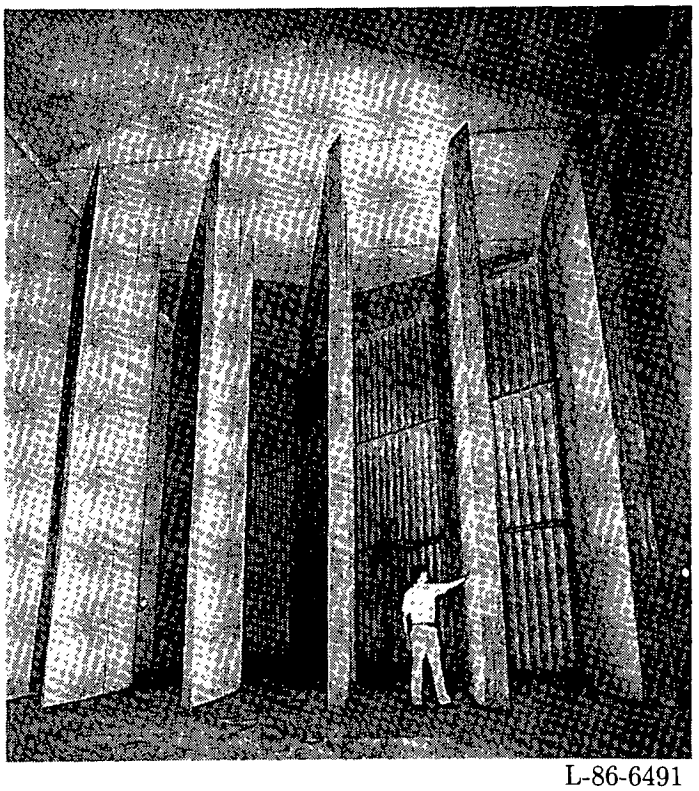

L-86-6491

(a) Vanes in open position.

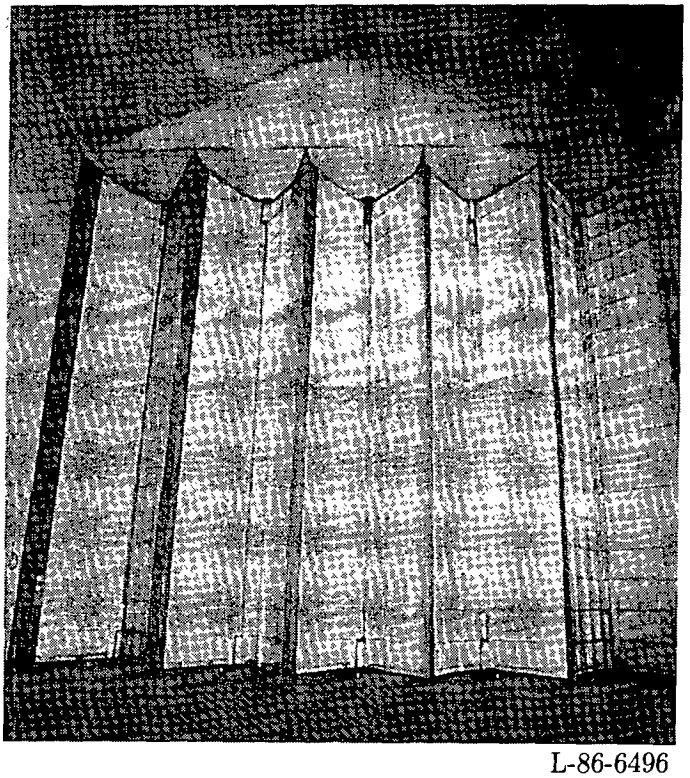

L-86-6496

(b) Vanes in closed position.

Figure 12. Photographs of flow-control vanes with added flap system and sketch of airfoil shape.

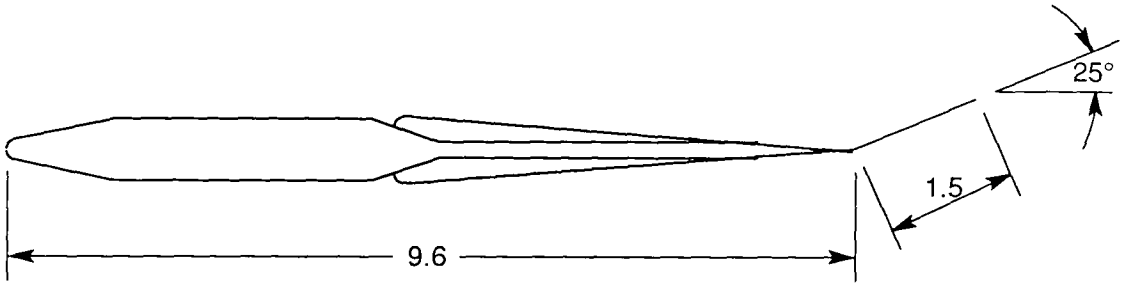

(c) Sketch of vane airfoil section in open position. Linear dimensions are given in feet.

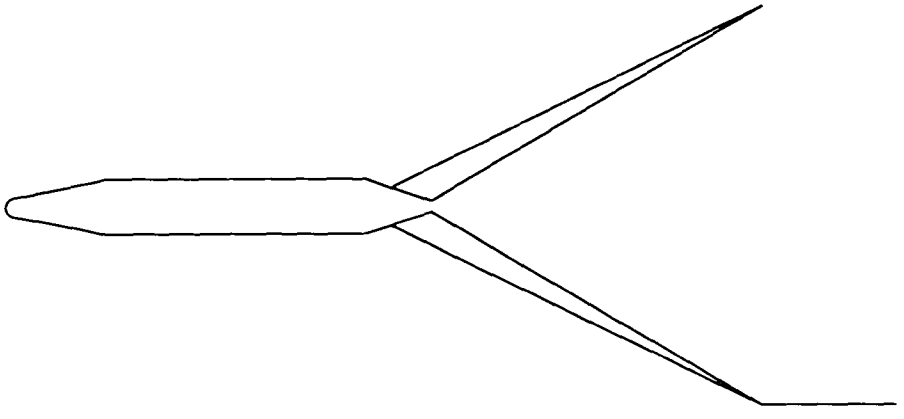

(d) Sketch of vane in closed position.

Figure 12. Concluded.

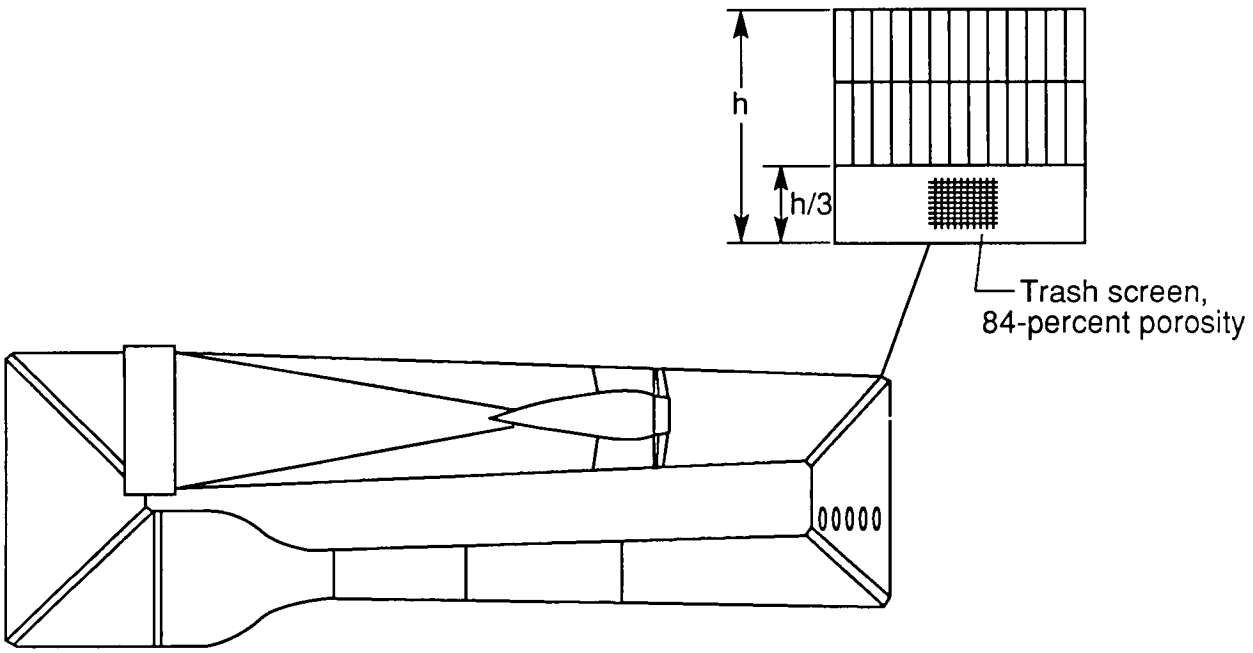

Figure 13. Sketch of debris-catching screen at second corner.

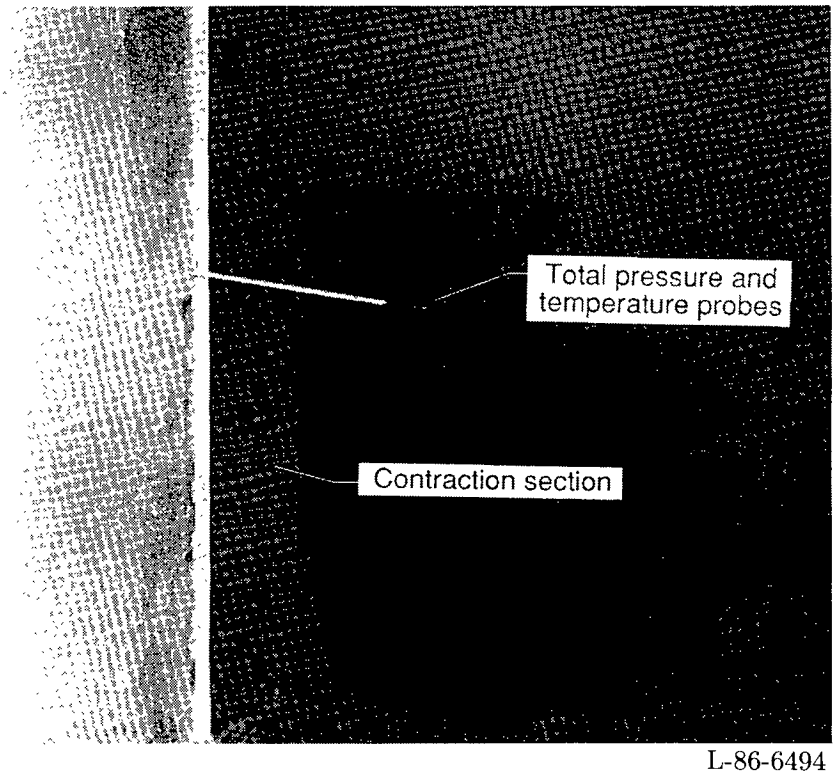

L-86-6494

(a) Total pressure reference probe.

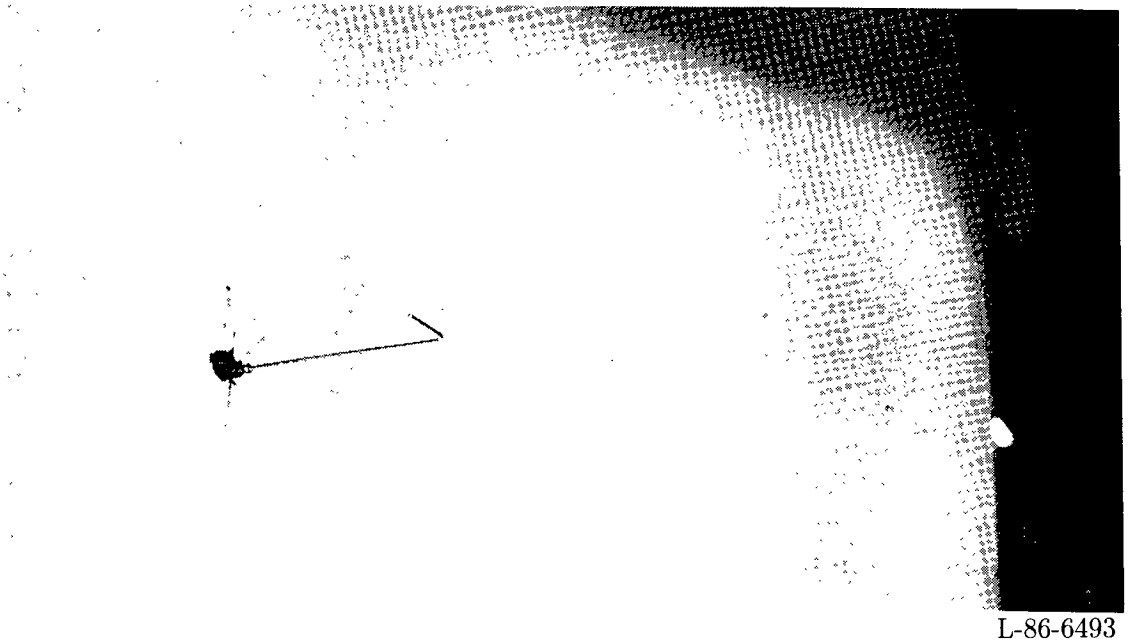

L-86-6493

(b) Static pressure reference probe.

Figure 14. Photographs of total and static pressure reference probes.

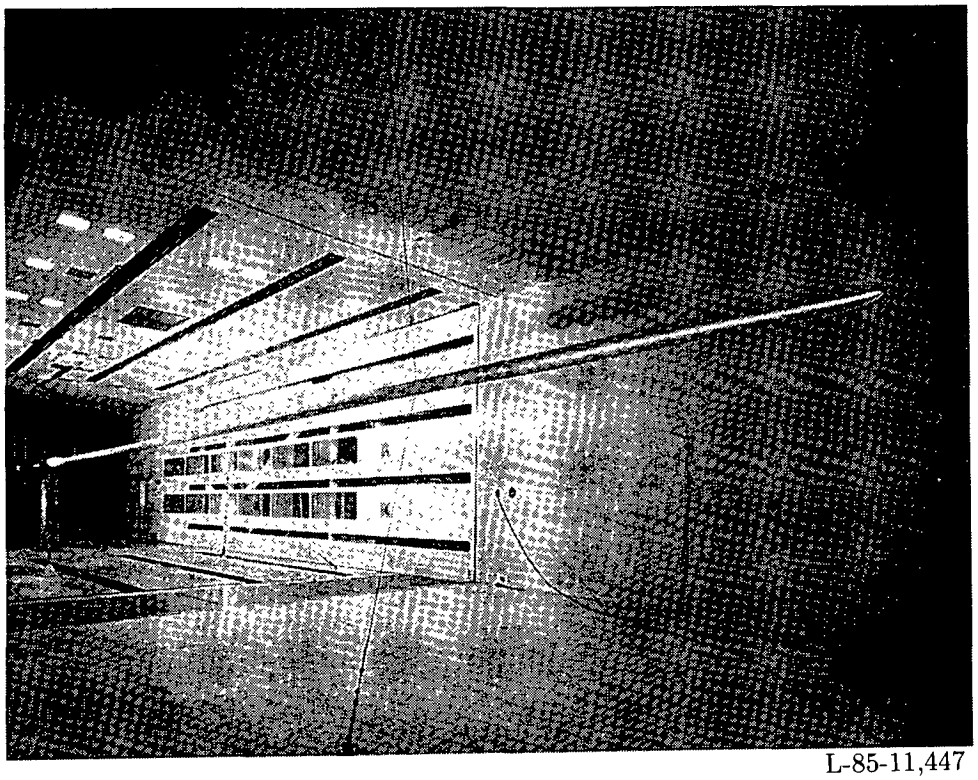

L-85-11,447

(a) Closed wind tunnel.

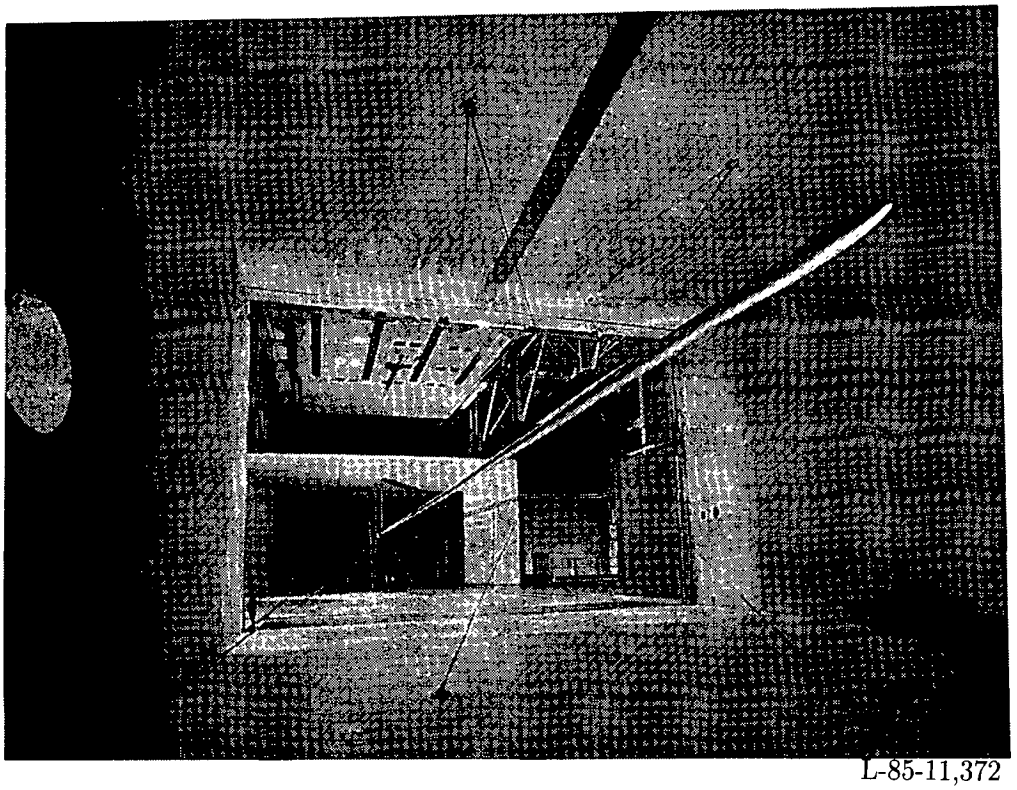

L-85-11,372

(b) Open wind tunnel.

Figure 15. Centerline probe mounted in test section.

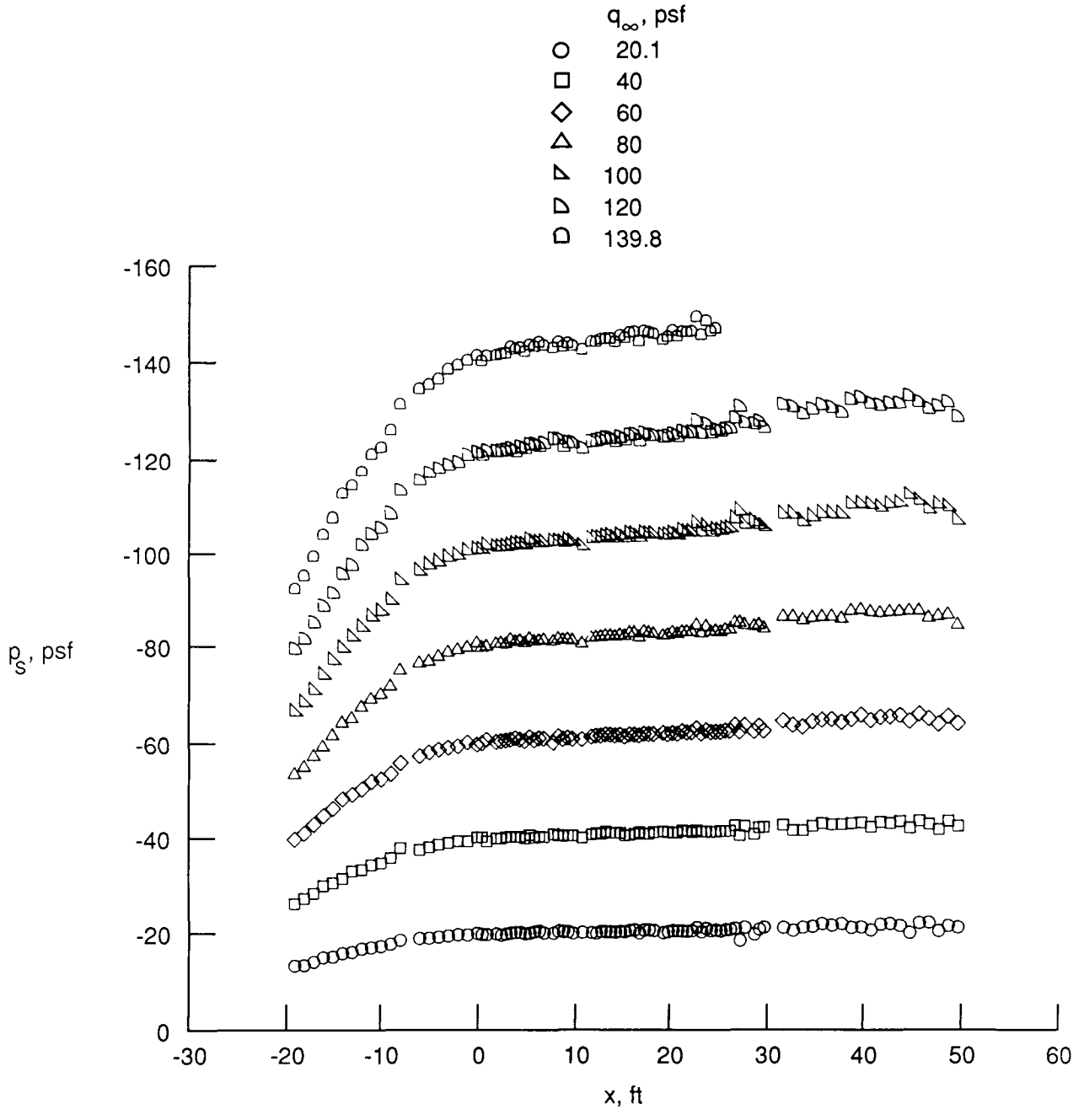

Figure 16. Longitudinal dynamic pressure distribution along centerline of closed test-section configuration with no floor boundary-layer control.

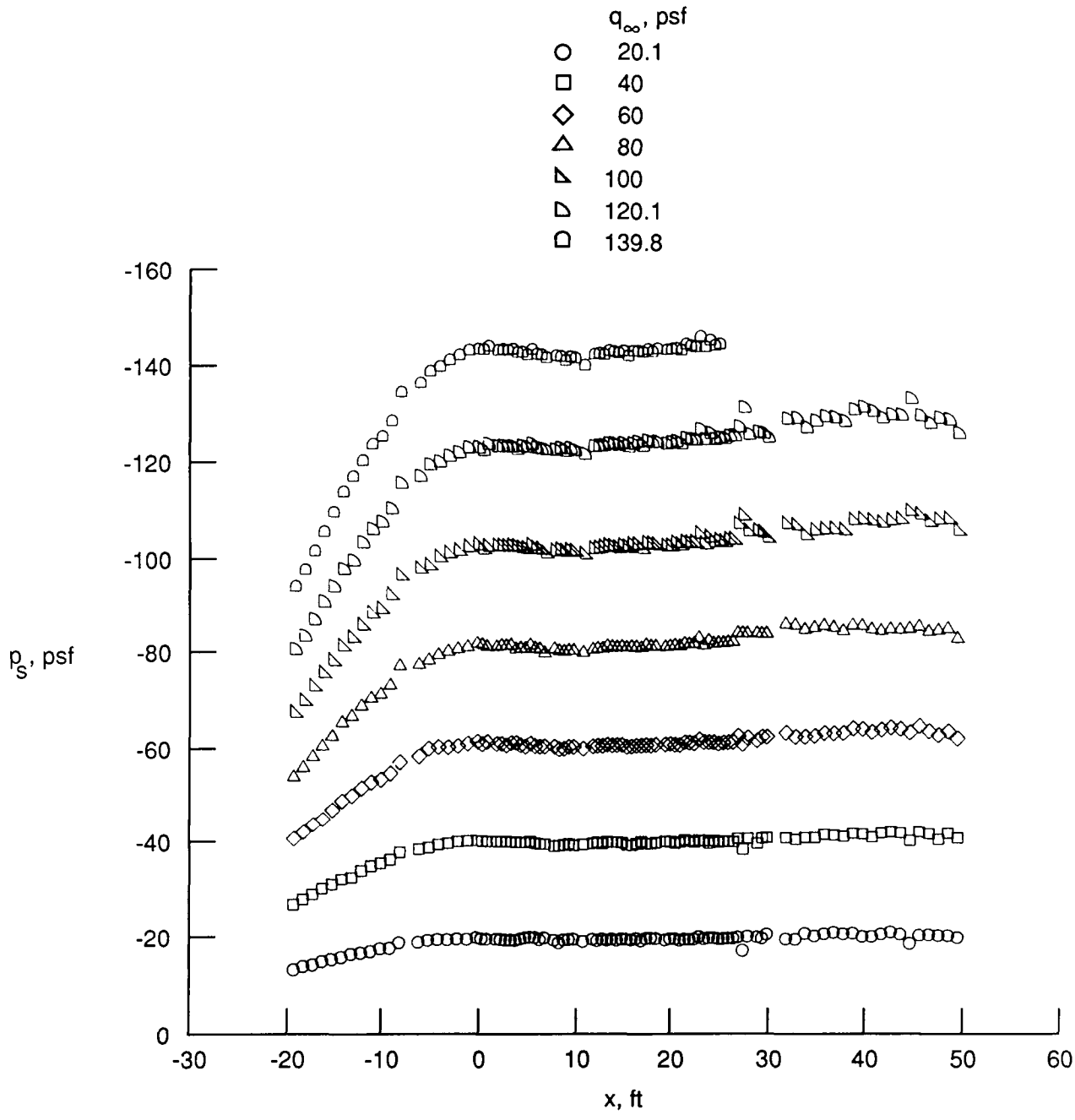

Figure 17. Longitudinal dynamic pressure distribution along centerline of closed test-section configuration with floor boundary-layer control.

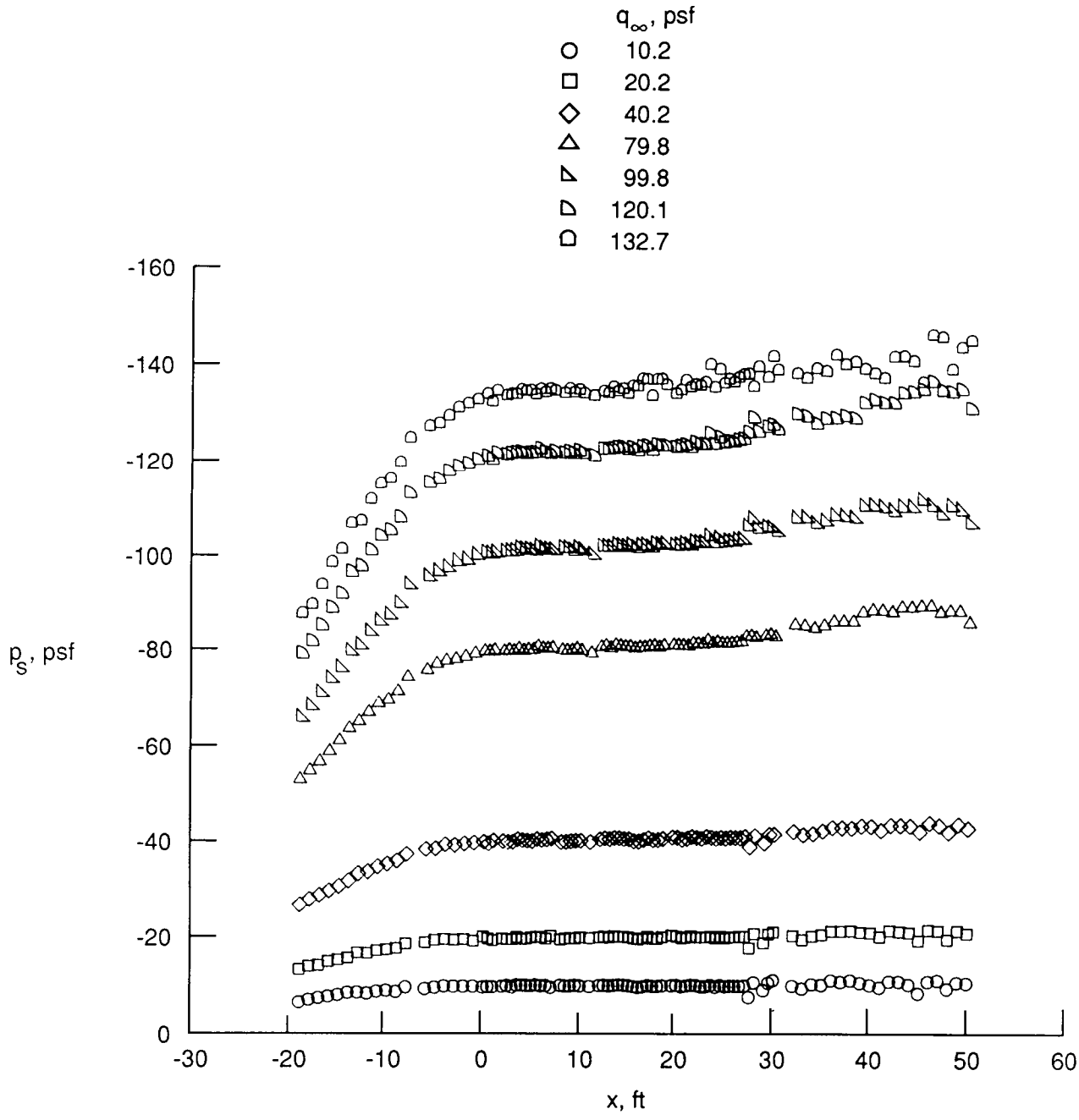

Figure 18. Longitudinal dynamic pressure distribution along centerline of closed test-section configuration with ceiling slots open and no floor boundary-layer control.

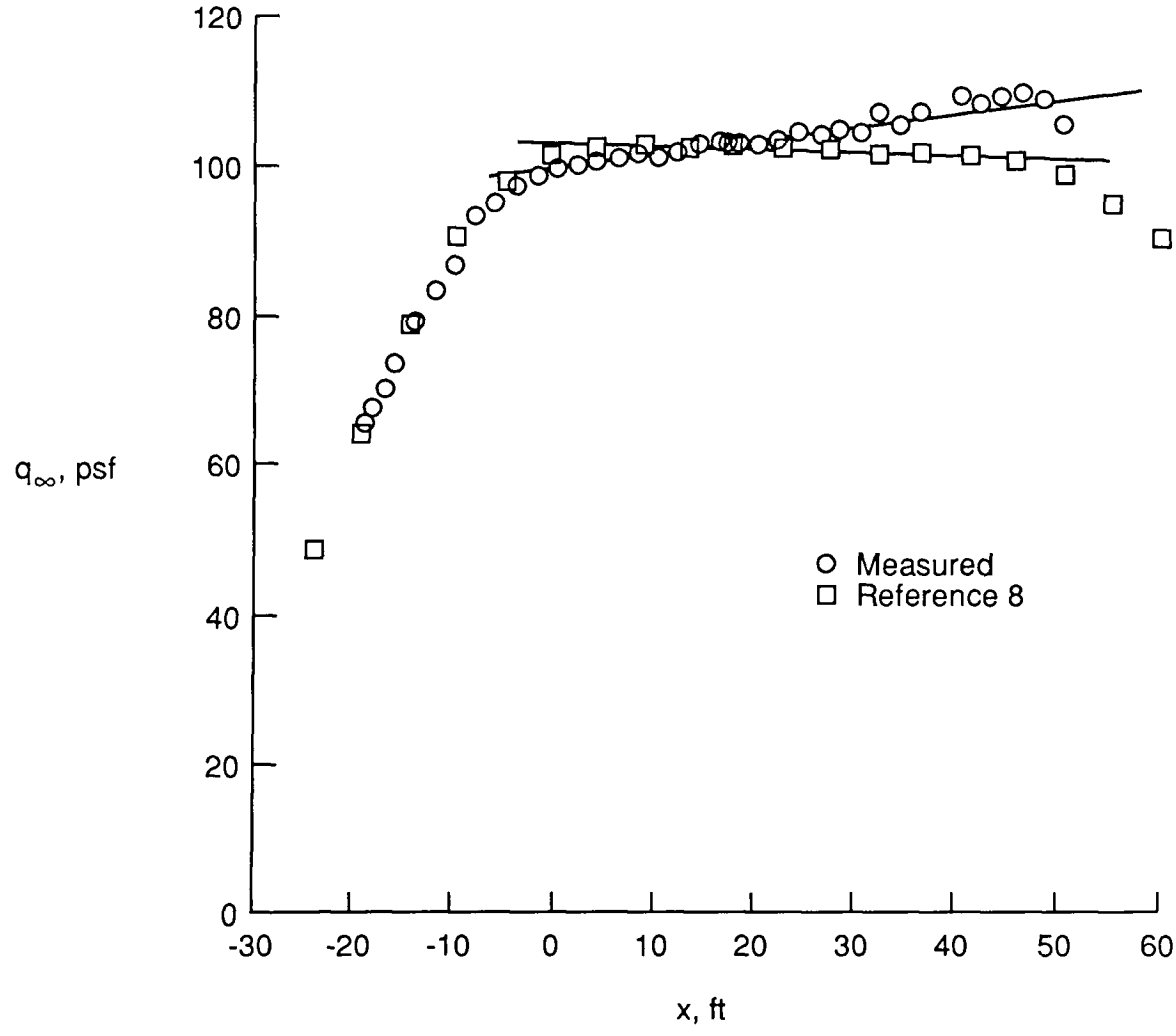

Figure 19. Comparison of measured and predicted dynamic pressure distribution along centerline of closed test-section configuration with no floor boundary-layer control.

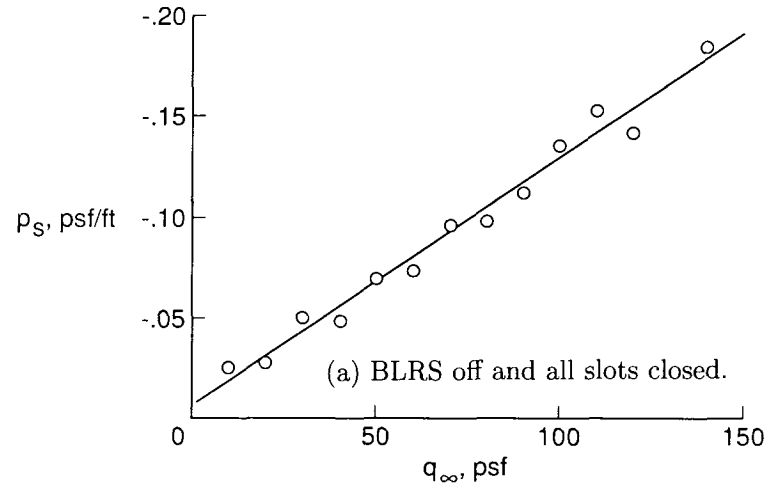

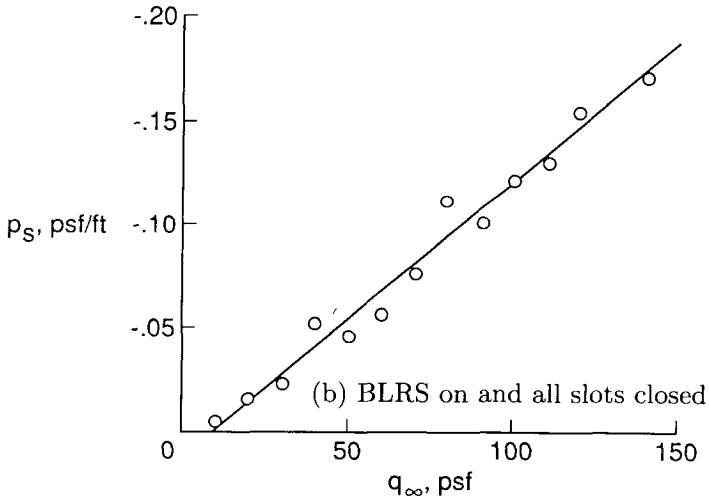

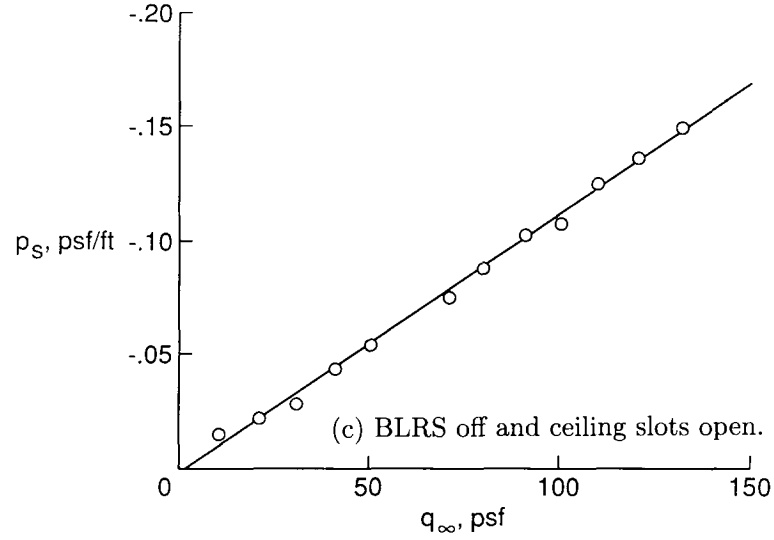

Figure 20. Static pressure variation through test section versus dynamic pressure for various test-section configurations.

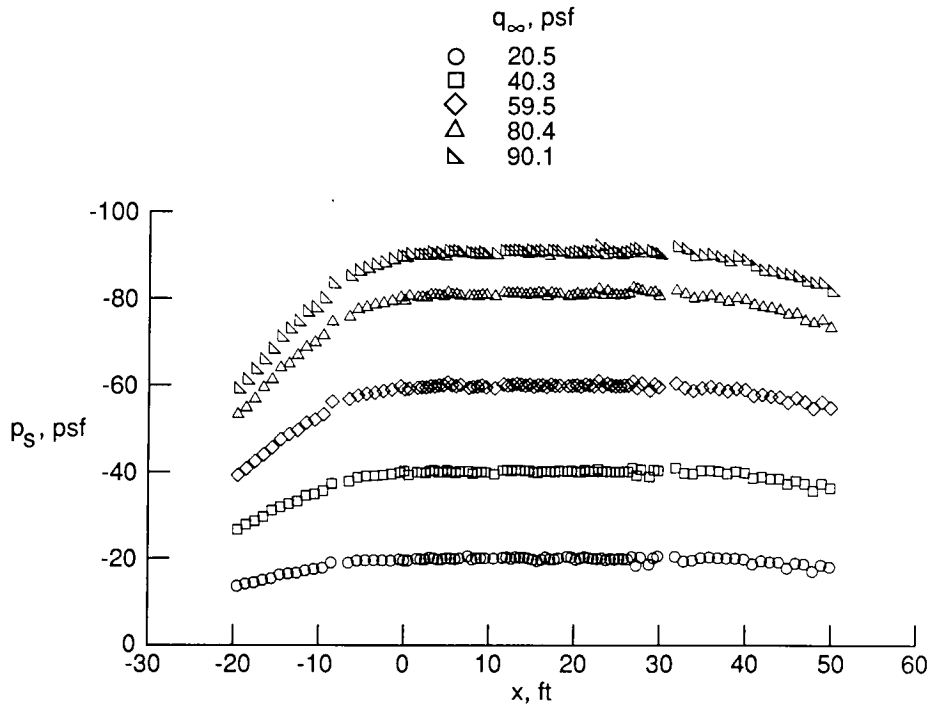

Figure 21. Longitudinal dynamic pressure distribution along centerline of open test-section configuration with no floor boundary-layer control.

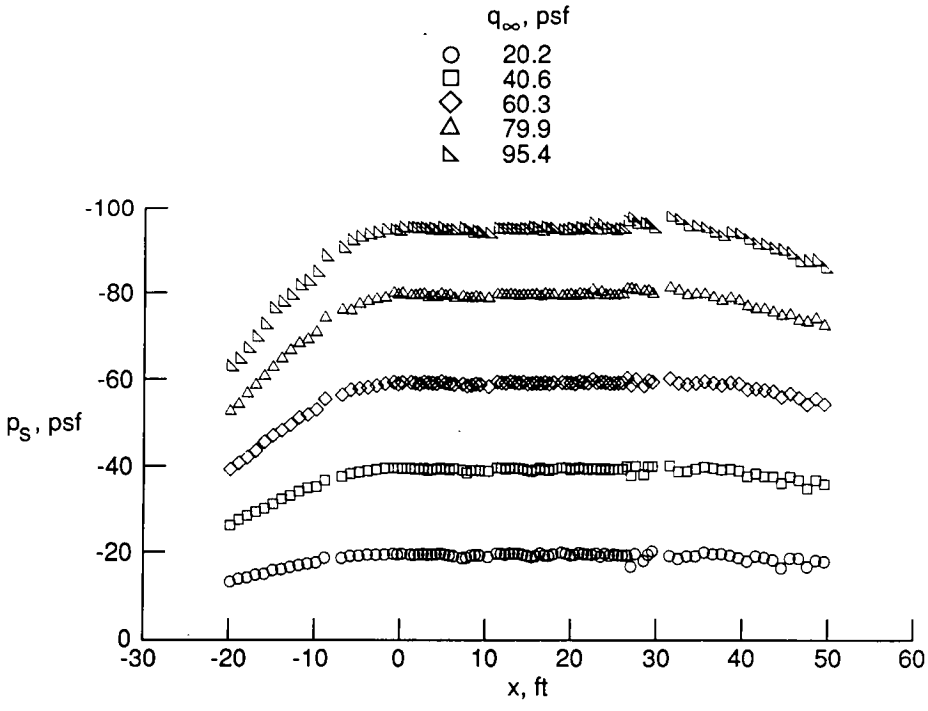

Figure 22. Longitudinal dynamic pressure distribution along centerline of open test-section configuration with floor boundary-layer control.

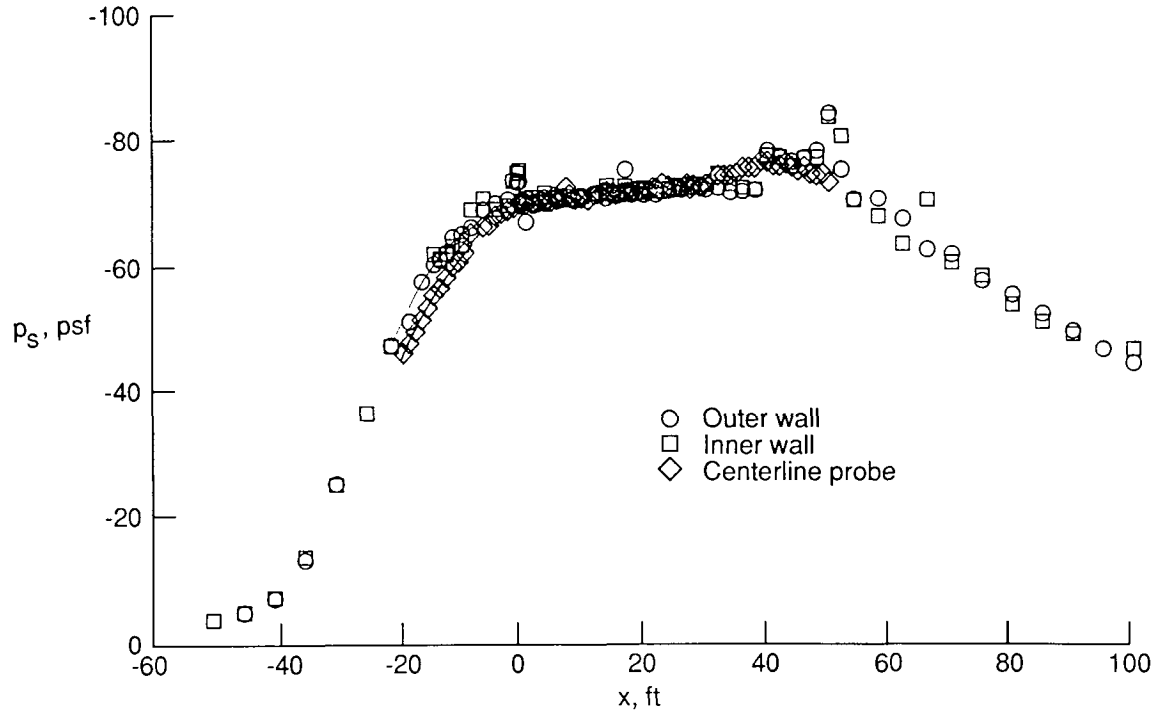

Figure 23. Static pressure data from tunnel stations −50 to 100 for closed test-section configuration with $q_\infty = 70$ psf.

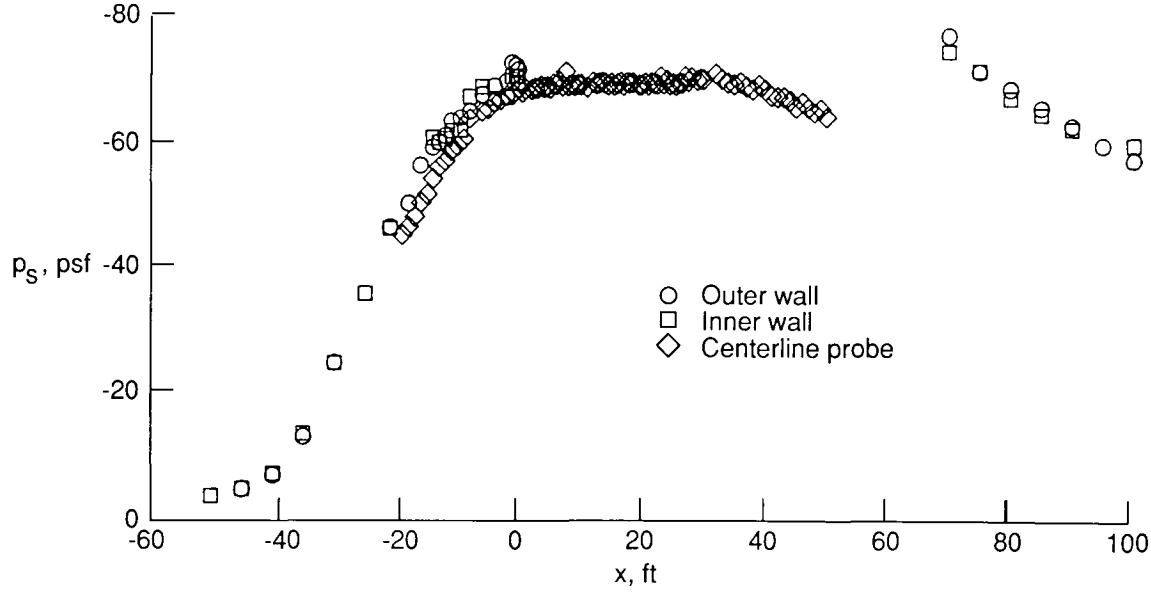

Figure 24. Static pressure data from tunnel stations −50 to 100 for open test-section configuration with $q_\infty = 70$ psf.

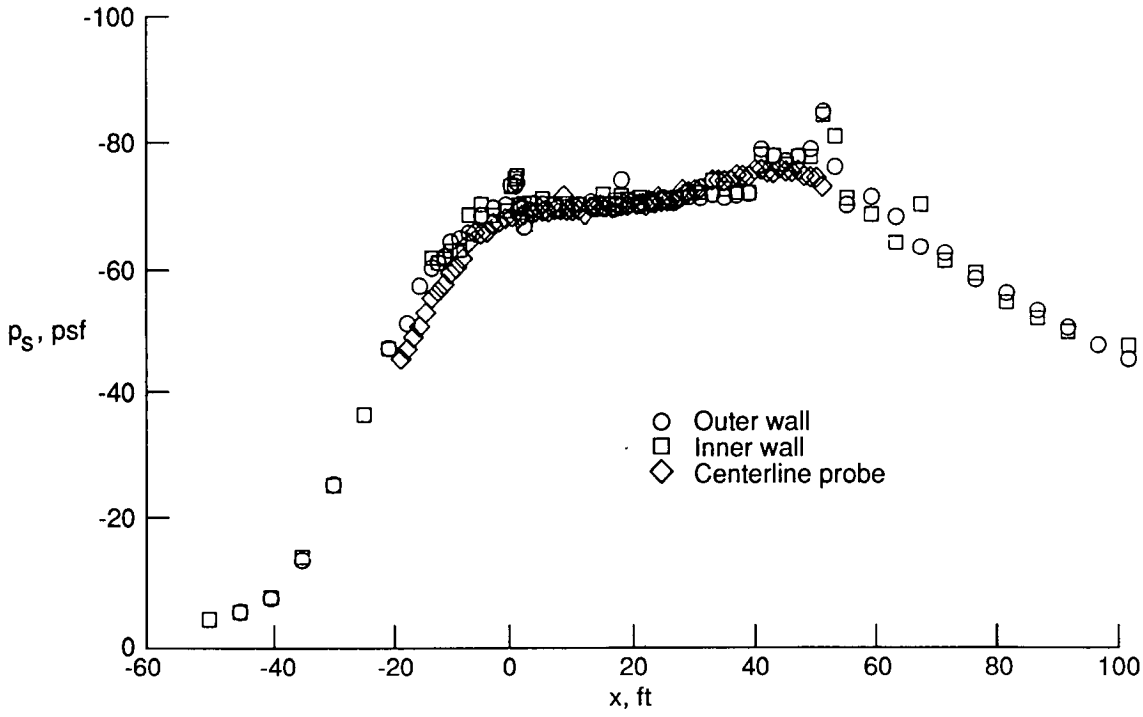

Figure 25. Static pressure data from tunnel stations −50 to 100 for closed test-section configuration with ceiling slots open and $q_\infty = 70$ psf.

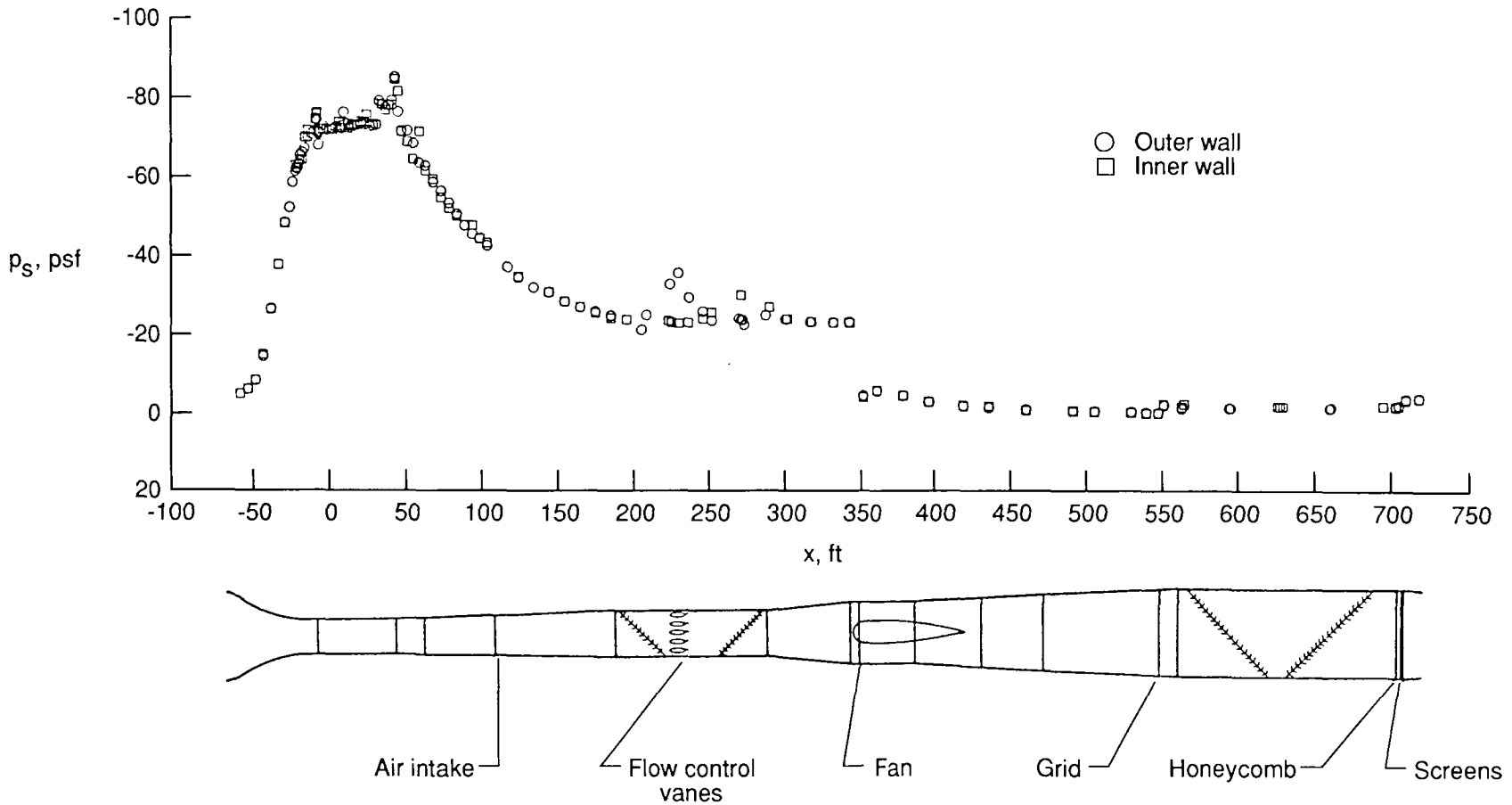

Figure 26. Static pressure distribution around entire tunnel circuit for closed test-section configuration with $q_\infty = 70$ psf.

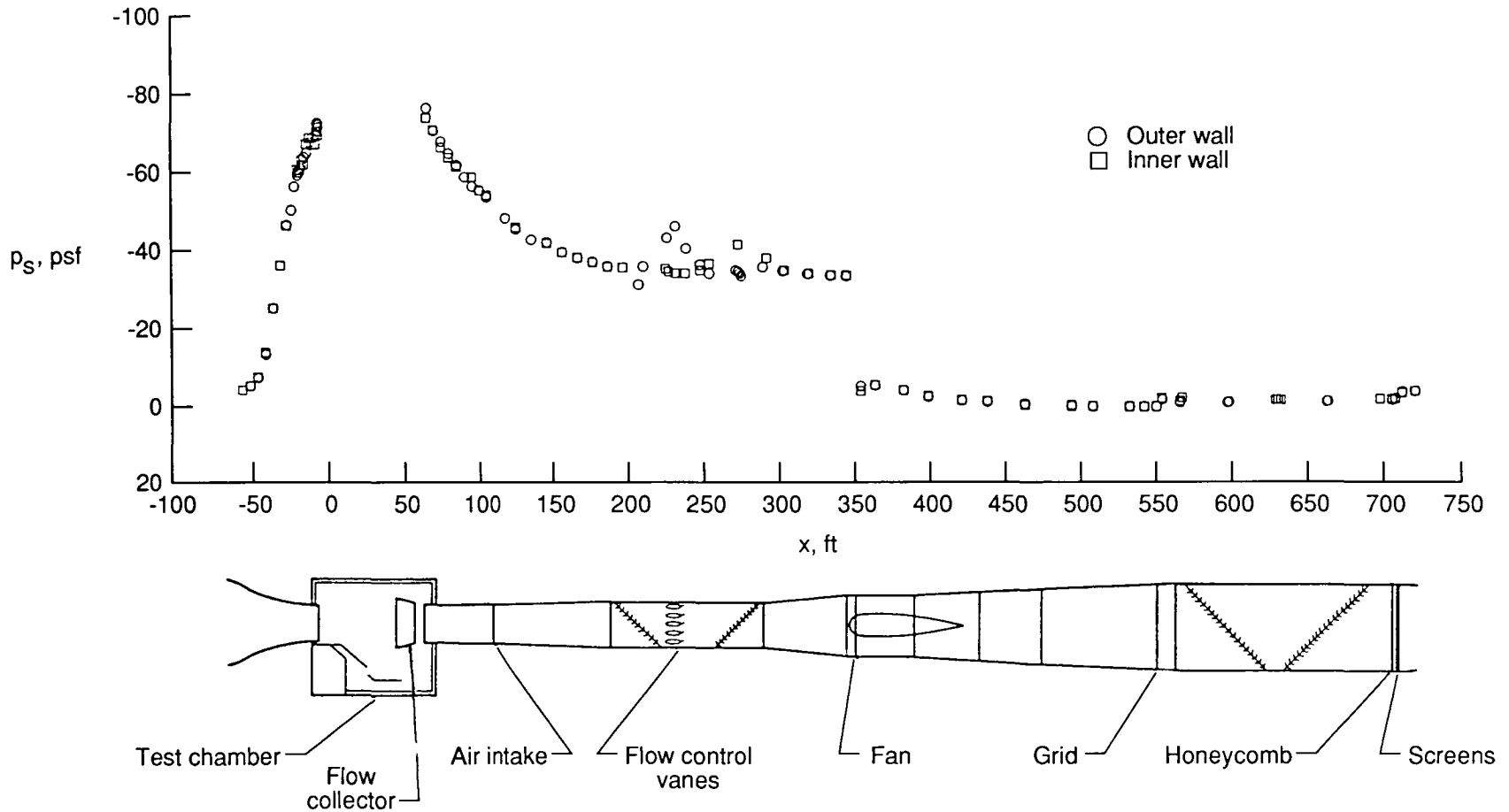

Figure 27. Static pressure distribution around entire tunnel circuit for open test-section configuration with $q_\infty = 70$ psf.

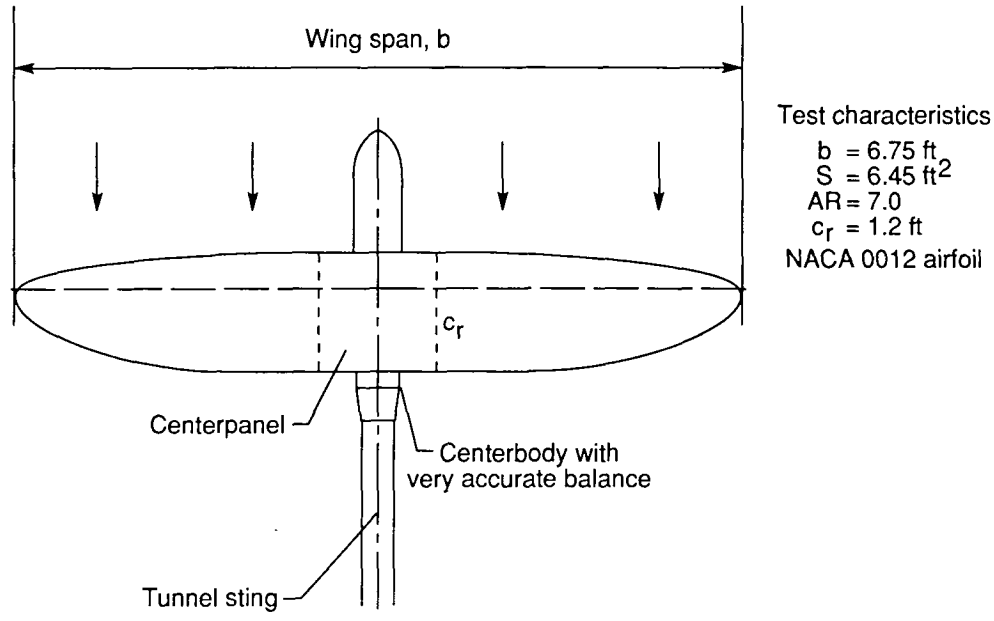

Figure 28. Sketch of elliptical wing model used in flow angularity test.

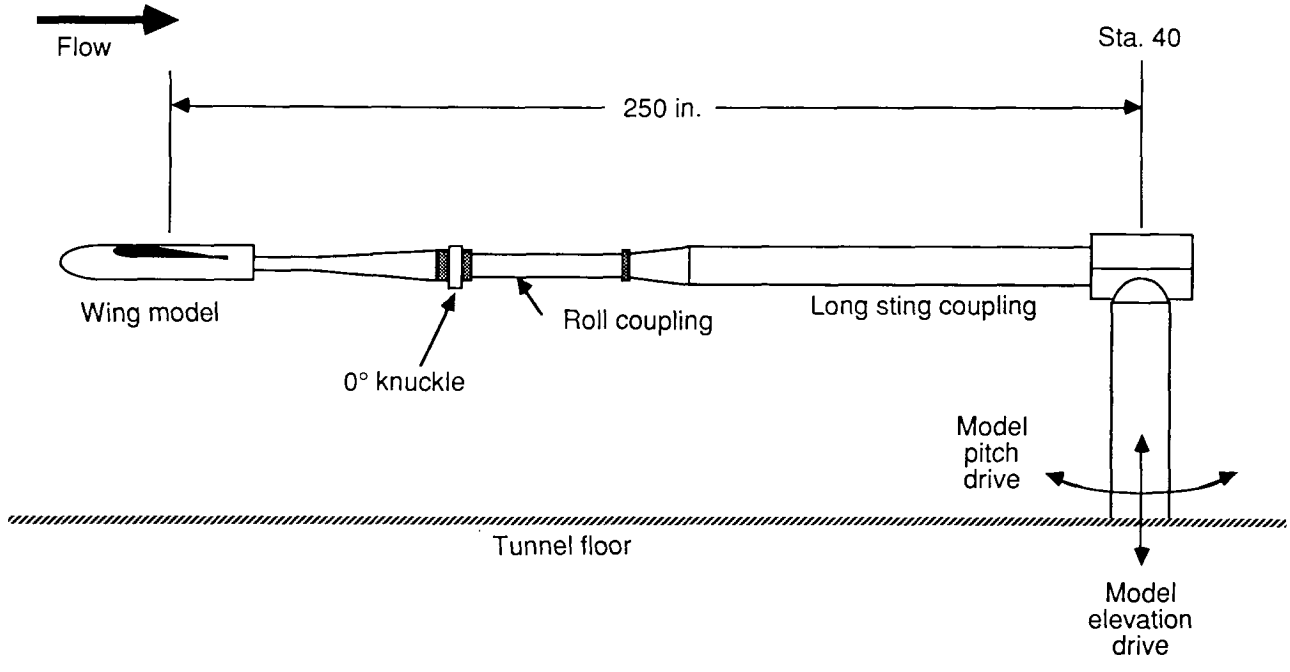

Figure 29. Sketch of elliptical wing model mounted in the 14- by 22-Foot Tunnel.

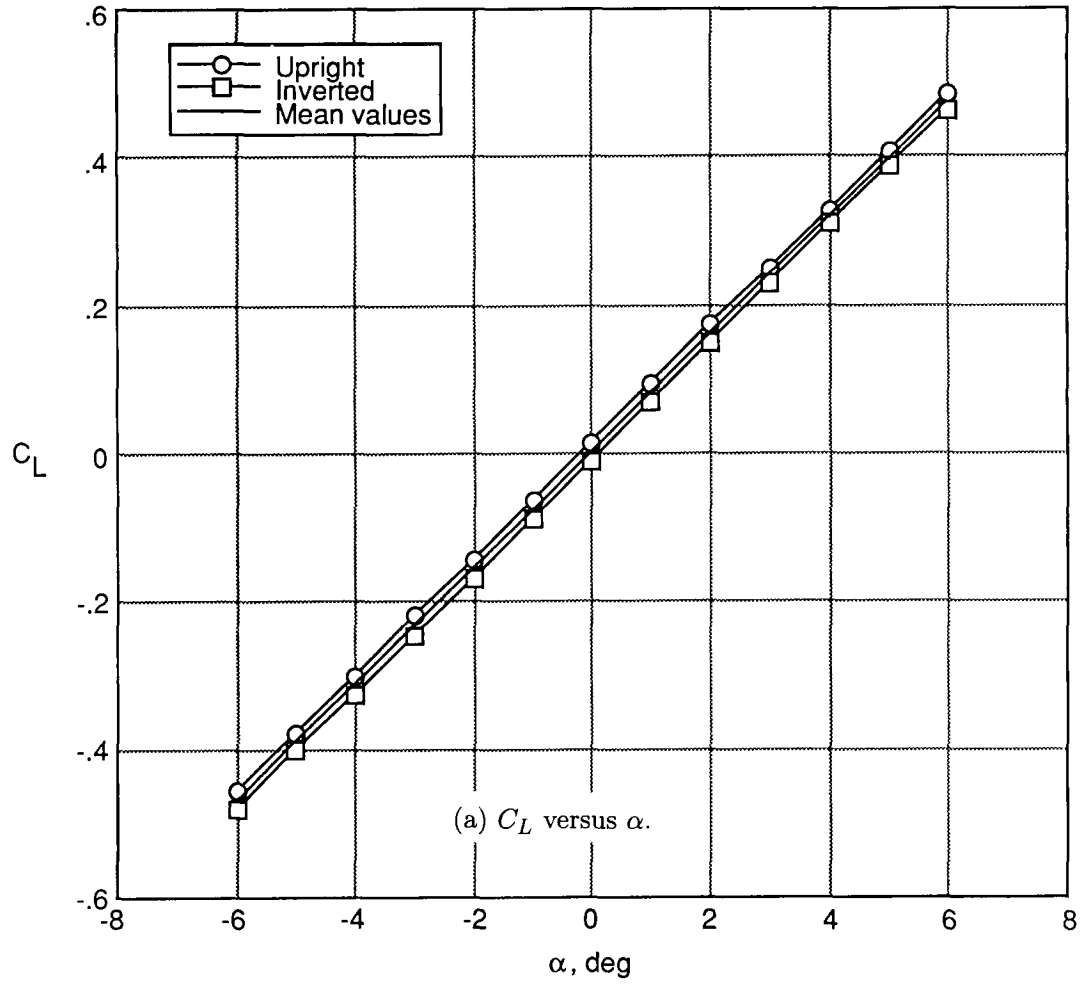

(a) C_L versus α.

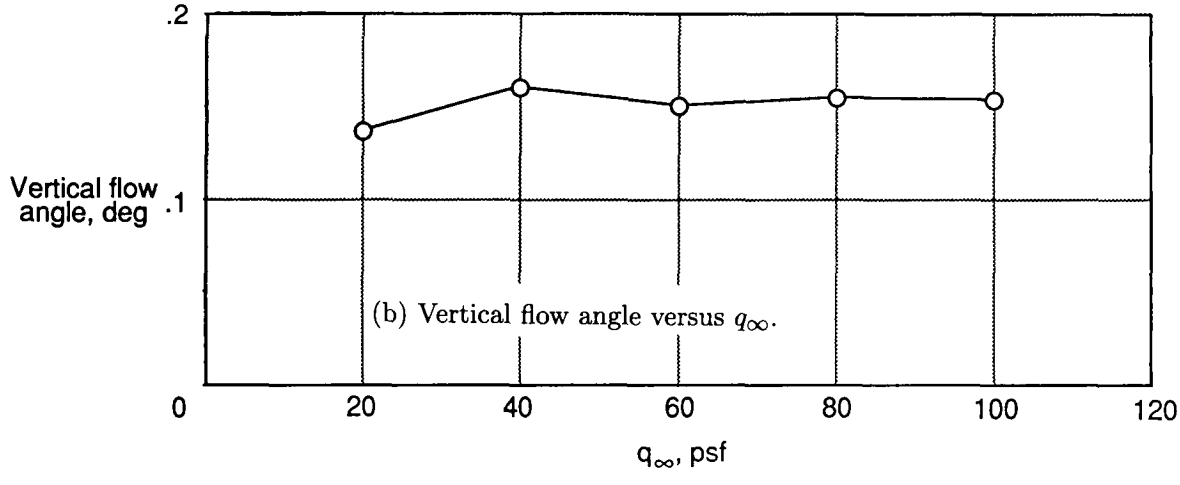

(b) Vertical flow angle versus q_∞.

Figure 30. Measurements of vertical flow angle using lift data of an elliptical wing at $q_\infty = 60$ psf.

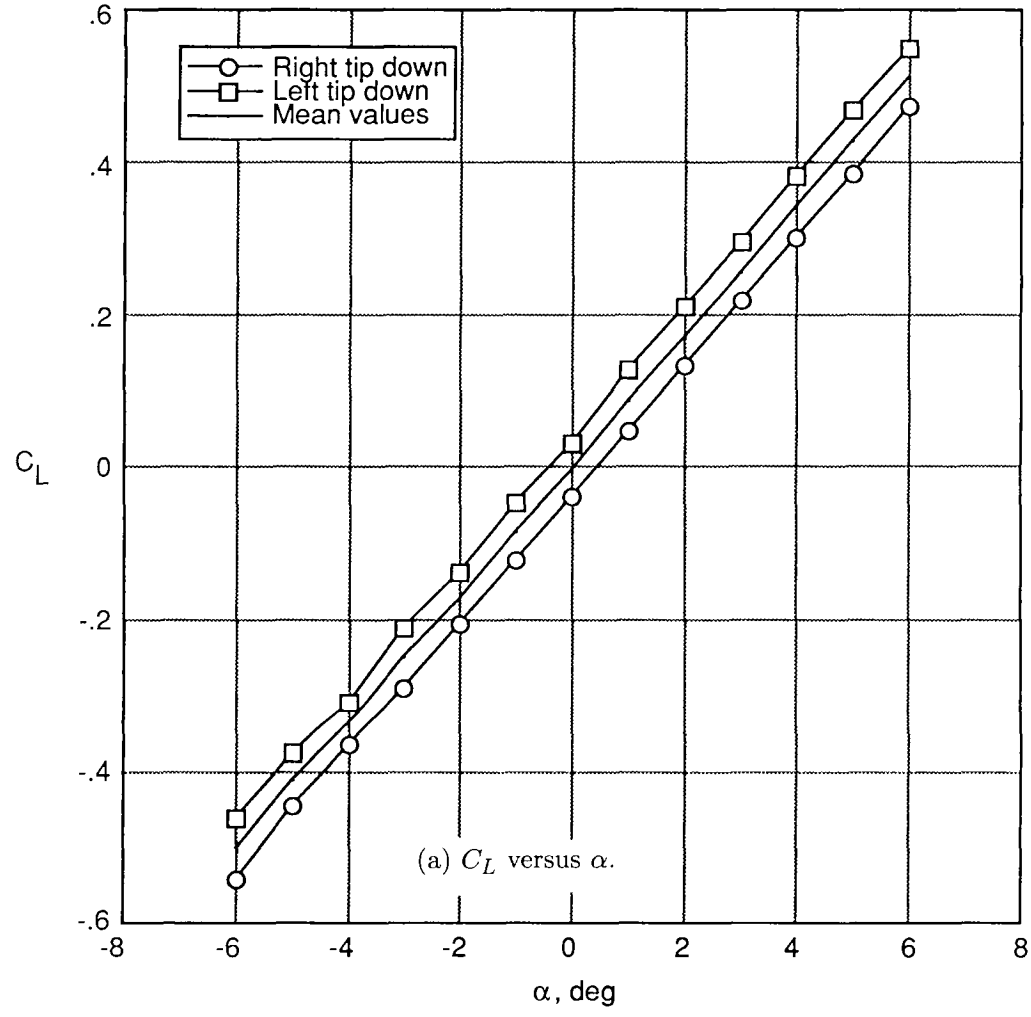

(a) C_L versus α.

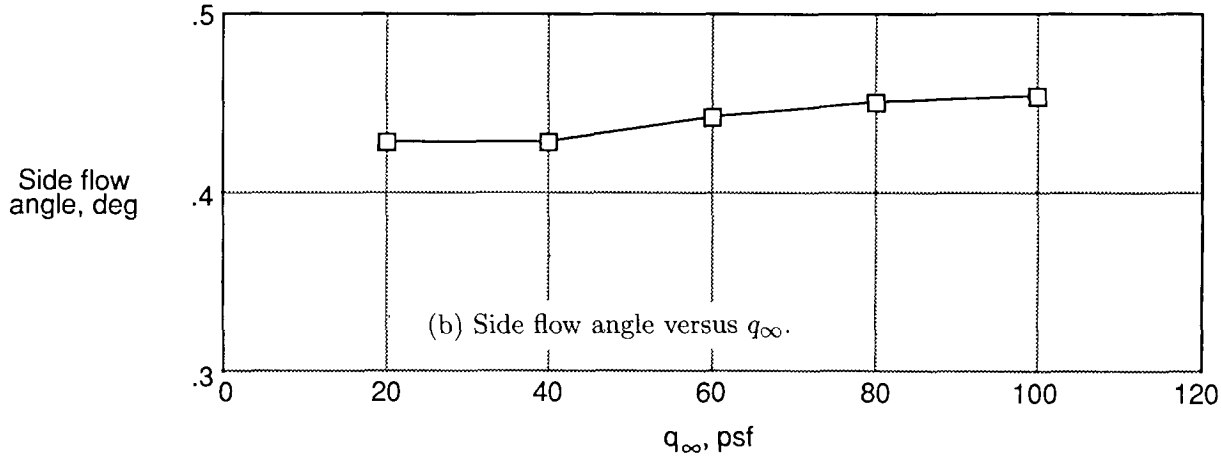

(b) Side flow angle versus q_∞.

Figure 31. Measurements of side flow angle using lift data of an elliptical wing at $q_\infty = 60$ psf.

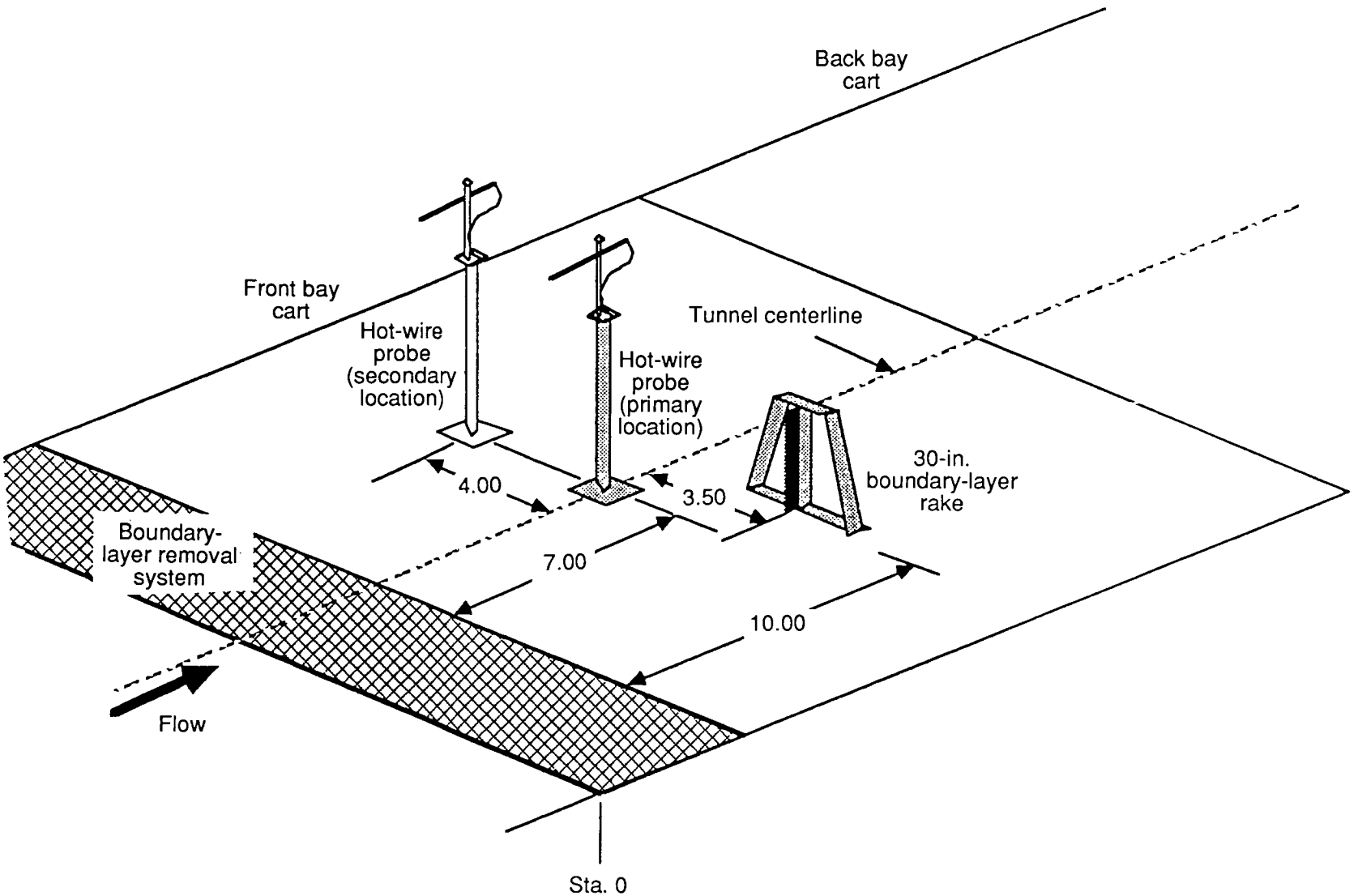

Figure 32. Sketch of hot-wire probe and boundary-layer rake location in the 14- by 22-Foot Tunnel. All dimensions are given in feet unless specified otherwise.

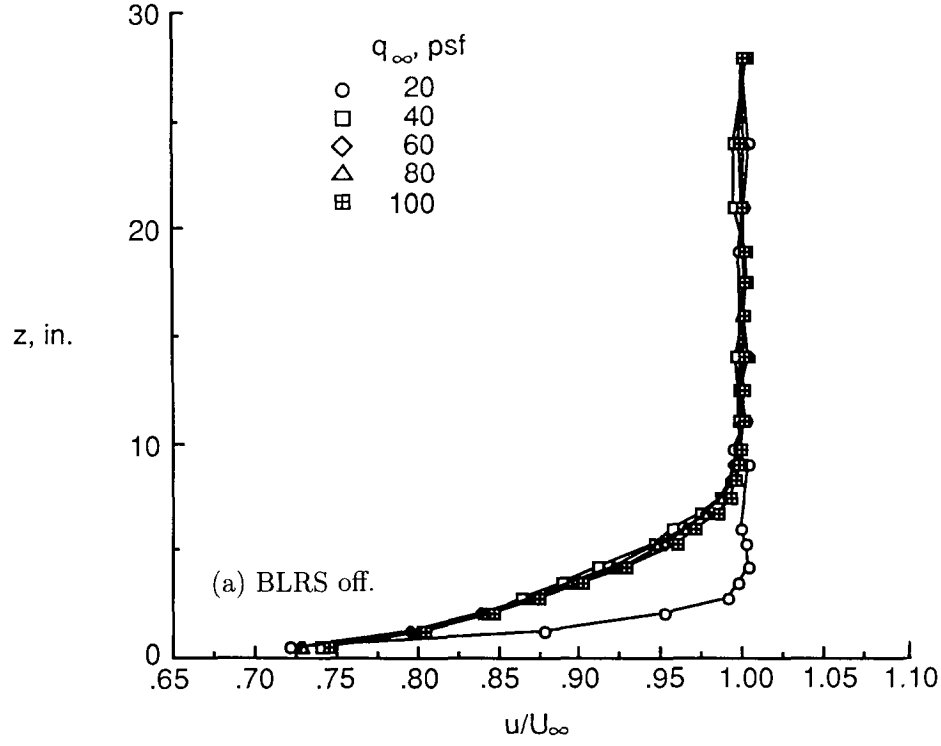

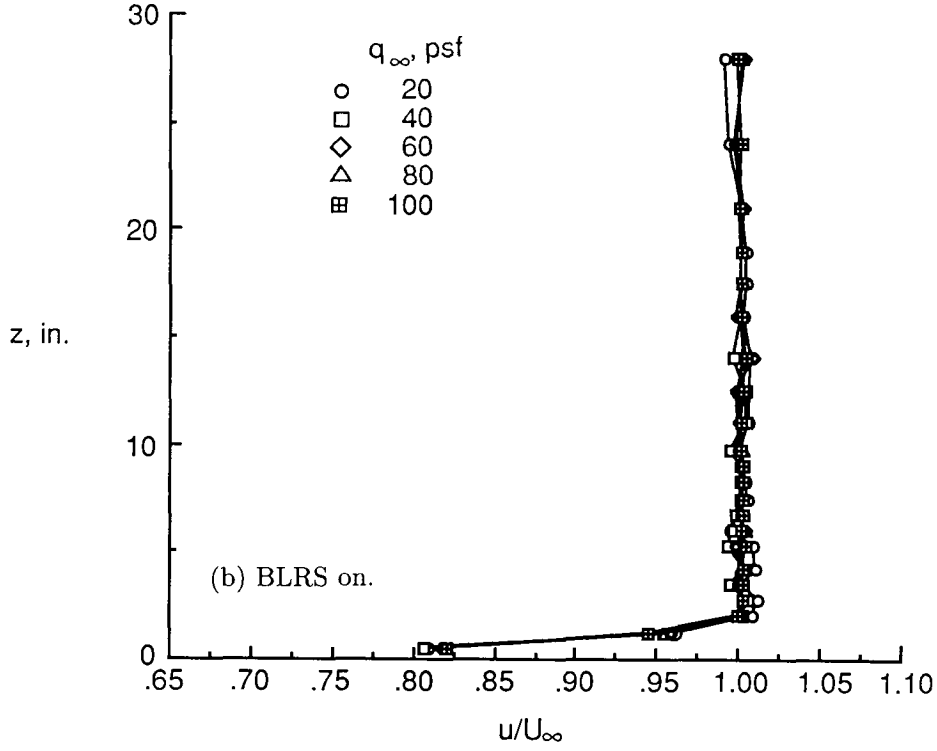

Figure 33. Velocity profiles displaying boundary layer of closed test-section floor at tunnel station $x = 17.75$ ft.

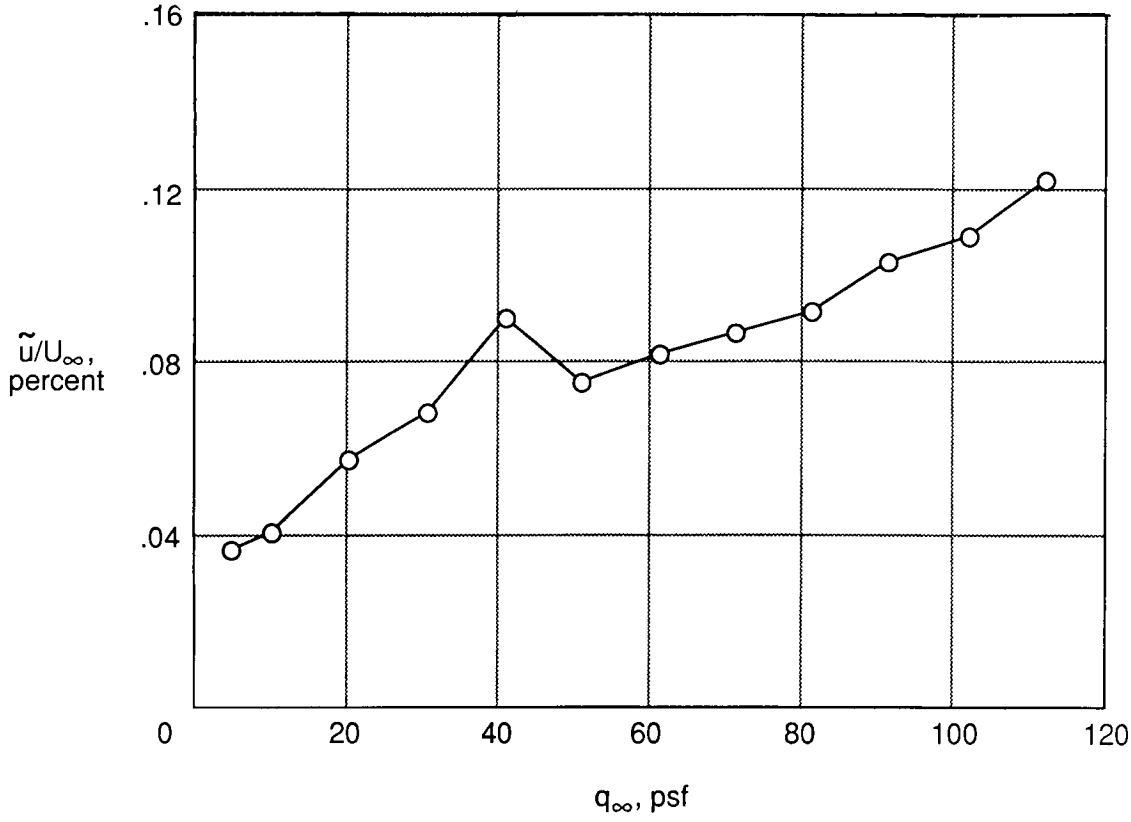

Figure 34. Effect of turbulence reduction system on longitudinal turbulence intensity for the closed test section.

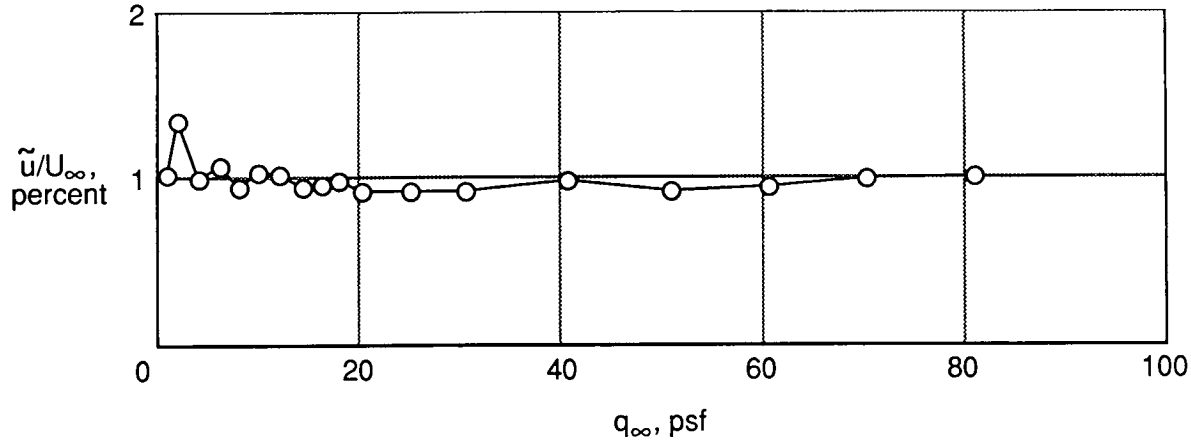

Figure 35. Effect of flow collector on longitudinal turbulence intensity for the open test section.

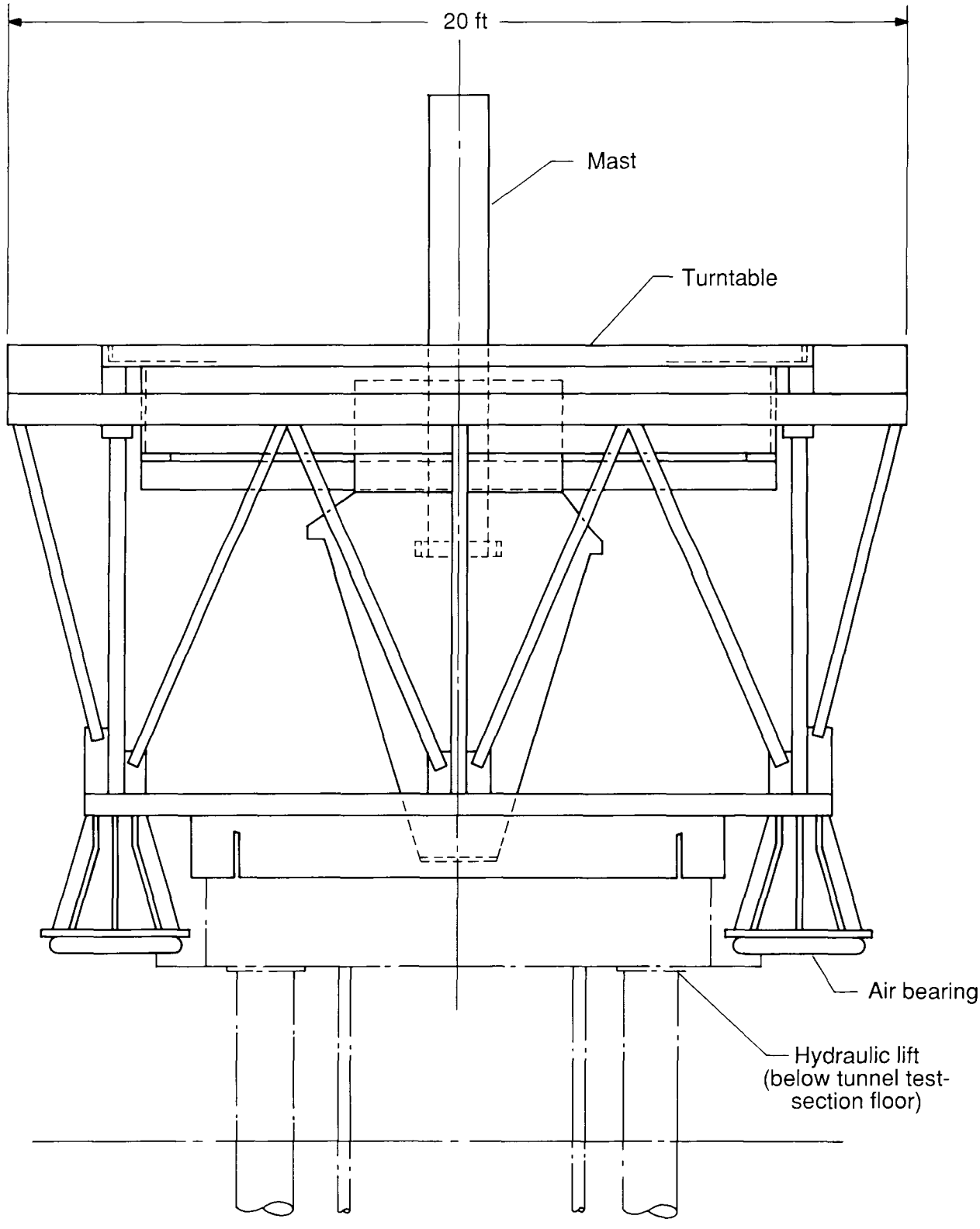

Figure 36. Schematic of model support carts 1 and 2.

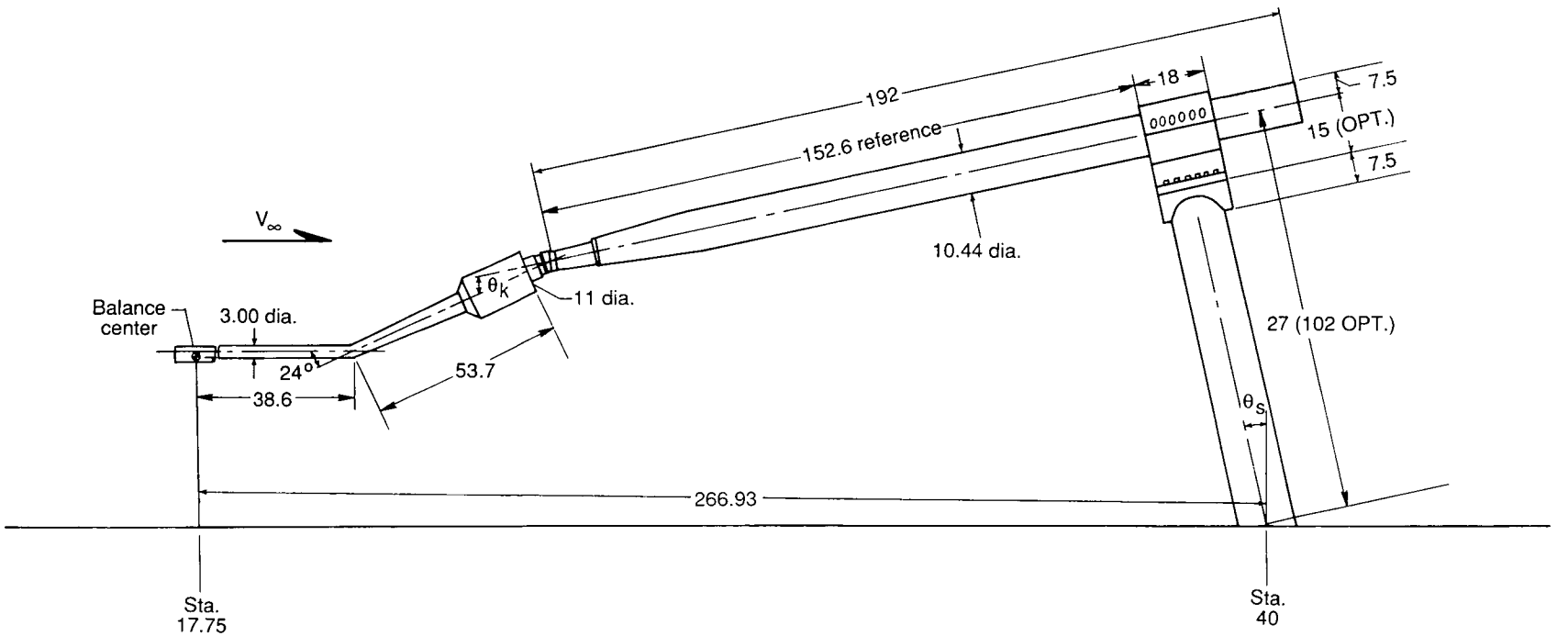

(a) Sting arrangement for 708-type balance.

Figure 37. Sting and balance combination commonly used in the 14- by 22-foot Tunnel. All linear dimensions are given in inches and tunnel sections are given in feet.

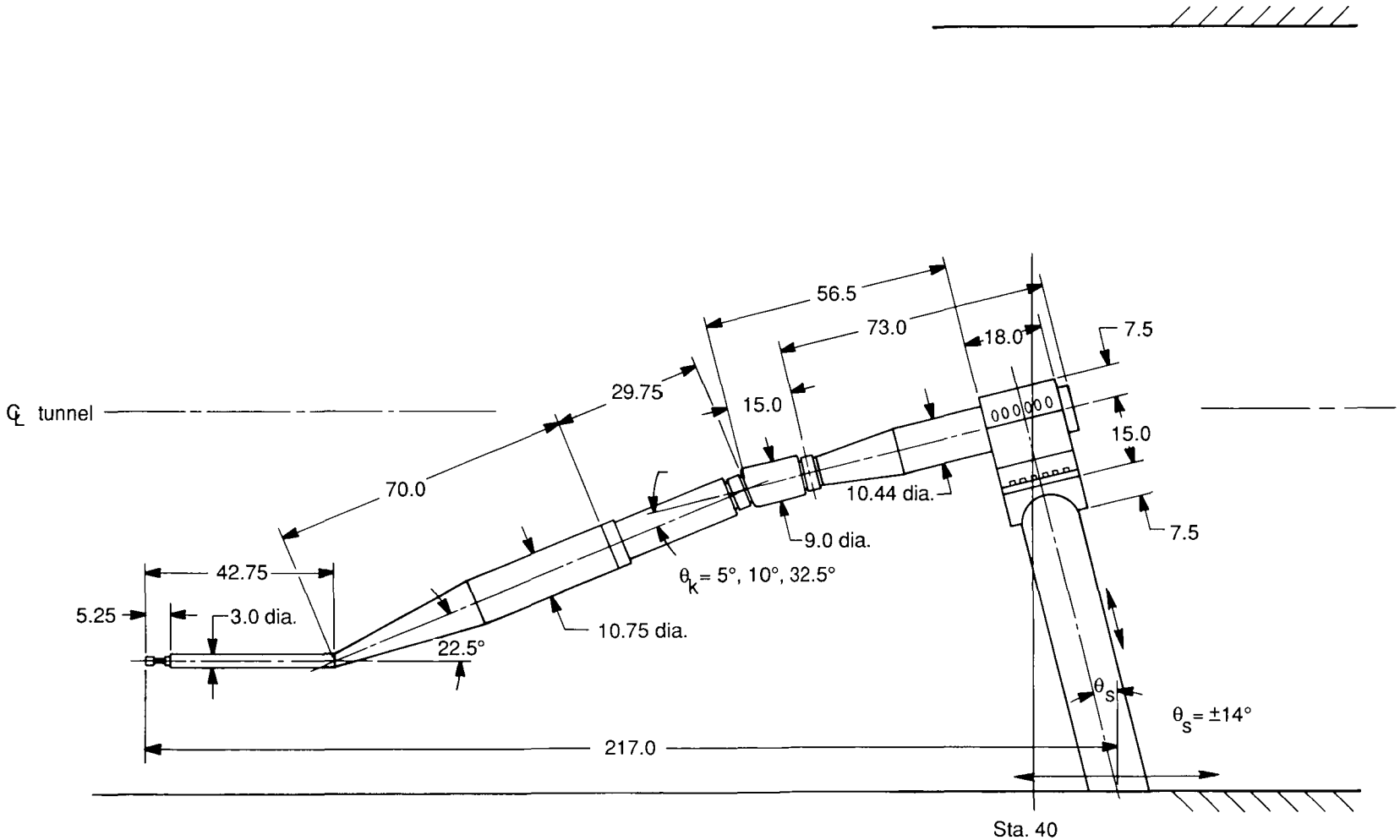

(b) Sting arrangement for 729-type balances.

Figure 37. Concluded.

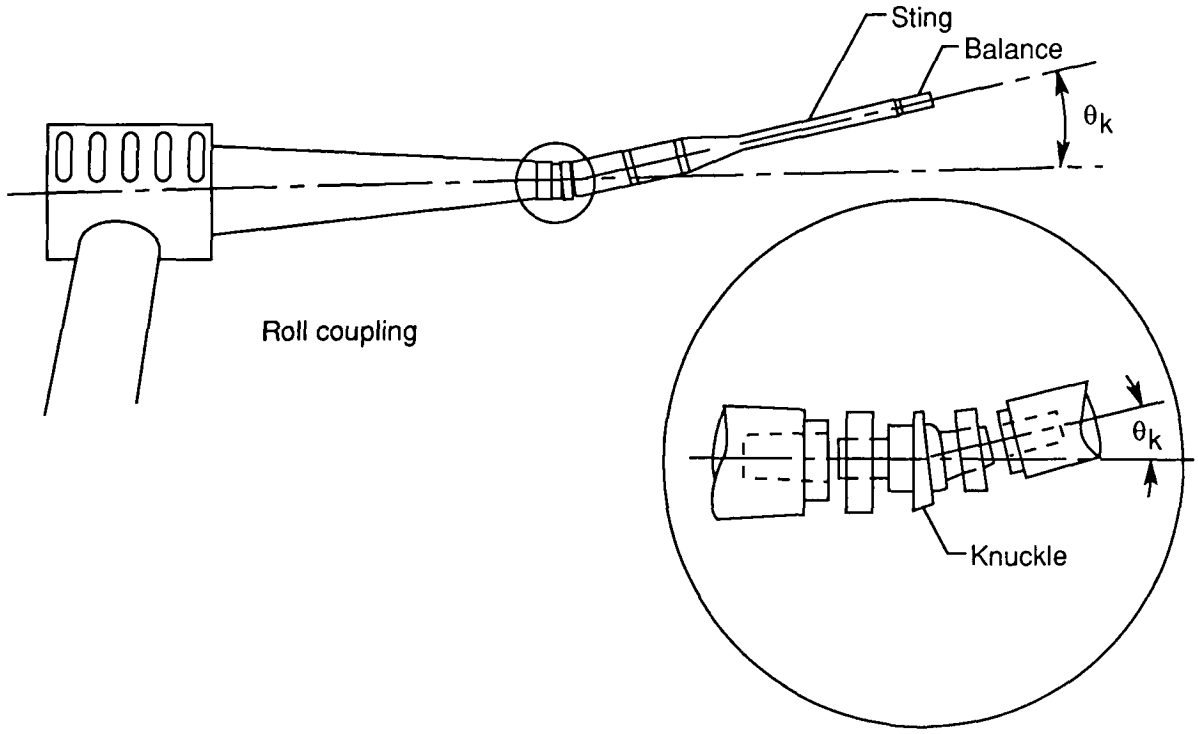

Notes:

1. Available knuckles (θ_k): 0°, 1°, 2°, 4°, 6°, 9°, 12°, 15°, 18°, 24°, 35°
2. Knuckles can be rolled 0°, 90°, 180°, and 270°.
3. Roll coupling can be set at nominal (±5° adjustment) angles of 0°, 90°, 180°, and 270°.

Figure 38. Small knuckle for use in sting assemblies.

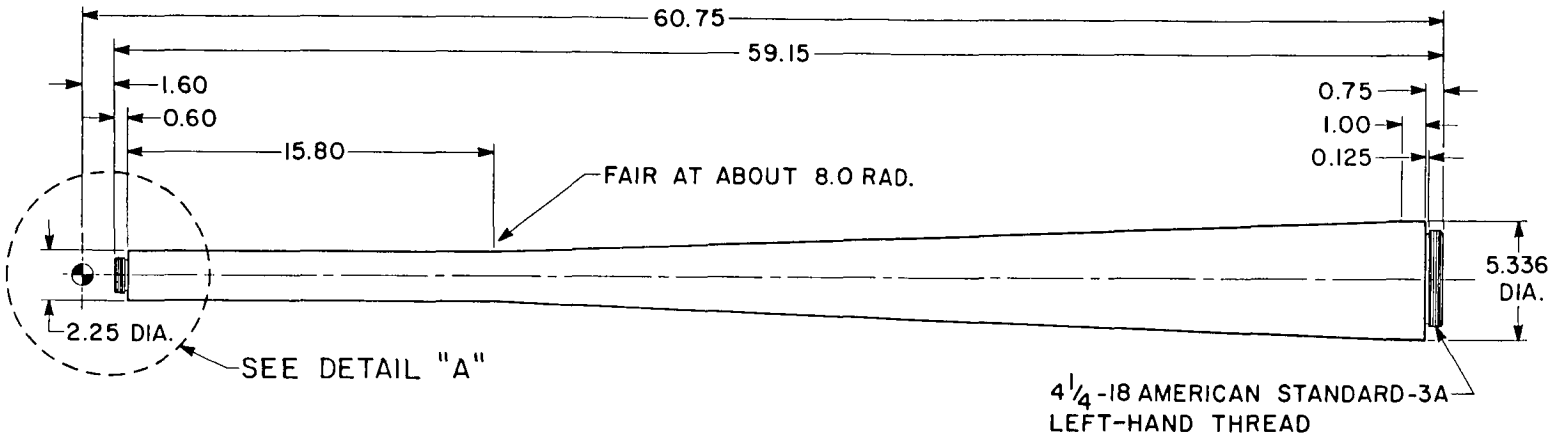

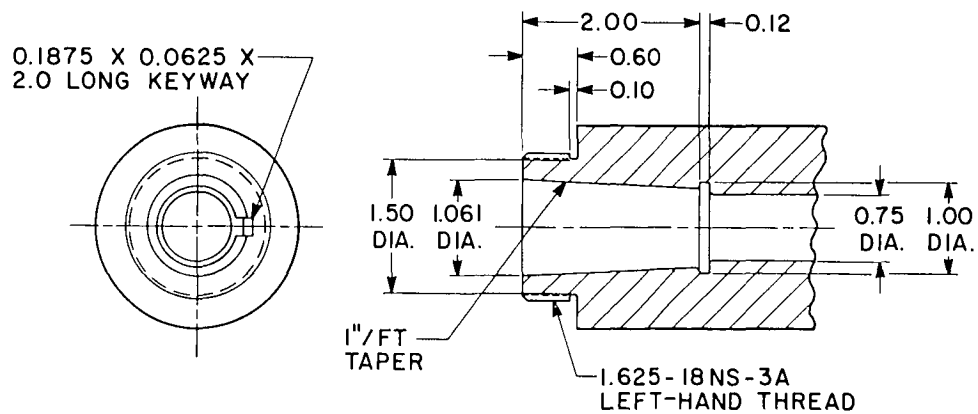

DETAIL "A"

(a) Used with 708-type balances.

Figure 39. Typical straight sting used in the 14- by 22-Foot Tunnel. All dimensions are given in inches.

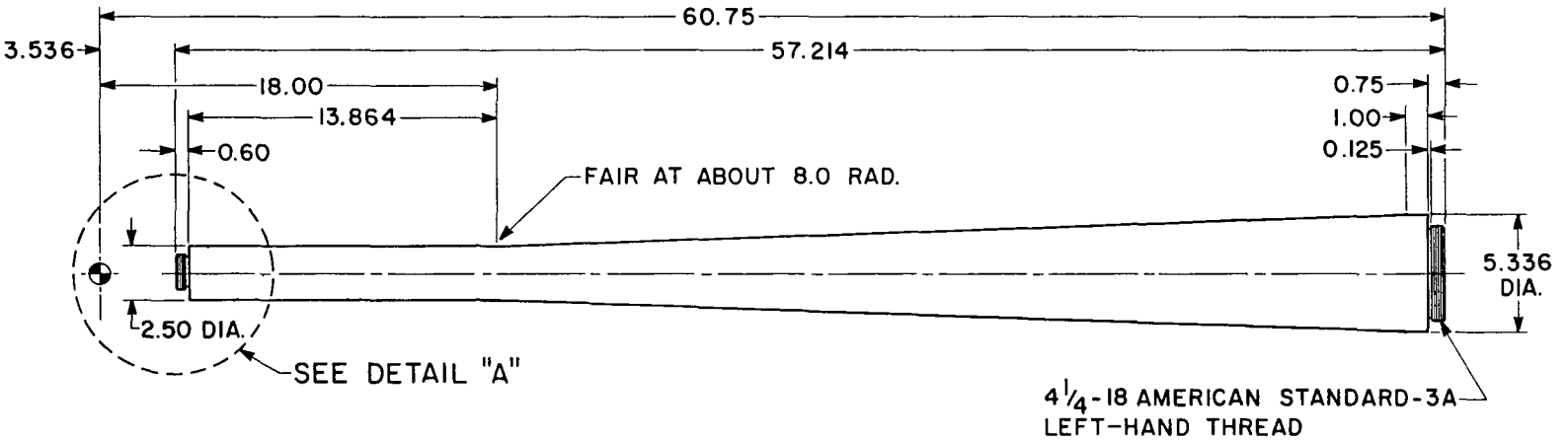

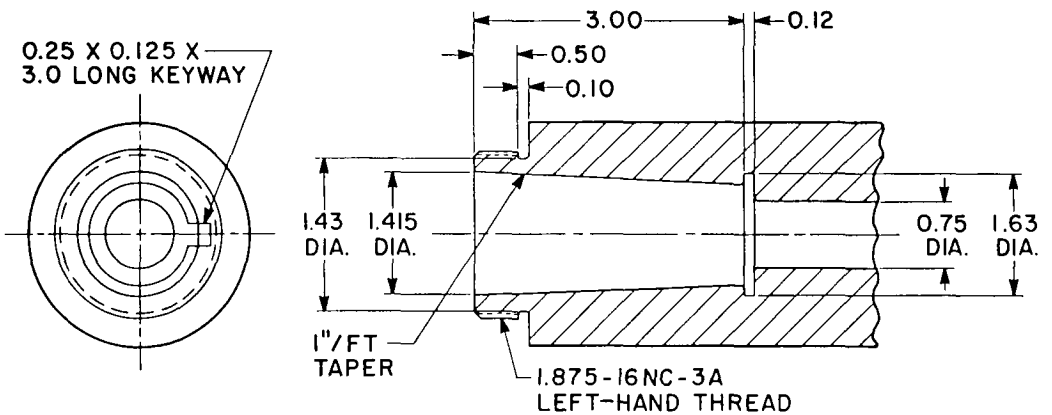

(b) Used with 729-type balances.

Figure 39. Concluded.

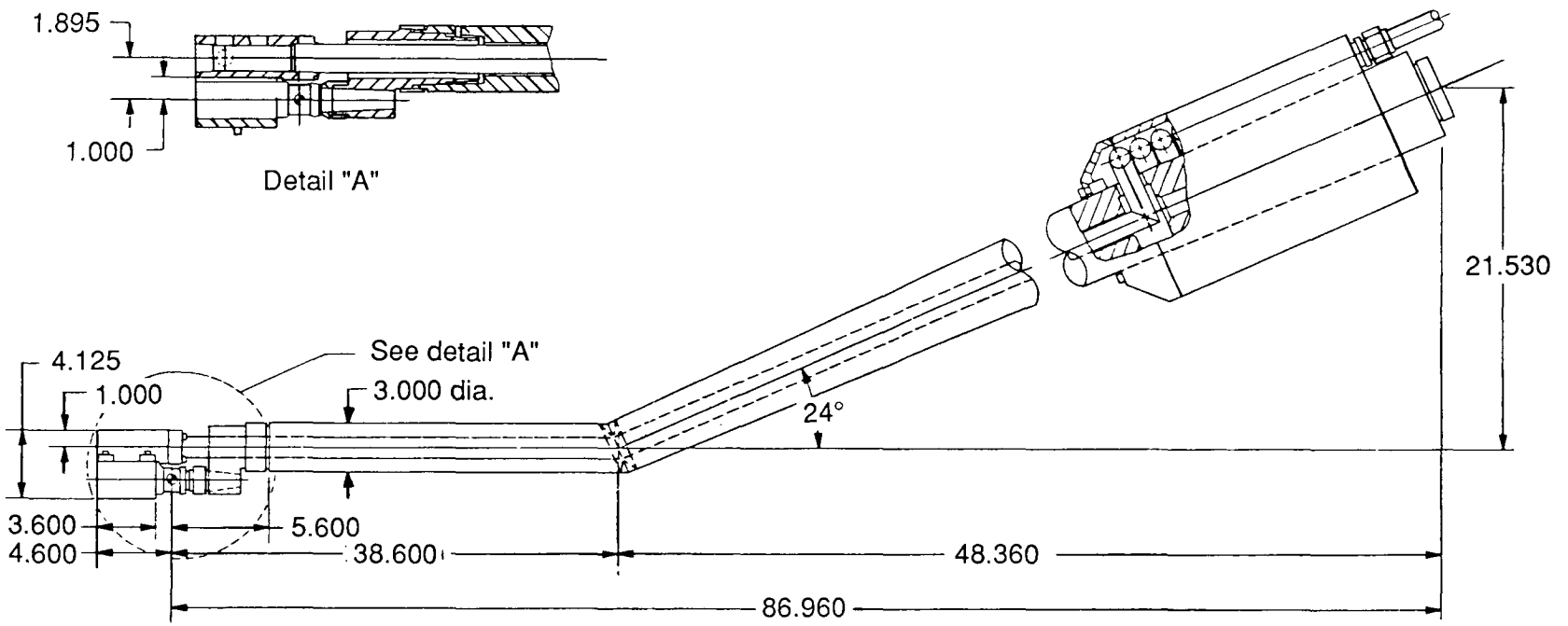

(a) Bent air sting using 708-type balances.

Figure 40. Sketch of air stings used in the 14- by 22-Foot Tunnel to get high-pressure air onboard the model. All dimensions are given in inches.

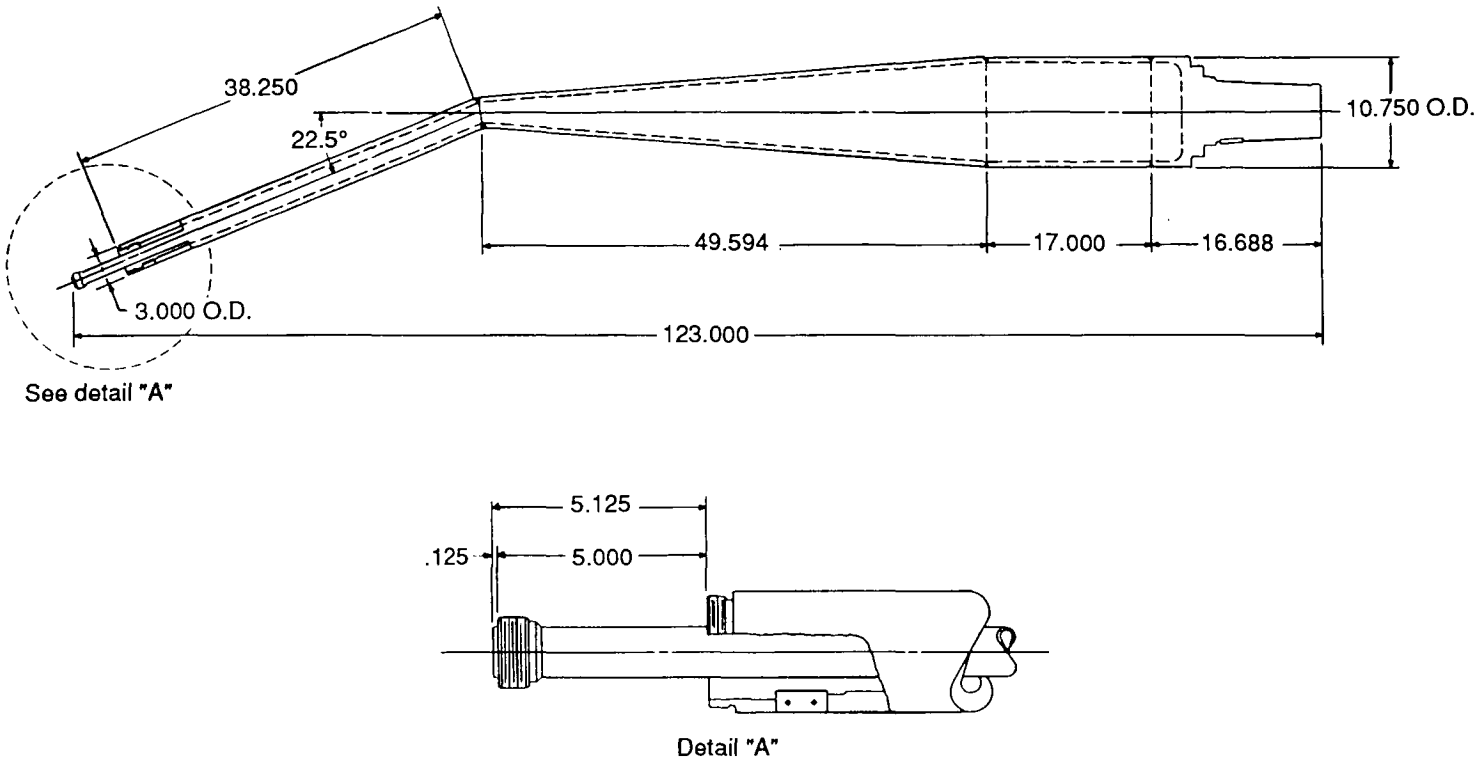

(b) Bent air sting using 729-type balances.

Figure 40. Concluded.

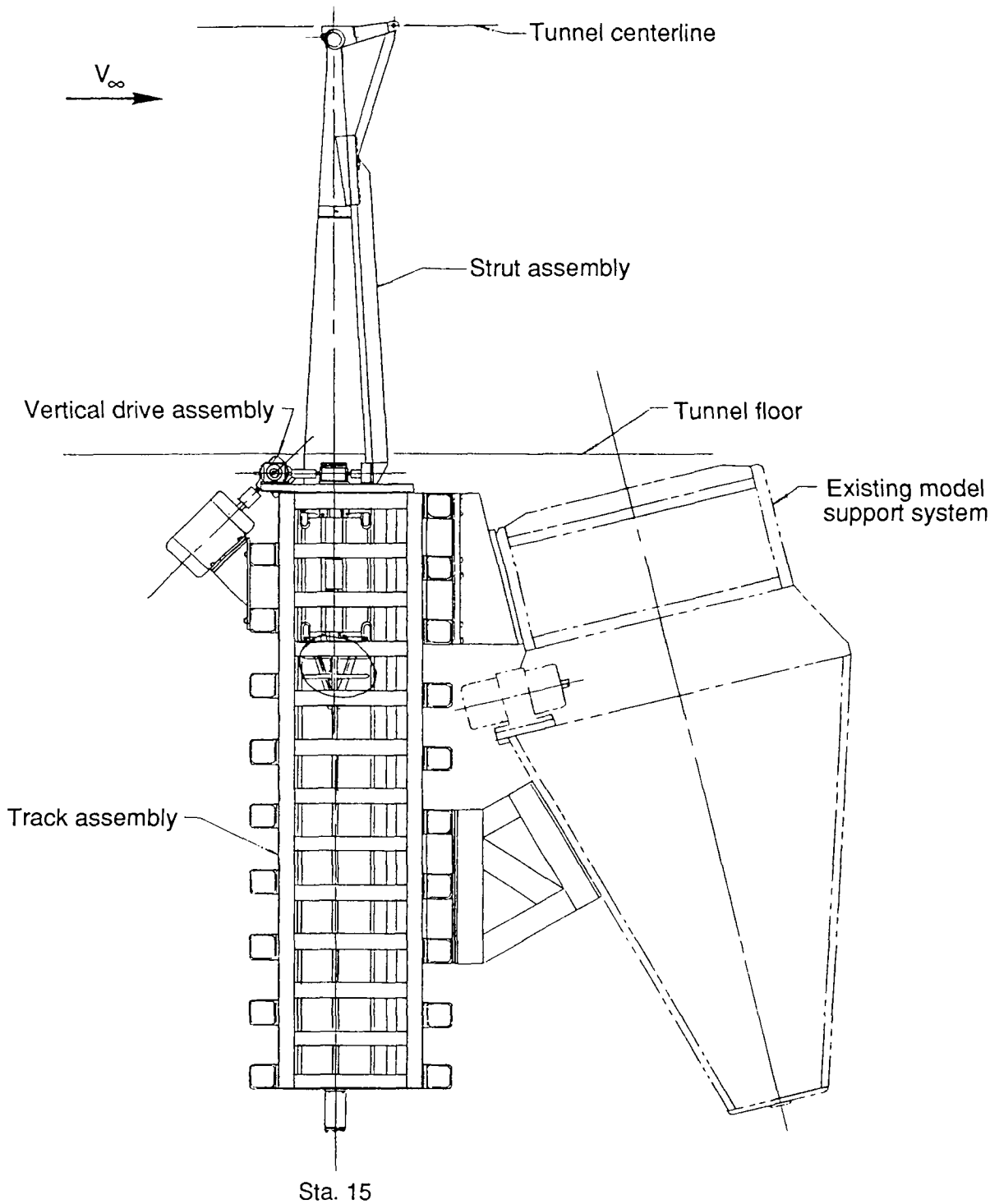

Figure 41. Vertical model support system mounted on model support cart 2 with capability to bring high-pressure air onboard the model.

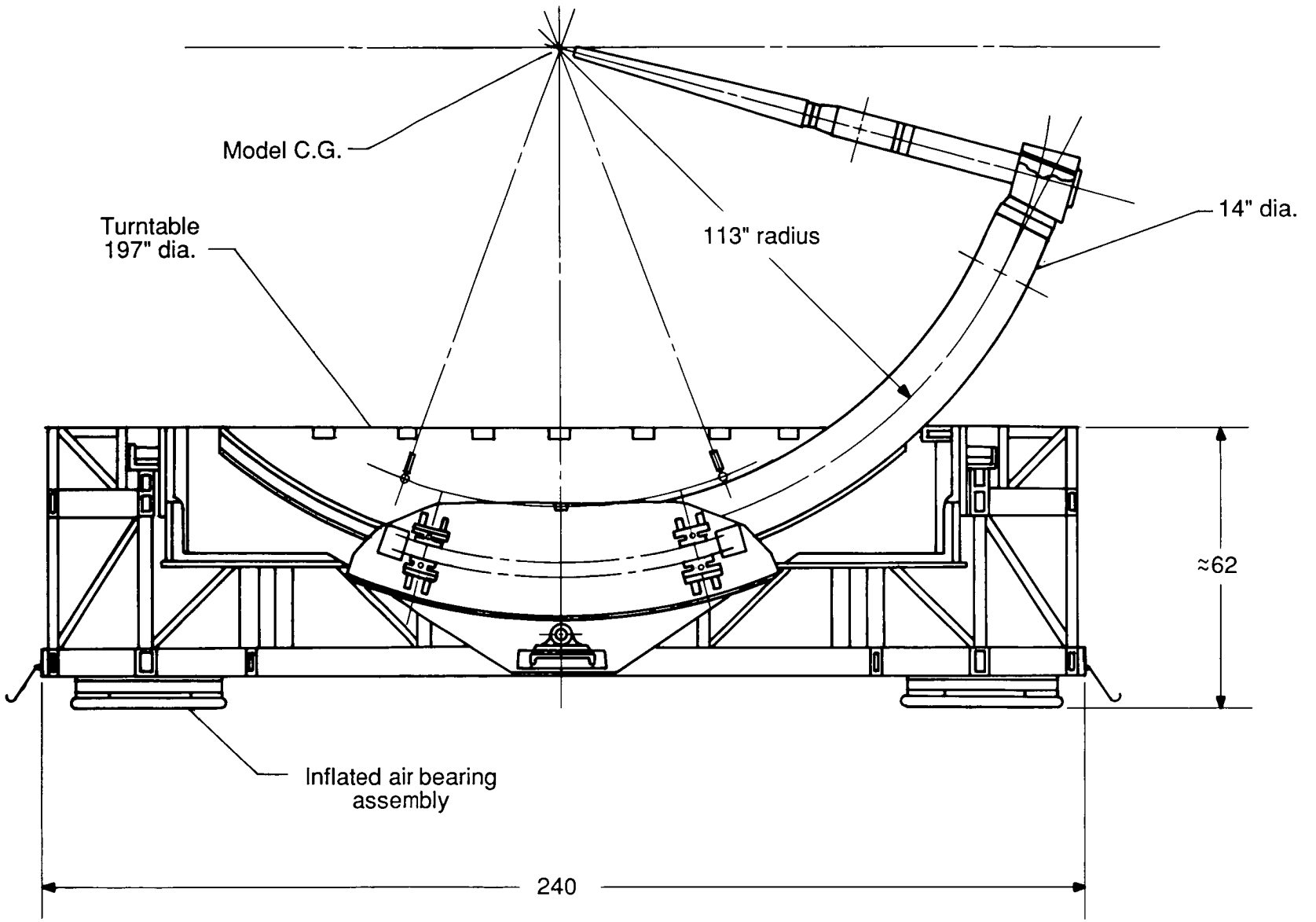

(a) Model support cart 3.

Figure 42. Sketches of model support carts 3 and 4. All dimensions are given in inches.

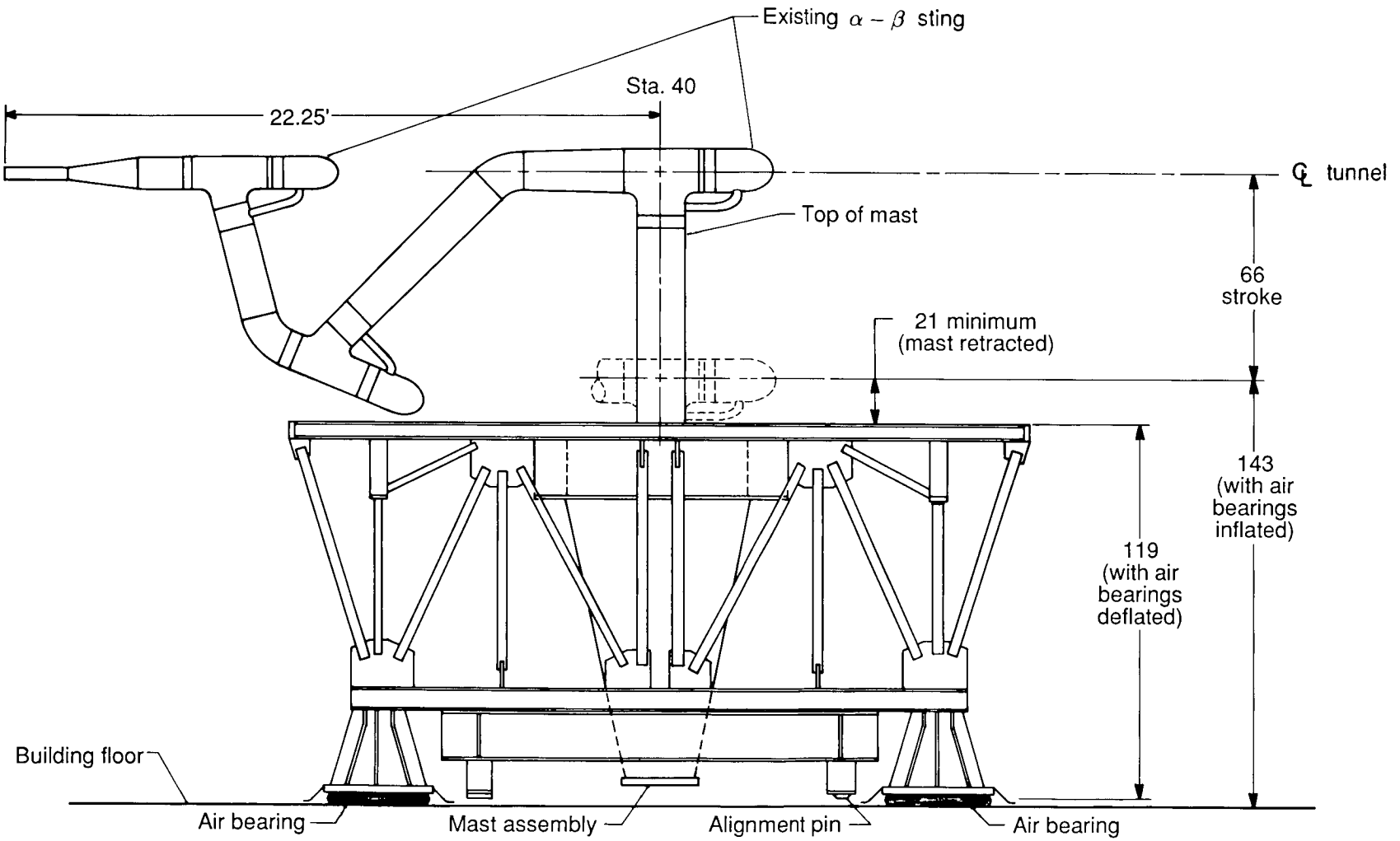

(b) Model support cart 4.

Figure 42. Continued.

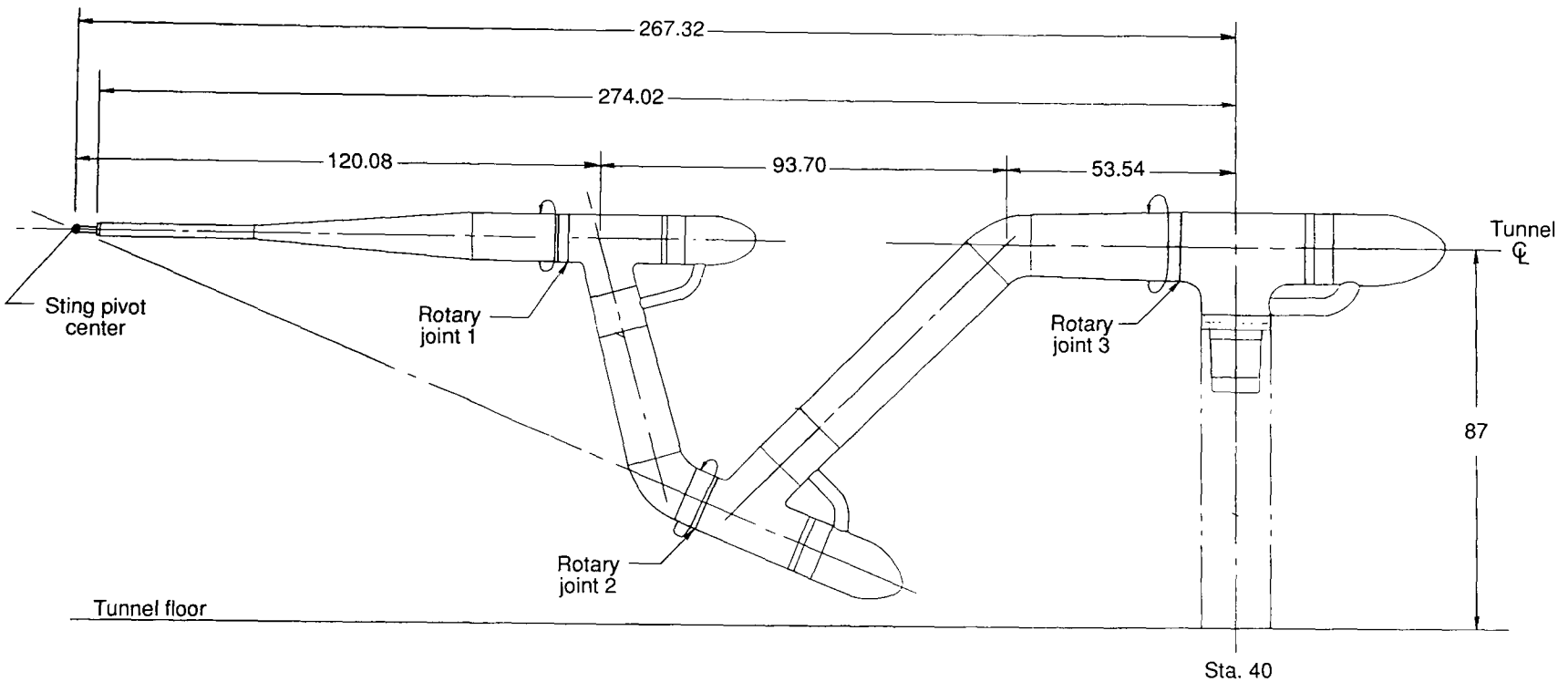

(c) $\alpha - \beta$ sting used on cart 4.

Figure 42. Concluded.

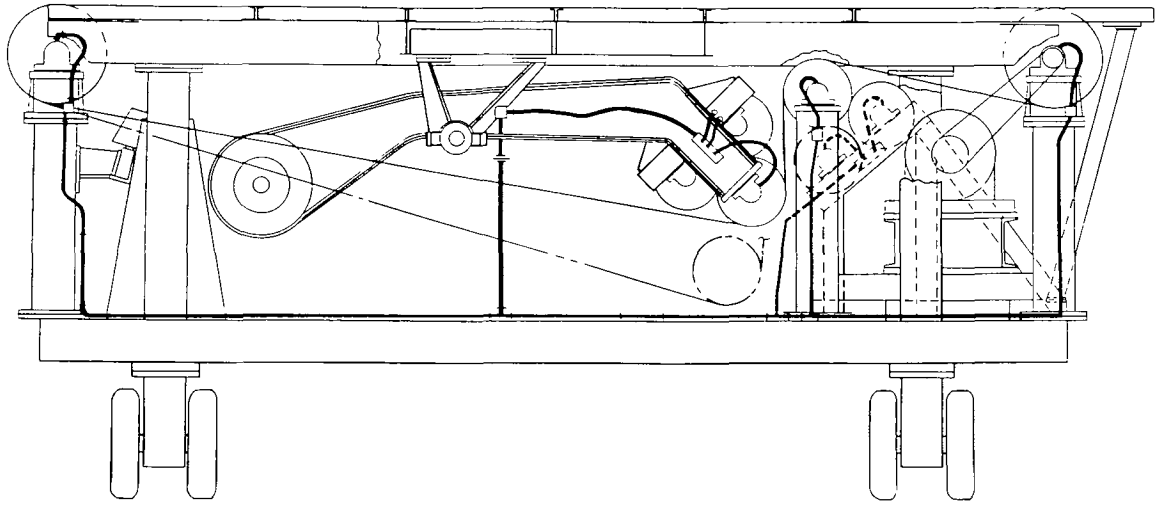

(a) Schematic of moving-belt cart.

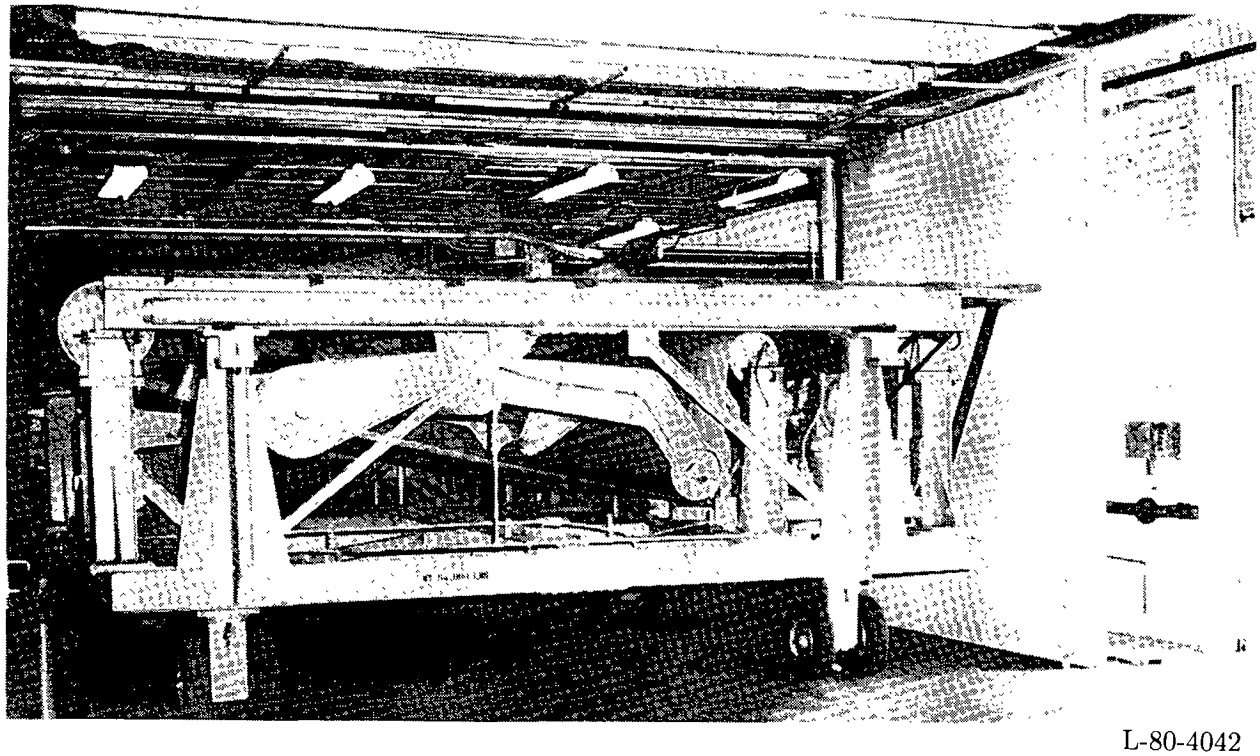

L-80-4042

(b) Photograph of cart prior to installation in the tunnel.

Figure 43. Moving-belt ground plane used in the 14- by 22-Foot Tunnel.

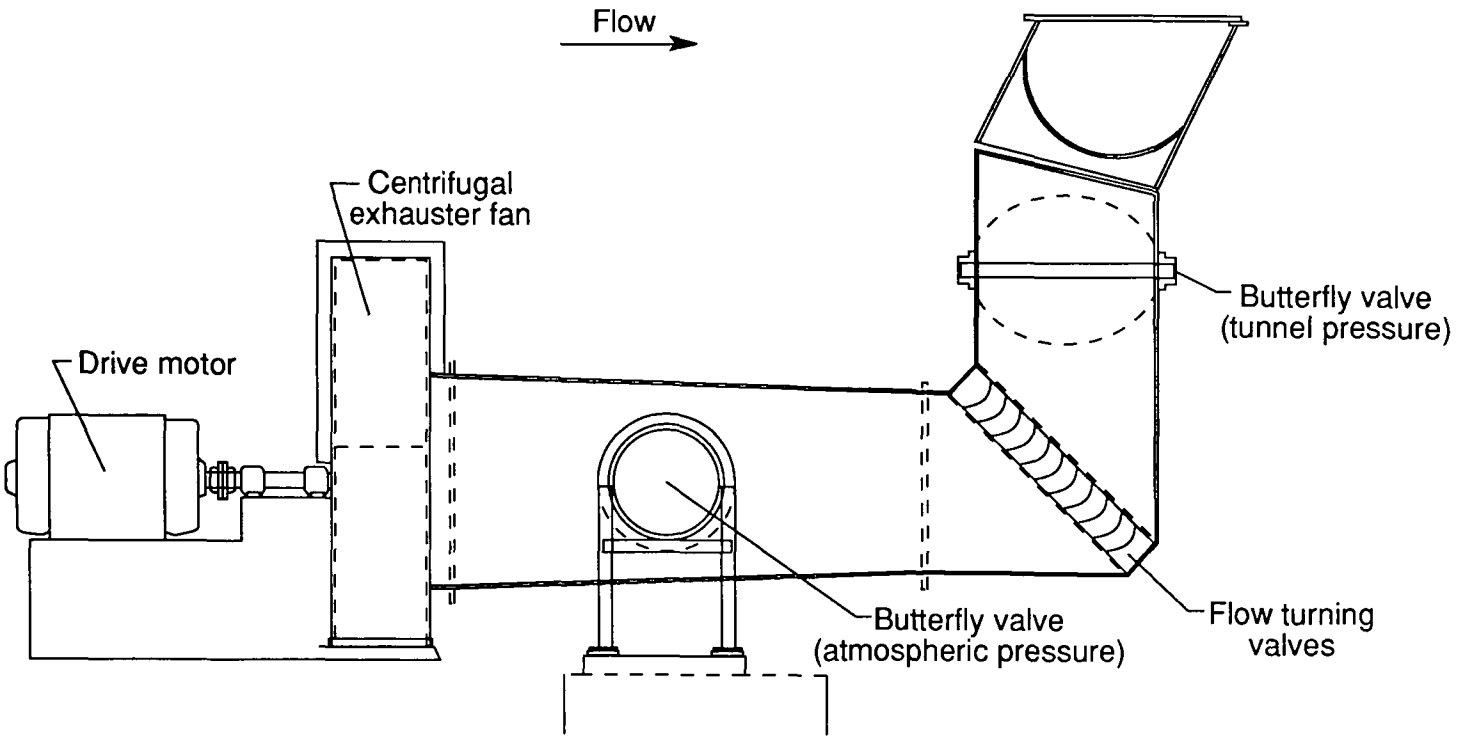

Figure 44. Schematic of boundary-layer removal system.

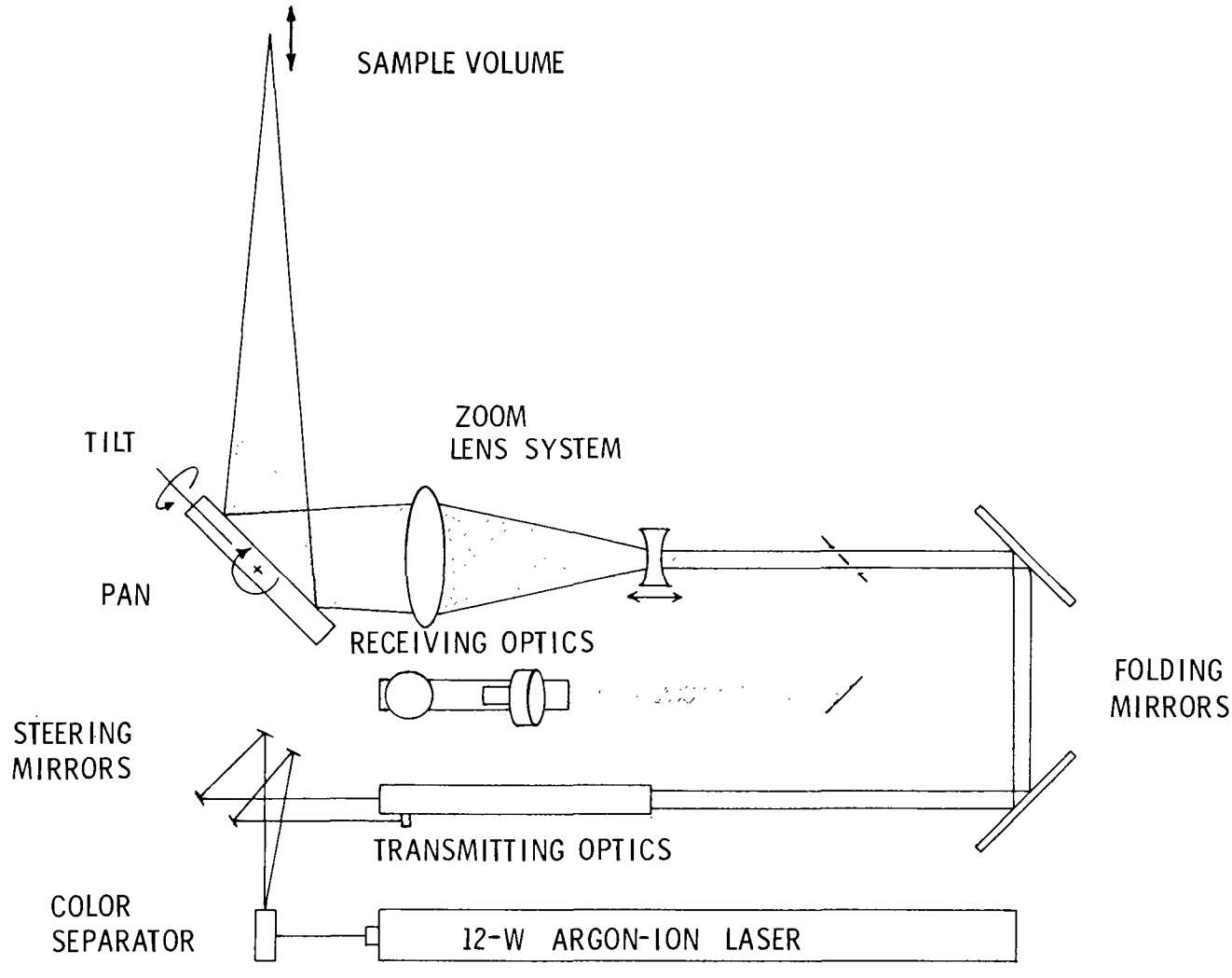

(a) Line diagram of the system.

Figure 45. Laser velocimeter (LV) used in the 14- by 22-Foot Tunnel.

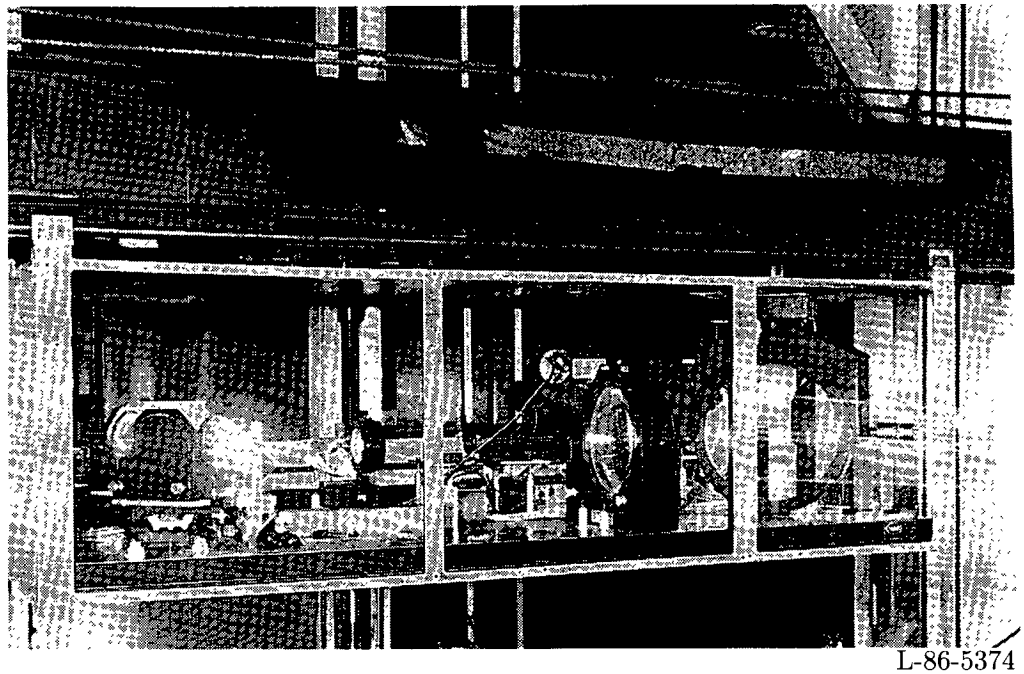

L-86-5374

(b) Photograph of LV system.

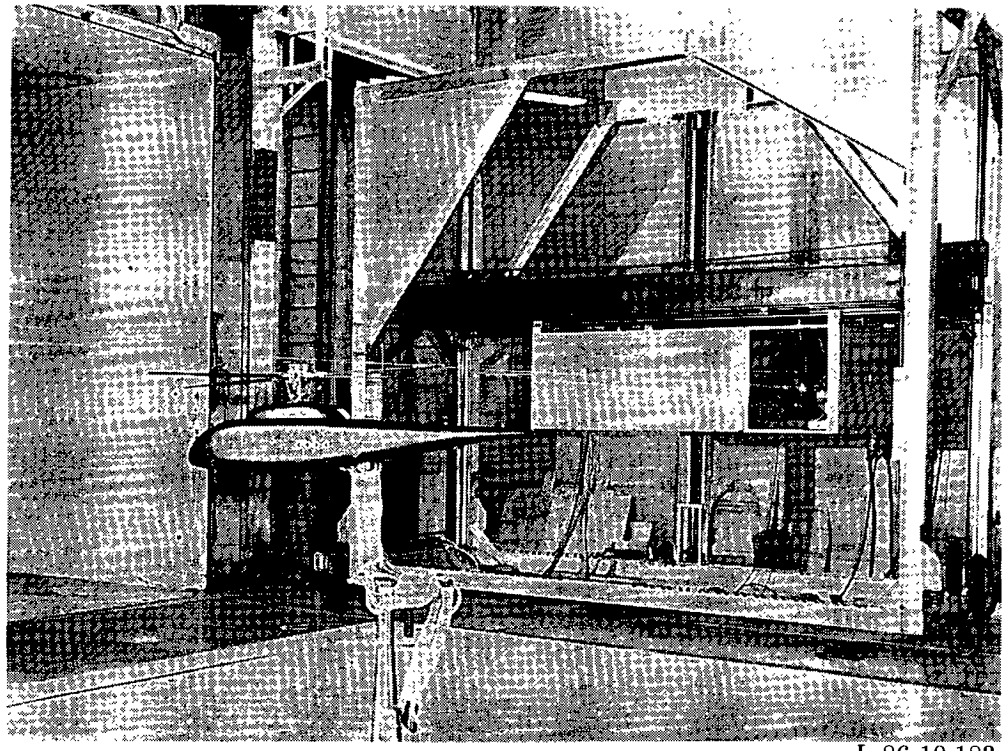

L-86-10,183

(c) x - y traversing rig of LV system.

Figure 45. Concluded.

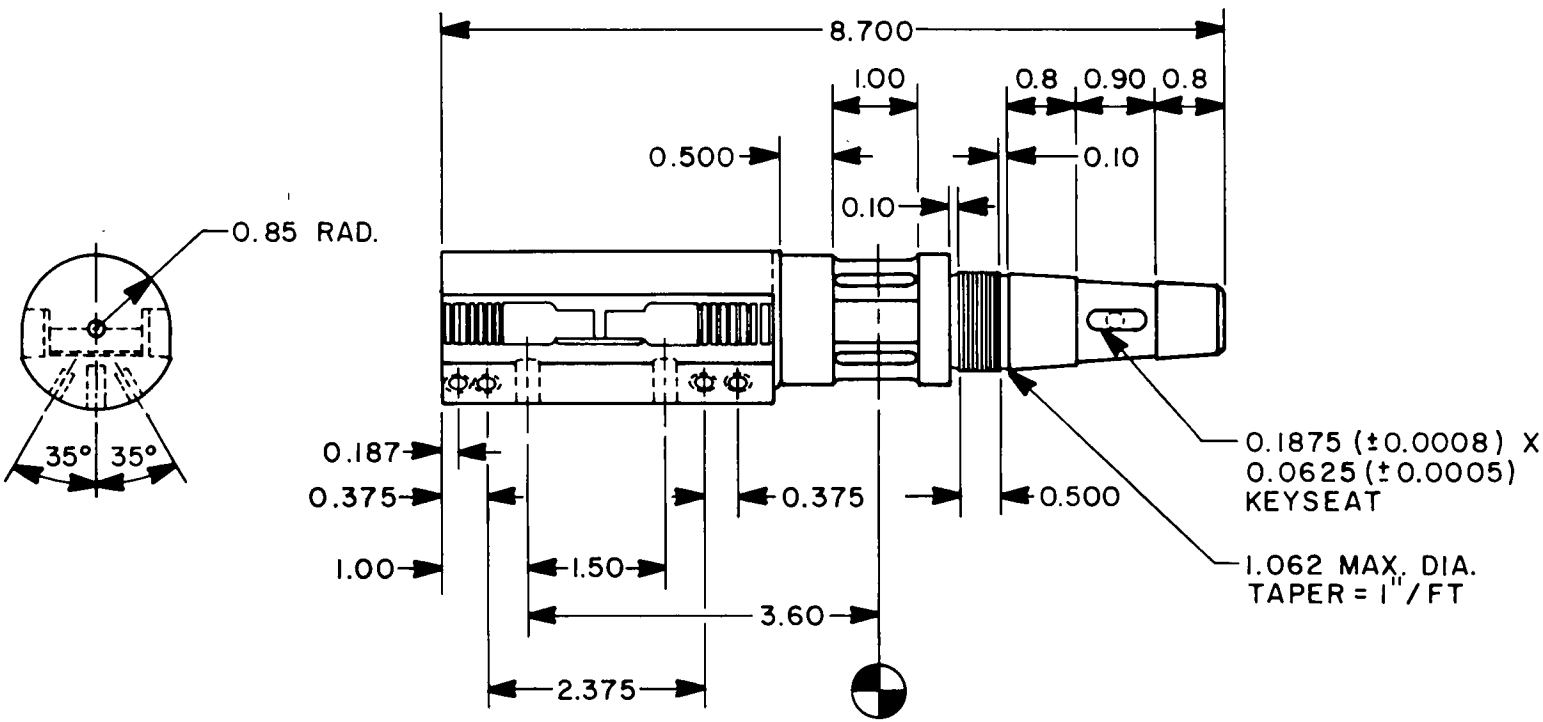

(a) 708-type balance.

Figure 46. Typical six-component strain gauge balances used in the 14- by 22-Foot Tunnel. Linear dimensions are given in inches.

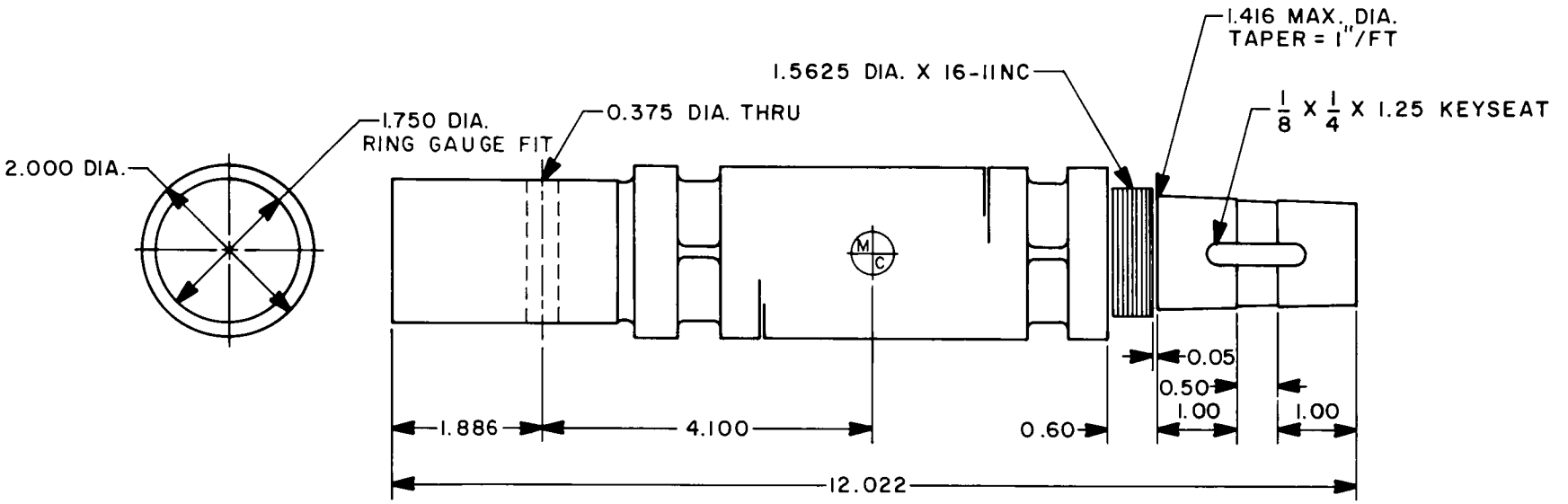

(b) 729-type balance.

Figure 46. Concluded.

NASA
National Aeronautics and Space Administration

Report Documentation Page

1. Report No.	2. Government Accession No.	3. Recipient's Catalog No.
NASA TP-3008		

4. Title and Subtitle	5. Report Date
The Langley 14- by 22-Foot Subsonic Tunnel: Description, Flow Characteristics, and Guide for Users	September 1990
	6. Performing Organization Code
7. Author(s)	8. Performing Organization Report No.
Garl L. Gentry, Jr., P. Frank Quinto, Gregory M. Gatlin, and Zachary T. Applin	L-16731
9. Performing Organization Name and Address	10. Work Unit No.
NASA Langley Research Center Hampton, VA 23665–5225	535-03-01-02
	11. Contract or Grant No.
12. Sponsoring Agency Name and Address	13. Type of Report and Period Covered
National Aeronautics and Space Administration Washington, DC 20546–0001	Technical Paper
	14. Sponsoring Agency Code

15. Supplementary Notes

16. Abstract

The Langley 14- by 22-Foot Subsonic Tunnel is a closed-circuit, single-return, atmospheric wind tunnel with a test section that can be operated in a variety of configurations—closed, slotted, partially open, and open. The closed test-section configuration is 14.5 ft high by 21.75 ft wide by 50 ft long with a maximum speed of about 338 ft/sec. The open test-section configuration, which has a maximum speed of about 270 ft/sec, is formed by raising the ceiling and walls to form a floor-only configuration. The tunnel may be configured with a moving-belt ground plane and a floor boundary-layer removal system at the entrance to the test section for ground-effects testing. In addition, the tunnel has a two-component laser velocimeter, a frequency-modulated tape system for dynamic data acquisition, flow visualization equipment, and acoustic testing capabilities. This report provides users of the 14- by 22-Foot Subsonic Tunnel with information required for planning experimental investigations including the use of test hardware and model support systems.

17. Key Words (Suggested by Authors(s))	18. Distribution Statement
Subsonic wind tunnel Langley 14- by 22-Foot Subsonic Tunnel Moving ground belt Hover test facility	Unclassified—Unlimited Subject Category 02

19. Security Classif. (of this report)	20. Security Classif. (of this page)	21. No. of Pages	22. Price
Unclassified	Unclassified	70	A04

NASA FORM 1626 OCT 86

NASA-Langley, 1990

For sale by the National Technical Information Service, Springfield, Virginia 22161-2171